INTERACTIONS OF 1.15 BEV/C K^- MESONS IN EMULSION

ANDREW L. HAMLIN
ALLEN G. MENKE
RONALD J. OBERLE
and
DAN J. WOLKENSDORFER

28

INTERACTIONS OF 1.15 BEV/C K^- MESONS IN EMULSION

By

Andrew L. Hamlin

Lieutenant, United States Navy,

Allen G. Menke

Lieutenant, United States Navy,

Ronald J. Oberle

Lieutenant, United States Navy,

and

Dan J. Wolkensdorfer

Lieutenant, United States Navy.

Submitted in partial fulfillment of
the requirements for the degree of

MASTER OF SCIENCE
IN
PHYSICS

United States Naval Postgraduate School
Monterey, California

1963

INTERACTIONS OF 1.15 BEV/C K^- MESONS IN EMULSION

* * * * * * *

Andrew L. Hamlin

Allen G. Menke

Ronald J. Oberle

Dan J. Wolkensdorfer

INTERACTIONS OF 1.15 BEV/C K^- MESONS IN EMULSION

By

Andrew L. Hamlin

Lieutenant, United States Navy,

Allen G. Menke

Lieutenant, United States Navy,

Ronald J. Oberle

Lieutenant, United States Navy,

and

Dan J. Wolkensdorfer

Lieutenant, United States Navy.

This work is accepted as fulfilling
the thesis requirements for the degree of
MASTER OF SCIENCE
IN
PHYSICS
from the
United States Naval Postgraduate School

ABSTRACT

1240 interactions in Ilford K-5 emulsion have been studied of which 1154 were 1.15 Bev/c K^- meson interacions. 21% of all interactions produced a charged Σ hyperon with a ratio of Σ^- to Σ^+ of 1.70. Nine possible examples of Ξ^- hyperons were observed as well as three possible examples of double hyperon production. From the characteristics of 54 stars in flight and nine disappearances in flight, it is estimated that in 14% of the interactions the K^- meson is re-emitted. 14.6% of all the K^- meson beam interactions produced a secondary star in flight and 2.5% produced a disappearance in flight. Stars in flight were interactions of the following particles with the indicated ratio: 3 π meson; 2 K meson; 5 baryon.

65 double centered stars were observed for a frequency of production of 5.6%. 45 had a connecting track of less than 6 microns. The mesonic to non-mesonic ratio of the complete group was found to be 5.6 ± 1.9. The short range double centered stars were emitted predominately in the forward direction to give a F/B ratio of 2.8. In at least 80% of these events the stars were an interaction in the heavy emulsion elements. An absence of recoils from the parent stars was observed and the short range stars had few short prongs from the bound lambda hyperon decay. These and other observations support the model proposed by Jones et al for the production of short range double centered stars. A difference was observed in the F/B ratio of the recoils from stars with nine or more prongs and stars with less than nine prongs. From this observation it is extimated that $29\% \pm 22\%$ of the single centered stars contain a bound lambda hyperon decay and hence are CFs. From the characteristics of five free Λ^0 decays, it is estimated that 20% of the beam K^- meson interactions produce a free lambda hyperon.

Without considering the emission of $\bar{K}^0$, strangeness is found to be conserved in 91% of all K^- beam interactions.

TABLE OF CONTENTS

LIST OF ILLUSTRATIONS

LIST OF TABLES

I

INTRODUCTION

The first indication of the existence of K^- mesons was reported by Le Prince-Reinquet and L'Herities in 1944 /1/. K^- mesons were first produced artificially in 1953 by bombarding targets with high energy proton and pion beams available from the Brookhaven Cosmotron. Fowler et al /2/ and Hill et al /3/, using a 1.5 Bev/c pion beam, found evidence for strange particle production. Hill et al /4/ and Hornbostel and Salant /5/ produced K^- mesons by bombarding targets with proton beams of 2.2 to 3.0 Bev/c. The first observation of charged Σ hyperons produced by K^- meson interactions was reported by Hornbostel and Salant /5/ in 1955.

Upon the opening of the Berkeley Bevatron, K^- meson beams of great intensity became available and investigation of their interactions increased. Barkas et al /6/ reduced the pion background which had plagued earlier beams. The beam intensity was improved by the use of absorbers followed by magnetic analysis for separation. Focussing improvements /7/, the coaxial velocity spectrometer /8/, and other techniques enabled greatly enriched K^- beams to be produced. The coaxial spectrometer reduced background contamination by a factor of about 700 /9,10/.

After the initial discovery of hyperfragments (HFs) in 1955 /11/, information about them accumulated at a brisk rate. Most of the data dealt with the characteristics of the light HFs ($Z \leq 5$). Developement of high energy K^- beams made examination of heavier HFs feasible, but work in this field did not begin until 1962. Recent studies have resulted in the proposal of a plausible model for heavy HF production by Jones et al /12/. They stated that most of the short range HFs are recoiling nuclei with a bound lambda hyperon (Λ^0). Independent studies by Davis et al /13/ and Fletcher et al /14/ reported results in agreement with this model. In addition, Davis found that the binding energy of the Λ^0 in the heavy HFs approached a value of 25 Mev. To date no study of heavy HF production has been coordinated with a detailed

observation of all interactions, and hence we have undertaken this task. To accomplish this we have returned to a previously unfinished analysis of 1.15 Bev/c K^- interactions. In the preliminary study several hundred stars were examined for the emission of mesons and hyperons and a search was made for cascade particles /15/.

This paper represents the results of an analysis of 1240 interactions. A detailed study of the characteristics of each star was made. The emission of hyperons, K mesons, pi mesons and hypernuclei was determined. Each star was studied under 2500X magnification for the existence of a double center, a recoil and Auger electrons. A search was made for free lambda hyperons emitted from these interactions, and five events were located. Our analysis is directed toward determining how often the strangeness of the K^- meson is accounted for by the emission of a visible strange particle or a neutral hyperon. The probability of a Λ° being trapped to form a hypernucleus can them be estimated. We also sought to correlate the observed characteristics of parent stars with recent developements in the proposed model for heavy HF production.

Our study is divided into three projects to examine the three basic types of strange particle production. The first part is an analysis of charged hyperon production. The second part is an examination of interactions in flight. The last part is a determination of the frequency of lambda hyperon production, both free and bound.

Each part is a complete study in itself, and represents the work of one or two individuals. Since all studies are closely related, they are combined into one paper to obtain completeness and to eliminate duplication in describing techniques and history.

II

EXPERIMENTAL PROCEDURES

A. The Emulsion Stack

A stack of 200 pellicles of Ilford K-5 emulsion, each 230 by 150 by 0.6 mm, was exposed to a 1.15 $\pm$ 0.10 Bev/c beam of K^- mesons developed at the Berkely Bevatron.

The beam was separated by the use of the Murray Coaxial Velocity Spectrometer /8/ and had less than 10% contamination of pion, muons, and anti-protons.

The physical positioning of the emulsion stack in the beam is shown schematically in Figure 1.

The exposed pellicles were processed and mounted at the Lawrence Radiation Laboratory at Berkeley.

All plates of this stack are presently at the United States Naval Postgraduate School, Monterey, California.

B. Scanning Techniques

The K^- stars analyzed in this paper were all located by the use of area scanning techniques. The principal biases of area scanning against small events, interactions with no dark prongs, and some directions of secondary particle emission are discussed later.

The area scanned was 100 mm long, and 80 mm wide, perpendicular to the beam, and centered at a point 50 mm downstream from the entering face as shown in Figure 2. The selection of this area was a compromise between the desire to bring to rest the more energetic evaporation particles, which are emitted approximately isotropically in the laboratory system, and the desire to bring to rest the energetic hyperons produced by the interactions within the available volume of the emulsion. The reactions which produce hyperons usually do not produce them backwards in the laboratory system, so as much emulsion as possible was desired "downstream" of the interactions studied.

The available mean distance in the emulsion downstream of the scanned area is approximately 180 mm and is adequate to stop any baryon with initial track ionization greater than twice minimum.

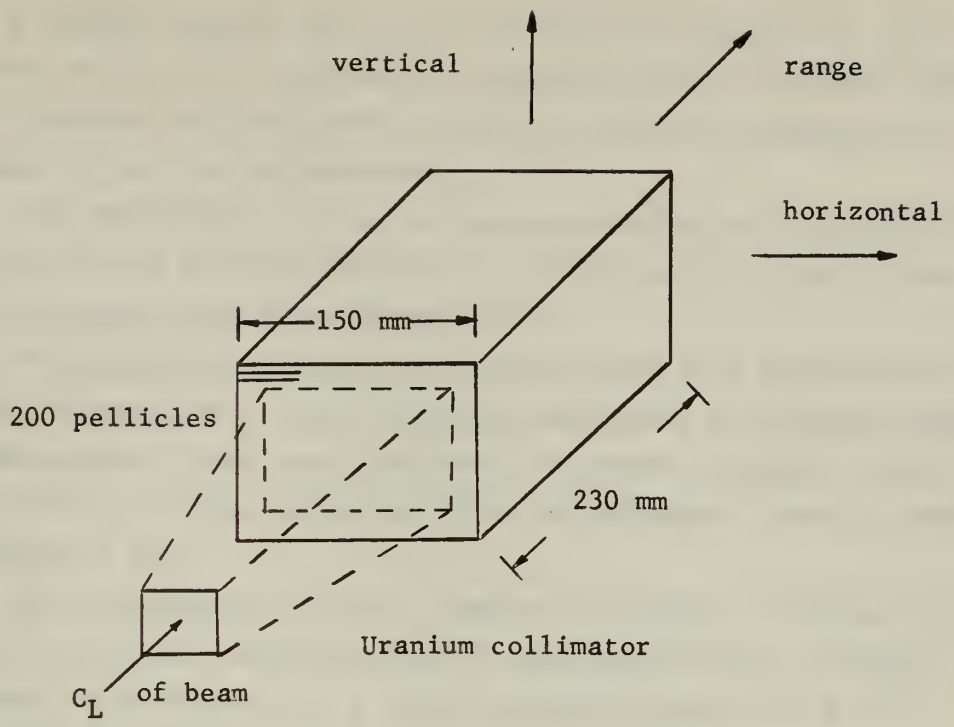

Figure 1. Geometry of the beam and the emulsion stack

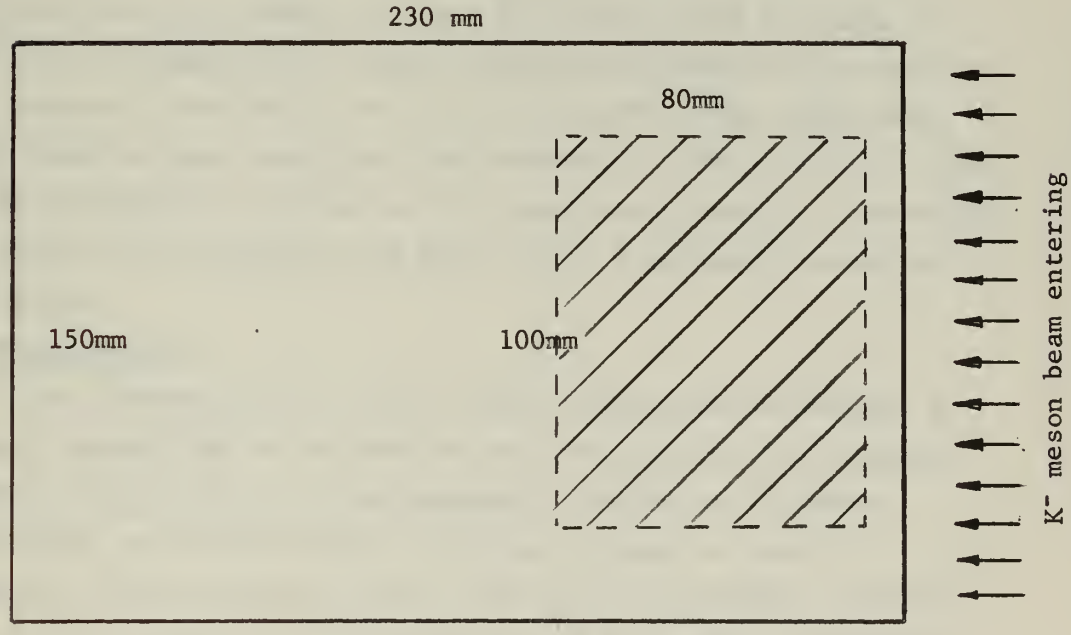

Figure 2. Diagram of the area scanned in each pellicle analyzed, the area completely scanned is shown by cross-hatched region

For a charged hyperon emitted in the forward direction at ionization twice that of minimum the moderation time is several times the lifetime, and the hyperon therefore probably decays prior to coming to rest in the emulsion.

The approximately 50 mm of emulsion available to stop particles emitted in the backward direction is sufficient to stop all protons of energy less than 130 Mev /16/.

The pellicles selected for scanning were B-86 through B-92. These pellicles were chosen because measurement of minimum tracks at the center of the face indicated the greatest density of minimum tracks in these pellicles. This experimental curve is shown in Figure 3 /17/.

The designated areas were completely scanned, yielding 1154 events definitely resulting from K^- meson interacions, assuming 7% beam contamination, in a total scanned volume of 27.9 cm^3, or 0.67% of the entire stack. The designated scanning area is shown in Figure 2.

C. Data Recording

All data are recorded on 8 by 10 1/2 inch McBee Keysort cards of the type shown in Figure 4. This system is based on the use of "edgepunched" cards allowing the specific information to be readily available when desired /18,19/. The large card size enables data resulting from analysis of the particular event to be permanently recorded on the event card. Each K^- interaction is listed on a separate card which gives a permanent record of the event.

D. Measurements

Any charged particle which moves through matter suffers a loss of energy due to excitation and ionization of the absorber atoms, the emission of electromagnetic radiation, Cerenkov radiation, or collision with a nucleus forming a "star". A charged particle moving through a nuclear photographic emulsion interacts in exactly the same manner and the energy transferred from the charged particle to the photographically sensitive grains forms a latent image when the energy transferred exceeds a certain threshold value. After development these latent images appear as "blobs" in the nuclear emulsion. The track formed by the

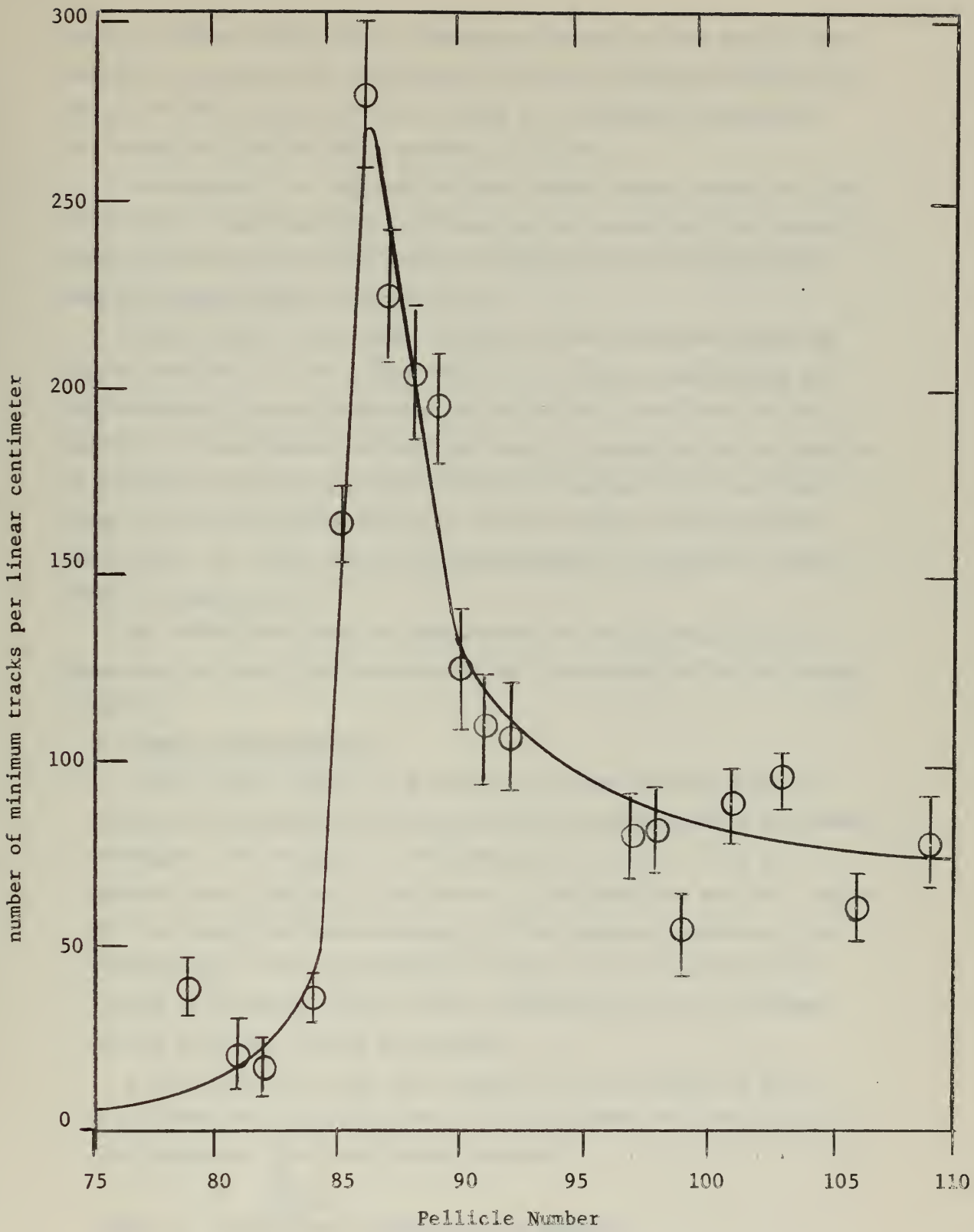

Figure 3. Experimental determination of the number of minimum tracks per linear centimeter at the center of the face as a function of pellicle number.

locus of these blobs gives a permanent record of the path of the particle causing these interactions and the measurable characteristics of the tracks provide a means for analyzing the nature and energy of the particle causing the track.

The energy of a charged particle which comes to rest in the stack can be most accurately determined by measuring the particle's range and calculating the particle energy using an empirically derived range-energy relation /20/.

Tracks which do not come to rest in the emulsion stack can not be analyzed by the method above. In these cases energy may be determined from a knowledge of the velocity and mass of the particle. Experimental determinations of ionization as a function of particle velocity have been made and together with the knowledge of the particle's identity provide energy determinations. The subject of track ionization measurements is covered in some detail in Appendix A.

The techniques used in measurement of track length and in computing and applying corrections are discussed in the following sections.

1. Range determination

The actual range of a particle in the nuclear emulsion cannot be measured directly, but must be approximated by summing straight line segments. Measurements are made of the projected track length in the plane of the emulsion and the length in the direction perpendicular to the emulsion surface. The measurement in the perpendicular plane must be corrected by use of a shrinkage factor which compensates for the collapse of the emulsion during processing.

Dividing the track into segments short enough to give a satisfactory approximation to straightness and summing over the segments, the total range becomes:

$$R = \sum_{k=1}^{n} r_k$$

where r_k is the total range of each segment.

All measurements were made using a microscope employing a rectangular stage and optic axis designed and equipped to measure translations along three mutually perpendicular axes,

the plane of the microscope stage being designated the X-Y plane. Carefully machined lead screws control movement in this plane with the amount of motion indicated directly by vernier equipped screw gauges. Lengths in the Z direction, defined as the optic axis of the microscope, are measured by vernier measurement of the displacement of the microscope objective. The measurement of length in the Z direction was accomplished by measurement of the displacement of the initial and final point of each segment and correcting the resulting length by use of the shrinkage factor.

For long tracks the distance between points in the emulsion is determined by the difference of coordinates of the points in the orthogonal frame above. The measured range of a particle in each pellicle becomes:

$$R = \sum_i \left\{ (x_{i+1} - x_i)^2 + (y_{i+1} - y_i)^2 + [S(z_{i+1} - z_i)]^2 \right\}^{1/2}$$

where x_i, y_i, and z_i are the coordinates of the initial point of the i^{th} track segment; x_{i+1}, y_{i+1}, and z_{i+1} are the coordinates of the final track segment; and S is the shrinkage factor.

For shorter track distances in the X-Y plane measurements were made by means of a calibrated reticle placed in one eyepiece and thus superimposed on the field of view. The measured range of a particle in each pellicle using the reticle method becomes:

$$R = \sum^{K} \left\{ l_i^2 + [S(z_{i+1} - z_i)]^2_{th} \right\}^{1/2}$$

where l_i is the projected length of the i^{th} track segment.

The selection of which measurement technique to use was determined by the length of the track segment. For track segments of length less than one millimeter the calibrated reticle method was used. The reticle used for all measurements spanned approximately 132 microns in the field of view (with 100X objectives and 10X eyepiece) and was calibrated to better than one part in 1350 /21/.

All ranges must be normalized to the standard conditions used in the Range-Energy relation. The corrections made for emulsion-density variations are based on Figure 4 and the exposure emulsion density of 3.8392 g/cc. Since the correction

is a function of velocity, each track must be considered separately. The emulsion-density variation errors are typically of the order of a few tenths of a percent of the measured range.

The sum of many straight line segments was used as an approximation in all measurements. The total projected length is the sum of the lengths of the chords joining successive points on the track; a new chord is started whenever there is a change of particle direction greater than 3 degrees. This approximation gives track lengths which are less than 0.1% short of the true length.

No error in energy determination was introduced by this approximation, since it was also used in establishing the Range-Energy relation /22/.

The systematic errors inherent in range determination are due to errors in the measurement of emulsion density and shrinkage factor /23/. The uncertainty in emulsion density of about 0.1% gives a range uncertainty of the same amount. The error due to shrinkage factor varies according to track geometry and must be calculated separately for each track. The uncertainty in shrinkage factor is about $\pm$ 1% and is reflected into the range as:

$$\Delta\beta = R\left(\frac{\Delta S}{S}\right) \sin^2\delta$$

where δ is the dip angle, i.e., the angle of inclination of the track to the emulsion surface as measured in the unprocessed emulsion.

The statistical errors inherent in range measurement are due to measurement uncertainty and range straggling. The magnitude of the Bohr straggling in nuclear emulsions has been calculated as a function of velocity /16/. Bohr straggling contributes most of the variance to the distribution of measured particle ranges. Measurement error varies with the particle, range, and the measurement technique and must be considered separately for each track.

2. Angular Measurements

The angle of primary interest in this analysis is the space angle between the incoming and outgoing particles. The space angle between two tracks cannot be measured directly but must be

calculated from the projected angle between the momentum vectors and the dip angle δ.

The projected angle (θ) is measured by using the hairline of the reticle and a goniometer and aligning the hairline above the track to be measured. All measurements are with respect to the incident particle vector using the shortest length of track consistent with reliable measurement. The observer standard deviation for the projected angle was found to be 0.2^{o}.

The dip angle (δ) is the angle of track inclination with respect to the surface of the emulsion in the unprocessed emulsion. The dip angle is calculated from the measured projected length (L) and the vertical distance ($S\Delta Z$). Using simple geometry, the dip angle (δ) becomes:

$$\delta = \tan^{-1} \frac{S\Delta Z}{L}$$

where S is the shrinkage factor, and ΔZ is the vertical distance in the processed emulsion.

The error in dip angle which arises from observer uncertainty is much greater than that for the projected angle and must be estimated for each track since it varies with dip angle.

3. Ionization

Measurement of a particle's range is the most accurate method of energy determination. For particles which cannot be measured in this way, an alternate procedure utilizing ionization measurements may be used. Since ionization is strongly velocity-dependent, it is possible to select an ionization parameter and perform measurements on particles of known energy to ascertain a calibration curve. The use of this calibration curve gives the velocity of any particle which has a known ionization value. This information, together with a knowledge of the particle identity, is sufficient to determine the energy of the particle at any point.

To minimize the possible personal error, the ionization parameter used was blob density (the number of blobs per 100 microns) rather than the more subjective grain density value.

A calibration curve for blob density as a function of velocity (β) was plotted for values of β between .110 and .92.

The calibration curve was formed using π mesons and proton tracks of known energy. The effects of nonuniformity of development were minimized by calibration through the entire pellicle thickness, and by using several pellicles.

Using the above calibration curve, the mean distance between "just resolvable" blobs (α) was found to be .61 microns. A blob density correction was plotted as a function of α for various values of dip angle. This dip angle correction was applied to all blob counts.

A more detailed treatment of this subject, together with the pertinent plots, may be found in APPENDIX A.

E. Shrinkage Factor

Since all measurements are made in the processed emulsion, while the interaction actually occurred in the unprocessed emulsion, a correction must be made to account for the differences between the processed and unprocessed emulsion. During processing, a collapse in the vertical dimension takes place because some of the constituents of the emulsion are removed; the ratio of the unprocessed thickness to processed thickness is therefore defined as the shrinkage factor. Changes occurring in the horizontal dimensions are considered negligible.

To obtain the true vertical dimension in the unprocessed emulsion, the measured distance in the processed emulsion must be multiplied by the shrinkage factor.

The following procedure was used to determine the shrinkage factor in this stack. Prior to processing, the densities of some sample pellicles were measured. The unprocessed thickness was later calculated from the density, weight, and area of each pellicle, the area being measured after processing. The mean processed thickness was measured and the shrinkage factor determined for each pellicle of the sample. Using these values and assuming that the remaining pellicles have a shrinkage factor equal to the average of the sample, the thickness at a standard reference point on each processed plate was measured and the original thickness calculated at these reference points.

The shrinkage factor at any time can be determined by measuring

the thickness at the reference point and computing the ratio of that value to the original thickness.

The determination of the shrinkage factor was made whenever range measurements were made.

F. Emulsion Density

The composition of an emulsion, and hence it's stopping power, varies with the relative humidity of the atmosphere with which it is in equilibrium. For accuracy, the relative humidity during exposure and the density of emulsion at standard conditions should be known, but a knowledge of the density of the emulsion at the time of exposure is usually sufficient. Since the Range-Energy relation is based on an emulsion with a standard density of 3.815 g/cc, corrections must be applied to track lengths measured in emulsions whose exposure density differed from that value.

The density of the emulsion in this stack was determined by weighing the pellicles both in air and in carbon tetrachloride. This method is described in detail in references /20,24/. The measurement error was estimated to be 0.1%.

The density of the stack was found to be 3.8392 ± 0.0029 grams per cubic centimeter or 0.634% more dense than the standard emulsion density of 3.815 grams per cubic centimeter.

The variation of proton range with emulsion density is shown in Fig. 4. For these values, the error due to emulsion density was less than the range measurement uncertainty and was neglected.

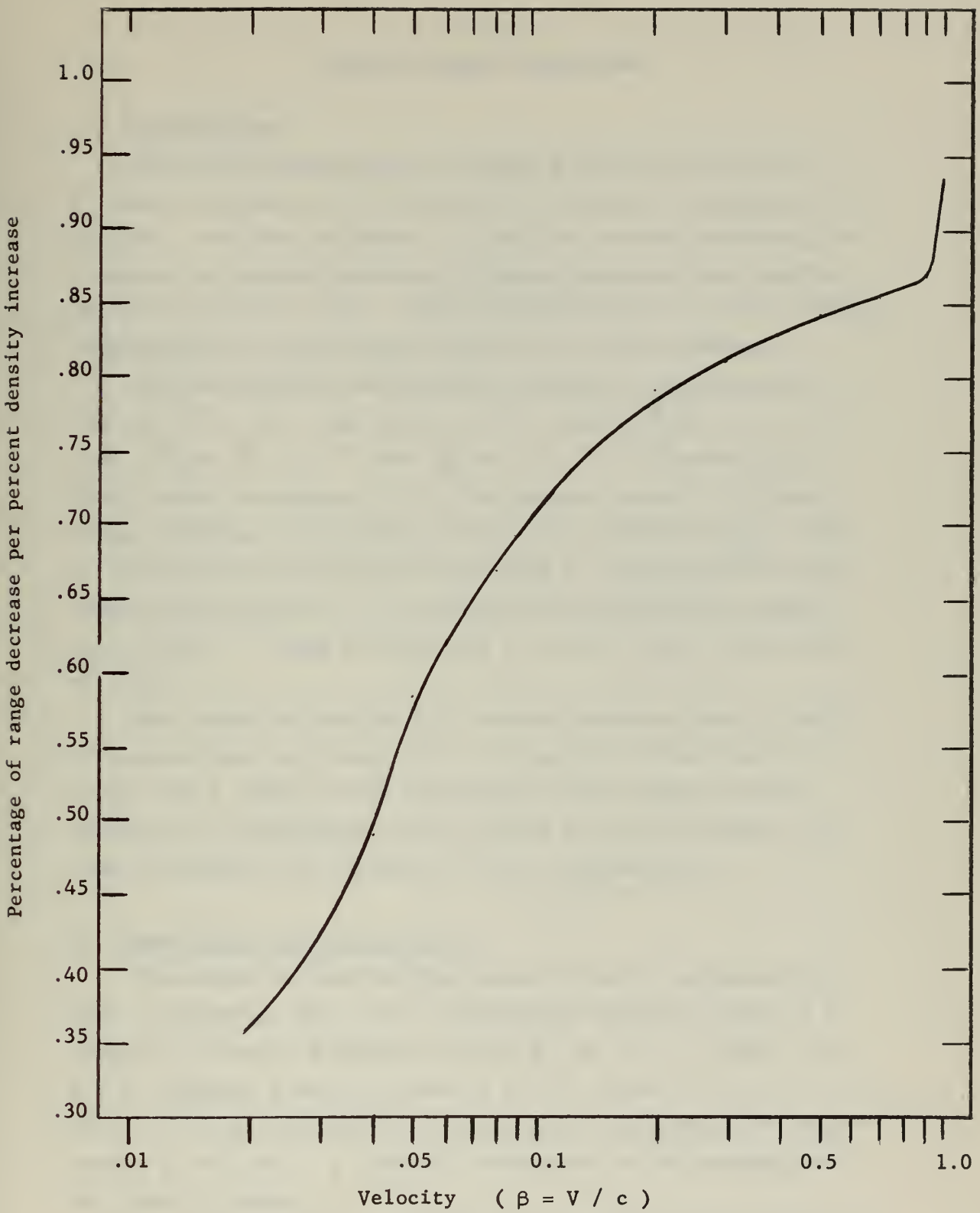

Figure 4. Variation of proton range with emulsion density. The percentage range decreases per percent density increase above the standard density of 3.815 grams per cubic centimeter plotted as a function of the velocity (β) of the particle.

III

CHARGED HYPERON PRODUCTION

A. Introduction

The first observations of charged Σ hyperons produced by K^- meson interactions were reported by Hornbostel and Salant /5/ in 1955. The first evidence of a decisive nature concerning the existence of charged hyperons in nuclear emulsions was reported in 1953 by Bonetti /25/ . Simultaneously York et al /26/ working independently noticed similar particles in cloud chambers.

The non-leptonic decay modes of charged Σ hyperons are $\Sigma^+ \rightarrow P + \pi^o$, $\Sigma^+ \rightarrow N + \pi^+$, and $\Sigma^- \rightarrow N + \pi^-$ with $\Sigma^+ \rightarrow P + \pi^o$ and $\Sigma^+ \rightarrow N + \pi^+$ occuring with nearly equal frequency./6,27/. The hyperon masses, lifetimes, energy spectra, and branching ratios have been determined. /24/

Much has been published concerning K^- interactions at energies up to 760 Mev. /28/ Some work has been reported using a 1.15 Bev/c K^- beam by Quassiati et al /29/ and by Barkas et al /30/.

The production and decay of charged hyperons from 1.15 Bev/c K^- interactions are discussed in this section. These data are drawn from a sample of 879 interactions. All prongs with the exception of approximately 10% of those of less than twice minimum ionization were followed to their terminations.

B. Nomenclature and Definitions

The system of notation introduced by the K^- Collaboration /31/ is employed. Thus, $F\Sigma^{\pm}\pi$ indicates a decay in flight of a positively charged Σ hyperon via the $\Sigma^+ \rightarrow N + \pi^+$ mode, and $R\Sigma^+p$ indicates a decay at rest of a Σ^+ via the $\Sigma^+ \rightarrow P + \pi^o$ mode. In cases of doubt as to the sign of the hyperon the superscript $\pm$ was used. A complete description of the nomenclature is listed in Table I .

A " short prong " is defined as a prong less than 30 microns in length.

A " recoil " is defined as any prong less than 6 microns long.

An "evaporation " prong is defined as any stable prong which comes to rest within a field of view of the star (using 22 X 10 power magnification).

A " fast poton " is defined as any stable prong which is not defined as an " evaporation prong ".

TABLE I

SUMMARY OF NOMENCLATURE

Term	Description
$R\,\Sigma^+_p$	$\Sigma^+ \rightarrow P + \pi^o$ at rest
$F\,\Sigma^+_p$	$\Sigma^+ \rightarrow P + \pi^o$ in flight
$R\,\Sigma^+_\pi$	$\Sigma^+ \rightarrow N + \pi^+$ at rest
$F\,\Sigma^+_\pi$	$\Sigma^+ \rightarrow N + \pi^+$ in flight
$F\,\Sigma^-_\pi$	$\Sigma^- \rightarrow N + \pi^-$ in flight
$R\,\Sigma^-$	Σ^- recognizable capture star at rest.
$F\,\Xi^-_\pi$	$\Xi^- \rightarrow \Lambda^o + \pi^-$ in flight
$R\,\Xi^-_\pi$	Ξ^- recognizable capture star at rest
$F\,\Sigma^\pm$ inter	$\Sigma^\pm$ interaction in flight

C. Hyperon Identification

Because charged hyperons are singly charged and have mass only slightly greater than the protonic mass, identification by means on ionization or multiple scattering versus range is difficult. Identification of those hyperons which come to rest in the emulsion is based upon terminal behavior. Terminal behaviors for hyperons are listed in Table II. Kinematic analysis

was used to ascertain the decay mode and identity of the hyperons which decayed in flight.

1. Decays at Rest

To be classified a decay at rest , the hyperon track must appear, by ionization and scattering,to stop; and the secondary particle must have energy compatible with a decay at rest. Since negatively charged hyperons are attracted by the Coulomb field of the nucleus and form capture stars, all hyperons decaying at rest into a minimum were designated to be positive.

2. Decays in Flight

For decays in flight, identification was made by kinematic analysis using knowledge of the momentum of each particle involved and the space angle between them. These observable quantities were checked against standard identification curves for heavy mesons and hyperons /32/ . An assumption as to the identity of the particles was usually immediately determined to be consistent with the observed data by reference to the appropriate family of curves for the decay mode in question. If the decay mode was dynamically consistent using the observed values, it was so identified.

TABLE II

TERMINAL BEHAVIOR OF HYPERONS

Decay mode	Behavior
$R\Sigma^+_p$	decay at rest with a proton emitted with range about 1680 microns.
$R\Sigma^+_\pi$	decay at rest with pion of near minimum ionization and a residual range of about 9.16 centimeters.
$R\Sigma^-$	small capture star at rest (see Table III for criteria of recognizability).

TABLE III

SELECTION CRITERIA FOR $R\bar{\Sigma}$ /33/

Recognizable	3 or more prongs of any length
	2 prongs, each of which is greater than 5 microns in length
	1 prong greater than 200 microns in length
Non-recognizable	hook ending
	single electron emitted
	blob ending

D. Experimental Results

1. Emission of Charged Hyperons

Using the relative populations of K : π : μ in the beam as estimated by Alvarez et al /34/ and using analysis by Barkas et al /30/ the completely analyzed sample of 879 interactions contains 93% or 817 events due to K^- mesons. The numbers of hyperons observed does not change because of this correction since the production of hyperons by pions of this energy was neglegible.

The total number of charged Σ hyperons recognized in 817 events is 123. The observed events were:

$R\Sigma^+_p$ 5
$F\Sigma^+_p$ 21
$R\Sigma^+_\pi$ 11
$F\Sigma^+_\pi$ 5
$R\Sigma^-_\pi$ 21
$F\Sigma^-_\pi$ 10
$F\Sigma^\pm_\pi$ 35
$F\Sigma^\pm_\pi$ 15

The relative numbers of $R\Sigma^+_p$ and $R\Sigma^+_\pi$ indicate good efficiency for the detection of minimum tracks.

The above values were corrected for possible observati-

onal losses as indicated below :

a. $R\Sigma^-$ Correction

Using the ratio of $R\Sigma^-_{total}$ to the recognizable $R\Sigma^-$ as reported by Davis and Skjeggestad /35/ to correct for the non-recognizable $R\Sigma^-$ capture stars, it is found that a correction factor of 3.61 must be used.

b. $R\Sigma^+$ Correction

All decays of this group should be detected and no correction is required or used.

c. $F\Sigma^+_p$ Correction

These events can simulate scatters if the proton is emitted with velocity in the laboratory system which is comparable to the hyperon velocity in the laboratory system. To minimize this bias , all scanners were instructed to record every scatter as a possible Σ^+ decay in flight by the proton mode. The events were later subjected to kinematic analysis, and several decays were found which simulated scatters. Based upon the known branching ratio for Σ^+ decay and the assumption that the decay is symmetric fore and aft in the center of mass system, the estimate of the corrected number of $F\Sigma^+_p$ decays becomes 26.

d. $F\Sigma^\pm_\pi$ Correction

No correction was made to the number of $\Sigma^\pm$ hyperons which were observed to decay in flight by the pion mode.

e. $F\Sigma^\pm_{inter}$ Correction

Interactions must be corrected by a factor of 1.1 to estimate the actual number using the same reasoning as Garelli et al /36/.

f. Charge Determination

Since the ratio of Σ^+_p to Σ^+_π should be unity and since the number of $\Sigma^\mp_p$ is known , the number of Σ^+_π which are in the sample of $\Sigma^\pm_\pi$ can be calculated. All remaining $\Sigma^\pm_\pi$ must be classified as

being negatively charged.

Using the observed values and the above corrections, the estimated Σ hyperon production was 185 distributed as follows:

$R\Sigma^{+}_{p}$ 5

$F\Sigma^{+}_{p}$ 26

$R\Sigma^{+}_{\pi}$ 11

$F\Sigma^{+}_{\pi}$ 20

$R\Sigma^{-}$ 76

$F\Sigma^{-}_{\pi}$ 30

$F\Sigma^{\pm}_{inter}$ 17

Estimated Σ hyperon production by 1.15 Bev/c K^- meson interactions was:

$\Sigma^{\pm}$ 21%

Σ^{+} 8%

Σ^{-} 13%

The ratio of negatively charged hyperons to positively charged was 1.7 . This value is in agreement with the results of a rough analysis of the reactions by which hyperons are produced and the reaction cross-sections. This value is in disagreement with that reported by Garelli et al /36/ which was 2.9 .

2. Energy and Angular Distributions of Charged Σ Hyperons

The energy distribution of the charged hyperons in the laboratory system is shown in Figure 5. The energy spectrum contains only the observed events, 123 , and no attempt has been made to correct for observational losses, which are small except in the case of $R\Sigma^{-}$ particles. A strong tendency toward low kinetic energy for the emitted hyperons indicates hyperon emission backward in the center of mass system with some possibility of inelastic scattering of the hyperon within the nucleus. Correction for the unobserved $R\Sigma^{-}$ events strengthens this conclusion.

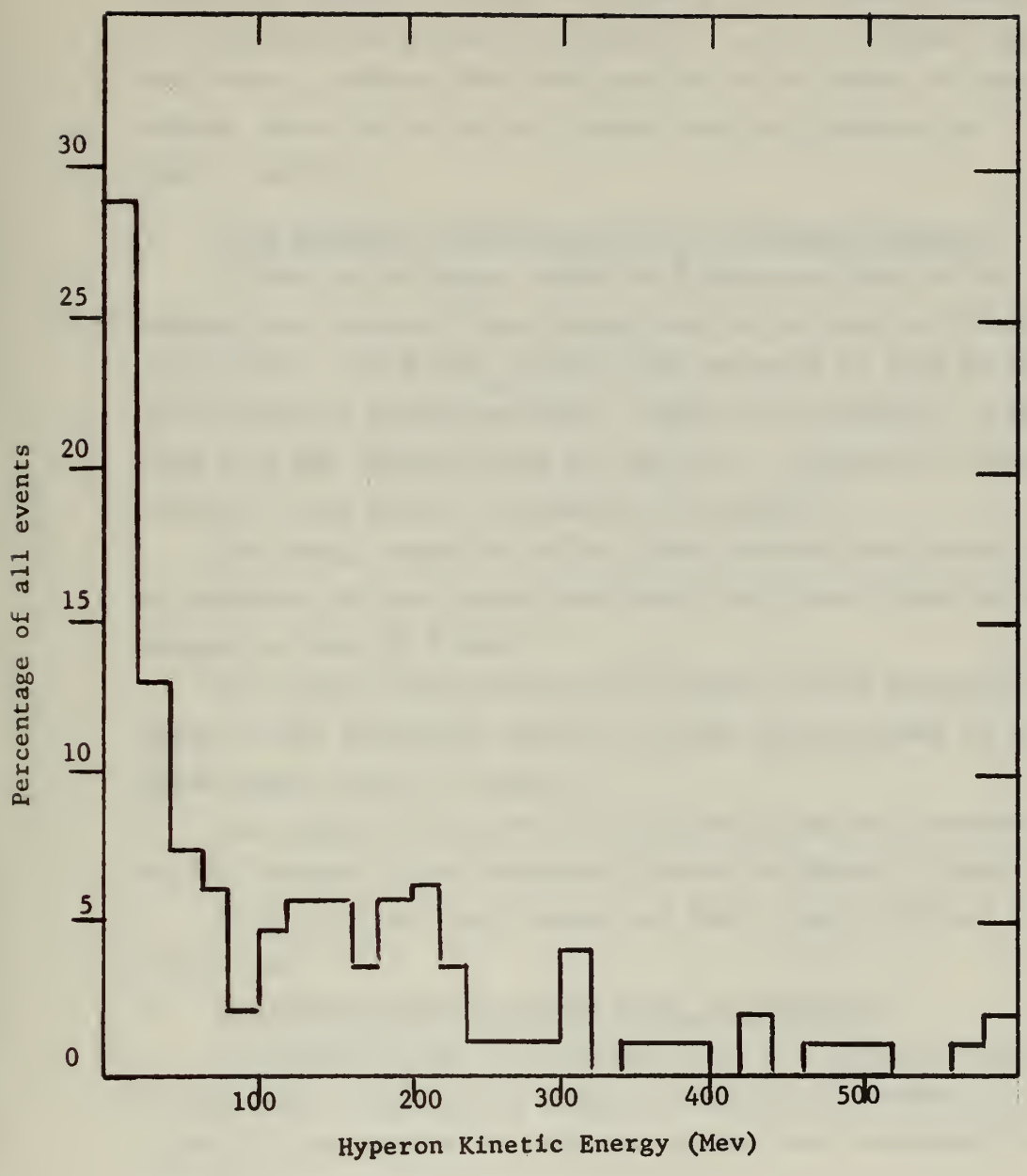

Fig. 5 Kinetic energy distribution of 123 Σ hyperons produced in 1.15 Bev/c interactions

The angular distribution of charged hyperons in the laboratory system is shown in Figure 6 . The forward peaking is expected from production kinematics , and no attempt has been made to reduce this distribution to the center of mass system, where it is now well known that the hyperons are peaked backward.

3. Pion Emission from Parent Stars of Charged Hyperons

In 54% of the parent stars of Σ hyperons there is no charged pion emitted, one charged pion is emitted in 34% of the events , and double charged pion emission is seen in 12% of all hyperon producing events. There is no instance in which more than two charged pions are emitted , although the production of four pions is energetically possible.

The energy spectrum of the pions emitted from parent stars of hyperons and the energy spectrum of all pions from the entire sample is shown in Figure 7 .

The angular distribution with resect to the incoming K^- meson in the laboratory system is shown for all pions of hyperon parent stars in Figure 8.

The angular distribution of emitted pions with respect to the hyperon in the laboratory system is shown in Figure 9.

No particular significance has been sought in these distributions.

4. Characteristics of Parent Stars of Hyperons

An investigation was conducted into the characteristics of the parent stars which exhibit recognizable hyperon production in an attempt to correlate parent star characteritics with hyperon production.

a. Prong Distribution

A histogram of the percentage of events as a function of the number of prongs per event for both all events of the sample and for those which produce recognizable hyperons is shown in Figure 10 . From examination of this plot 34% of all events producing a hyperon have 9 or more prongs, which is characteristic of heavy nuclei (Ag or Br), while

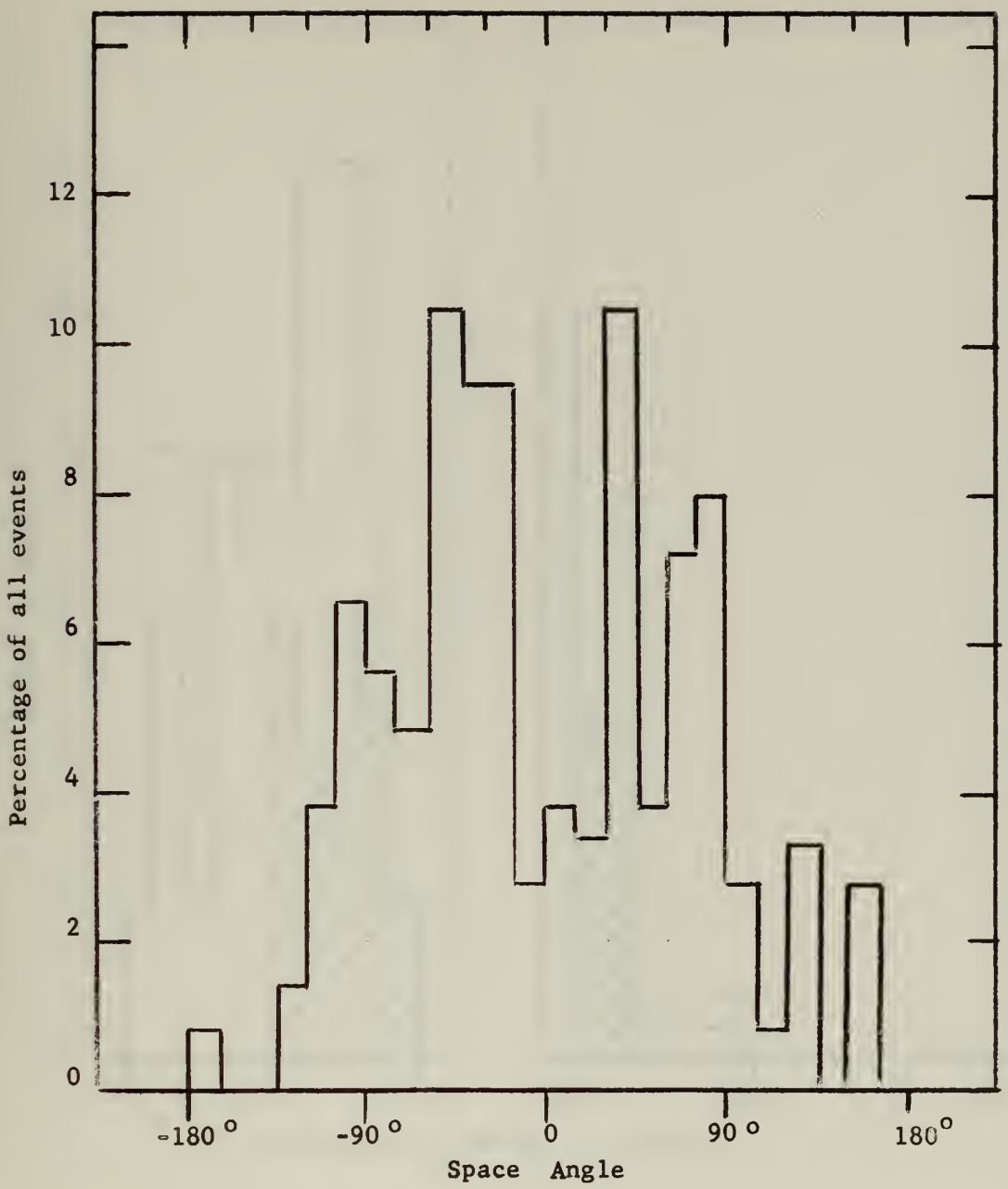

Fig. 6 Space angle distribution in the laboratory system of the emitted hyperon in 123 events with respect to the incoming K^- meson.

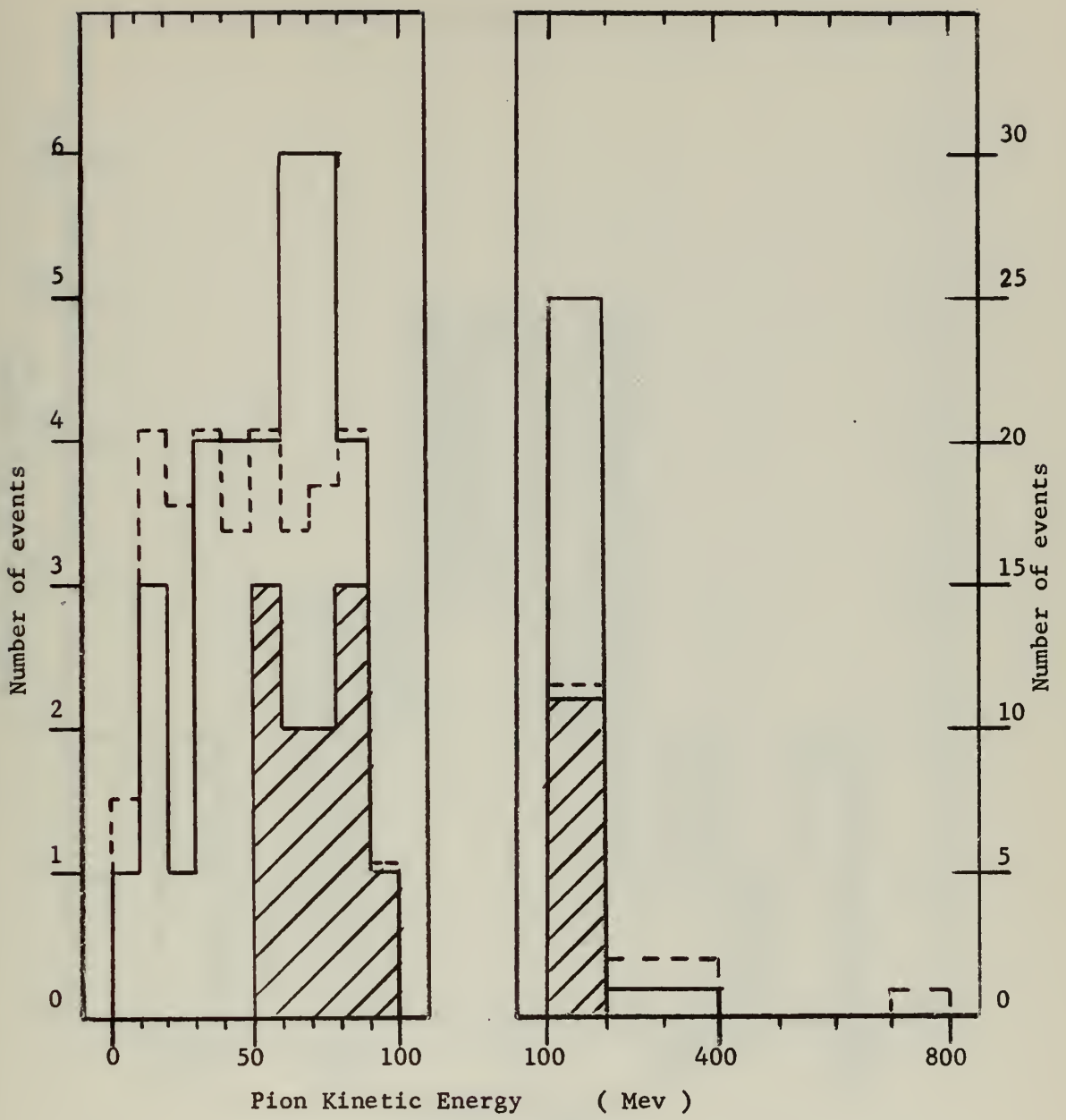

Fig. 7 Pion kinetic energy of 49 parent stars of hyperons, the cross-hatched portion indicating events in which two pions were observed. The dashed outline indicates the distribution of the entire sample normalized to 49 events.

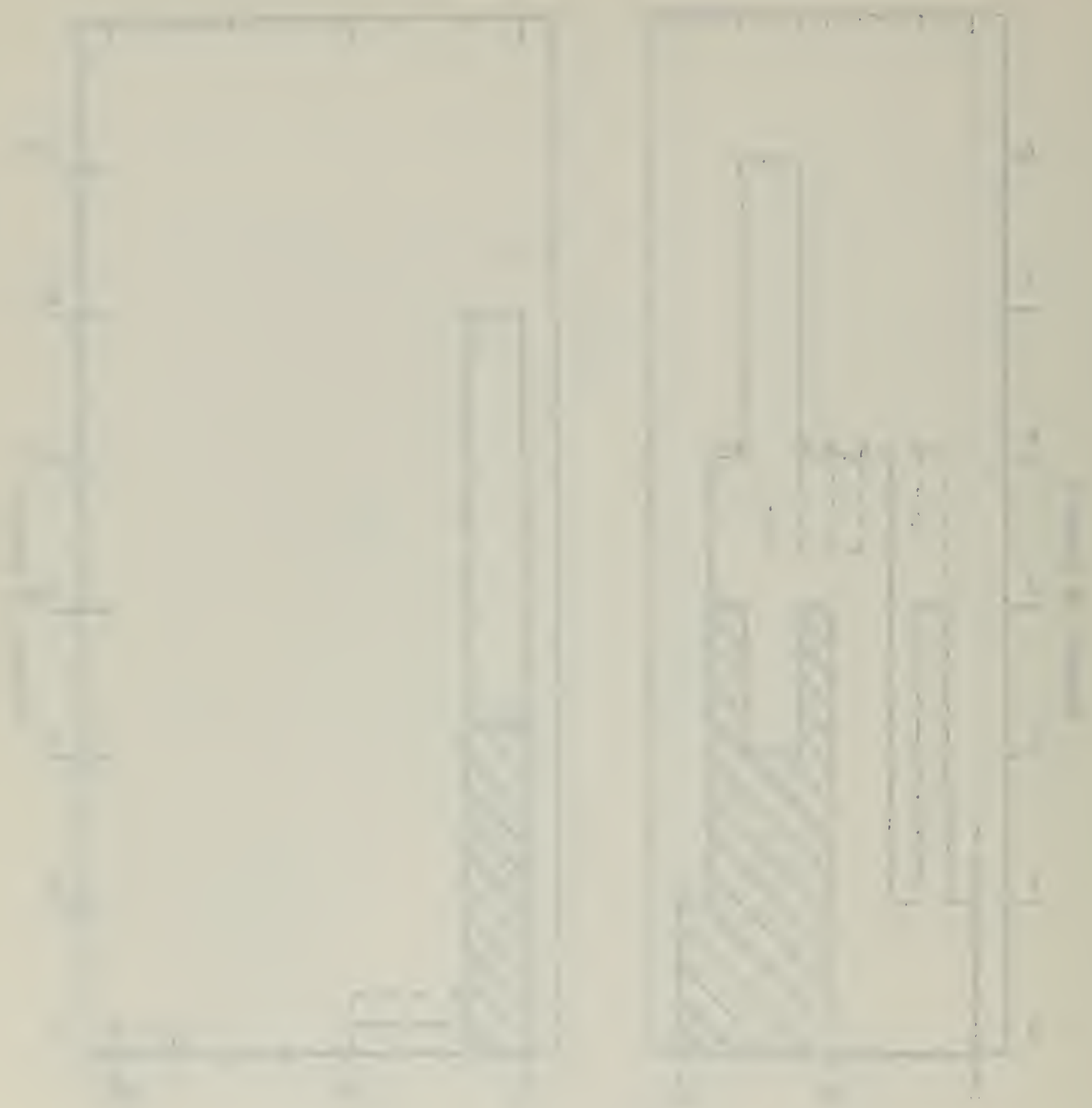

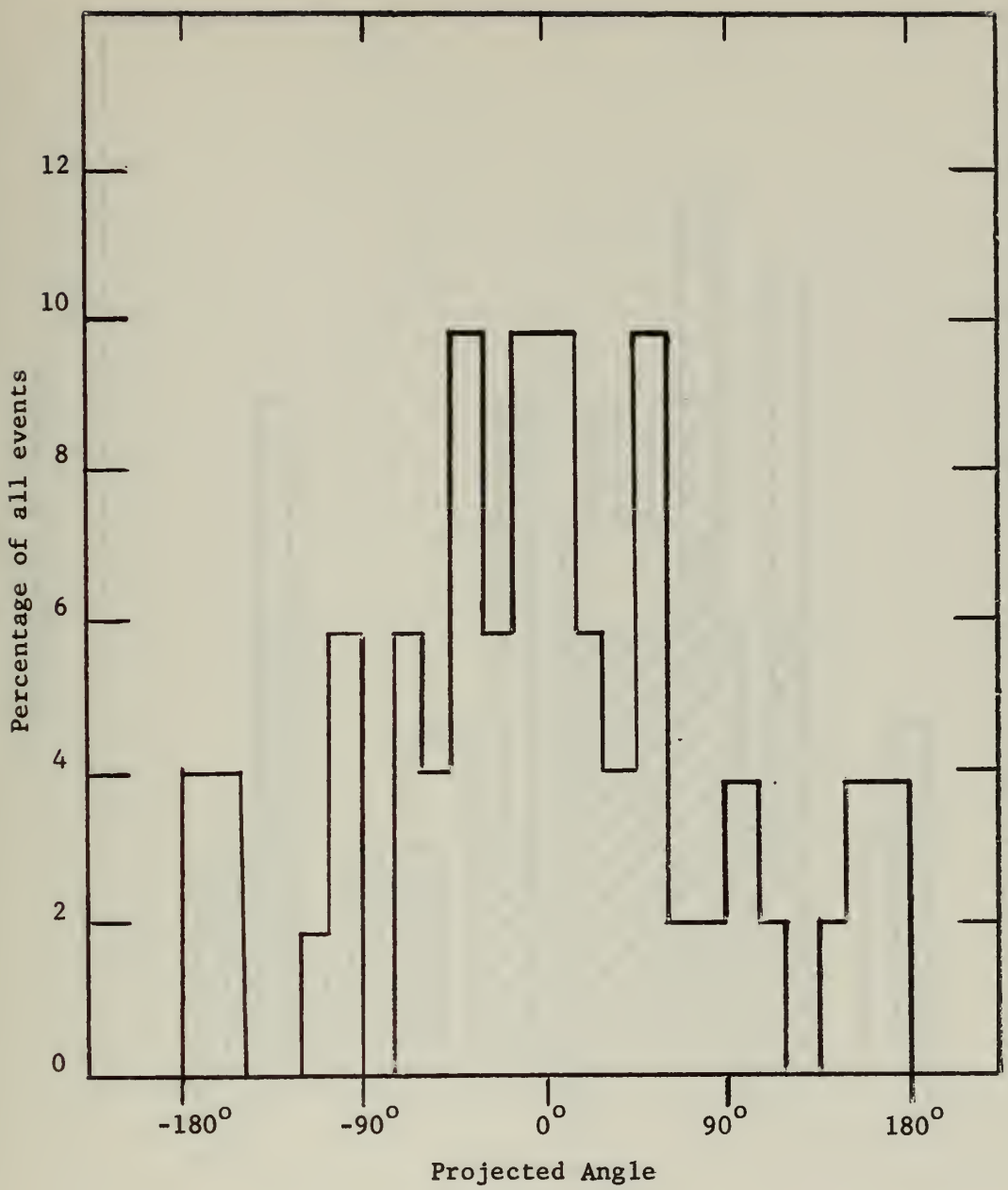

Fig. 8 Angular distribution (projected) in the laboratory system for pions emitted from hyperon parent stars for 49 events

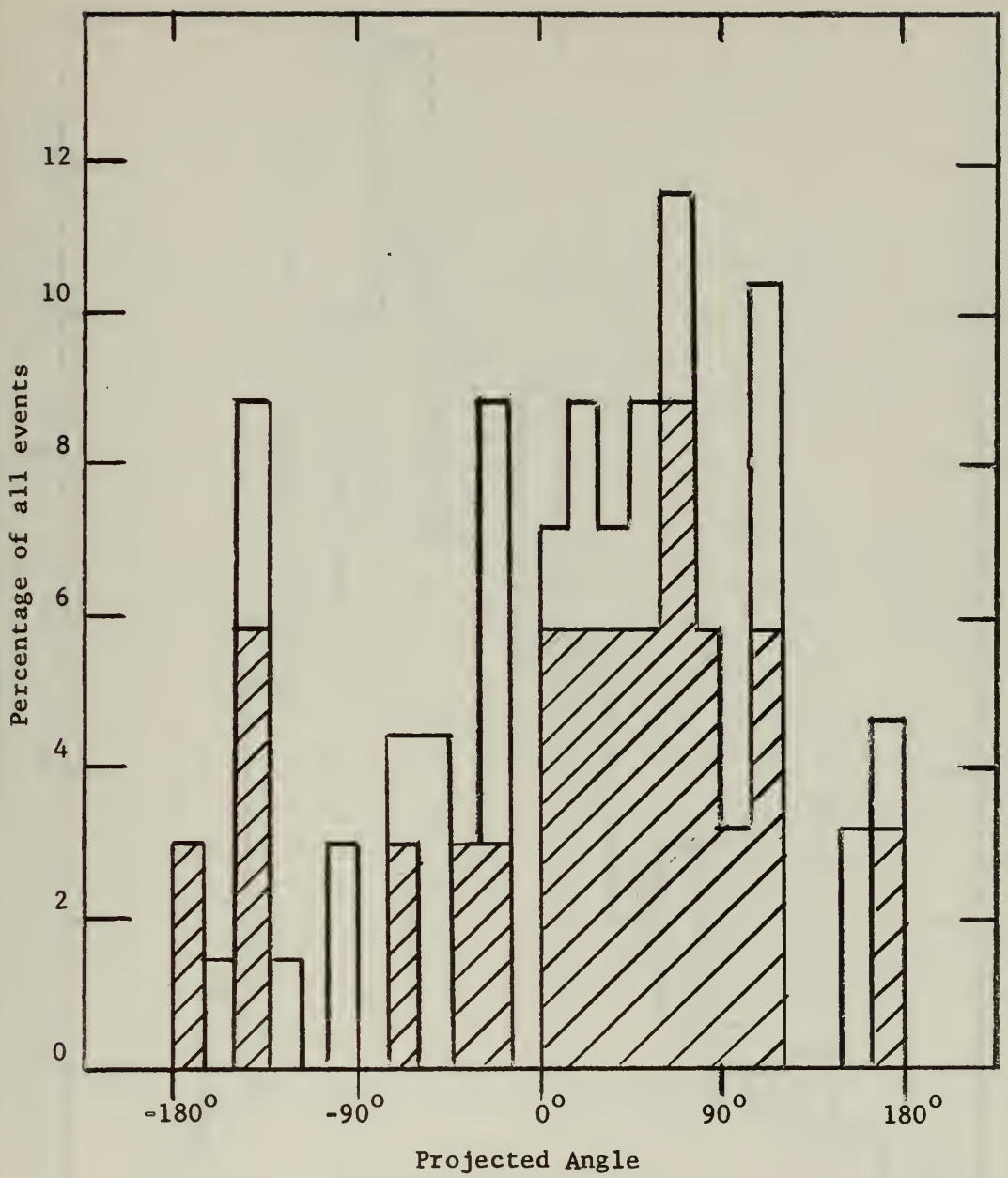

Fig. 9 Projected angular distribution of pions with respect to the emitted hyperon in the laboratory system. The cross-hatched area indicating pions from events with two pions.

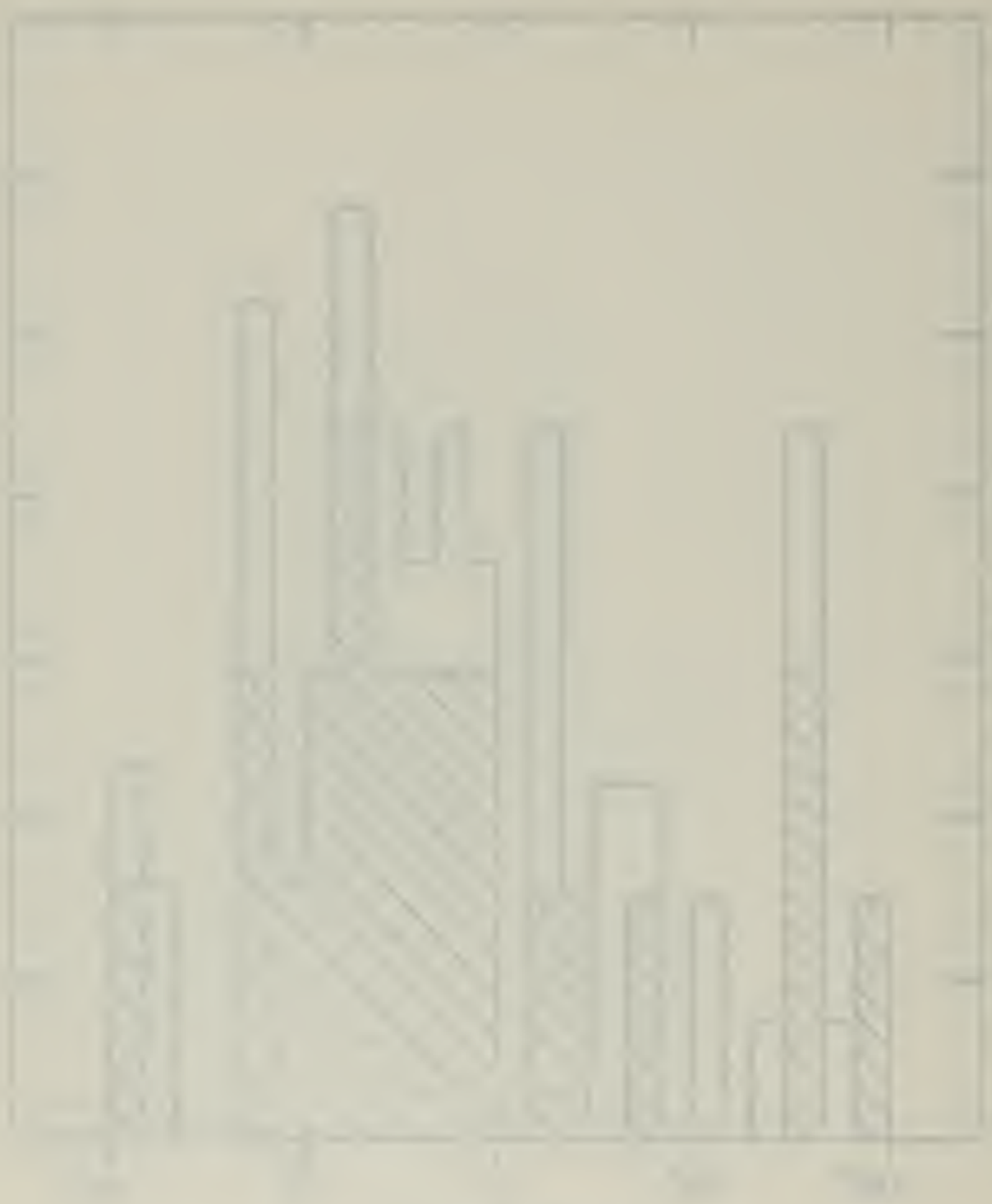

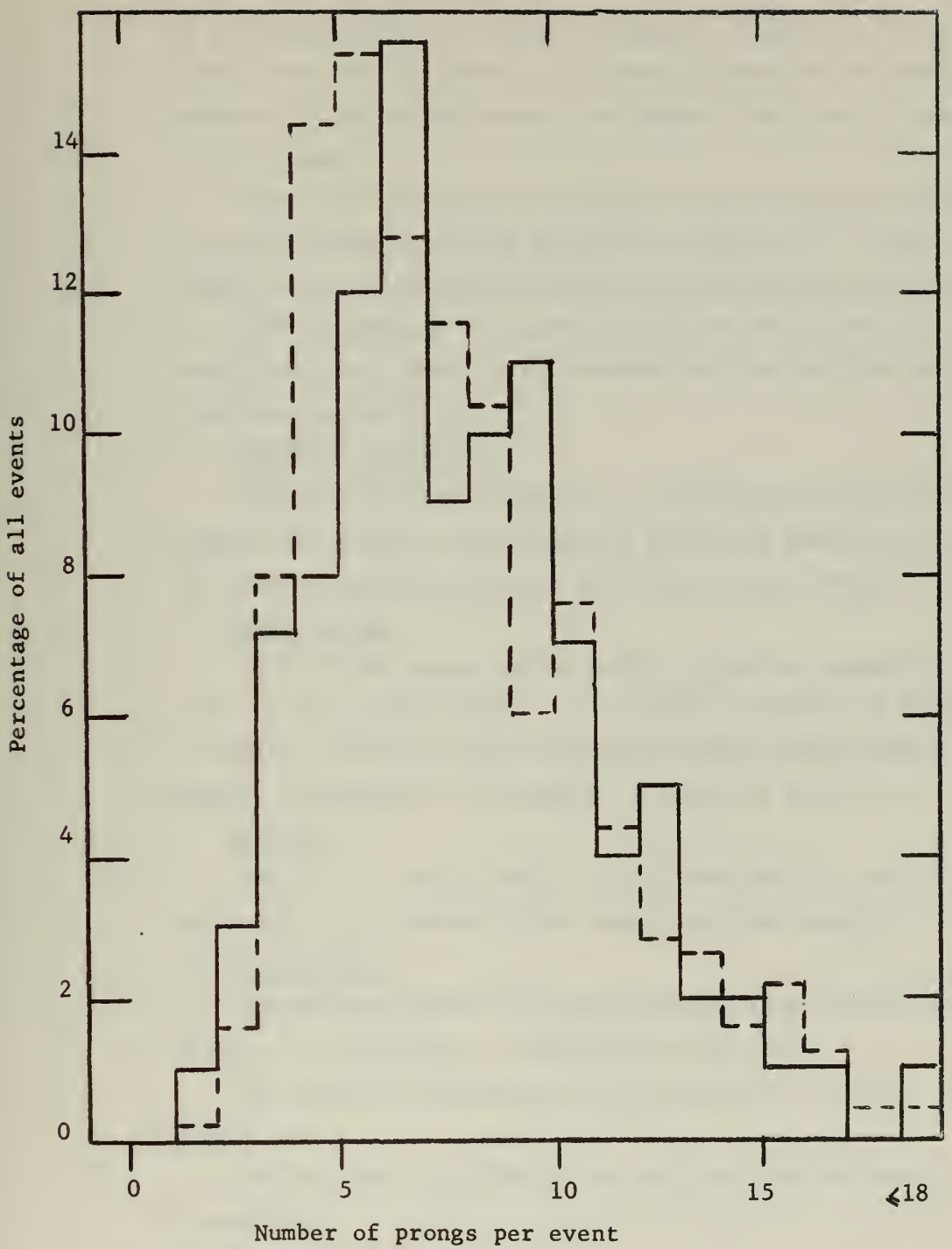

Fig. 10 Prong distribution of parent stars of hyperons with the dashed outline indicating the distribution for all events of the sample.

only 22% of all events display 9 or more prongs. This implies a slightly greater tendency for hyperon production by K^- interactions with heavy elements, however it is concluded that the frequency of hyperon production by heavy elements is not significantly different from that by the light elements.

Since all the interactions were located by area-scanning no 0 prong stars are plotted in Figure 10. A bias toward more easily noticed events was expected, but from the small percentage of 2 and 3 prong events it was assumed that the 0 and 1 prong events are rare and the scanning bias neglegible.

b. Electrons and Blobs

Within statistical limits , no difference was noted between the relative ocurrence of electrons and blobs on the hyperon parent stars and all stars of the sample.

c. Short Prongs

15 % of all events which exhibit hyperon production also contain short prongs, i.e. prongs less than 30 microns in length. 33% of all stars in the sample exhibit short prongs. The number distribution is shown in Figure 11 .

d. Recoils

33% of all parent stars of hyperons exhibit recoils, while 35% of all stars of the sample exhibit recoils.

e. Fast Protons

Parent stars which produce hyperons also produce one or more " fast protons " with 93% probability.

The number distribution of fast protons is shown in Figure 13.

The angular distribution of fast protons is shown in Figure 14.

f. Evaporation Prongs

The evaporation prongs from parent stars emitting charged hyperons is approximately isotropic in the laboratory system indicating neglegible motion of the nucleus during the interaction and immediately afterward. The distribution

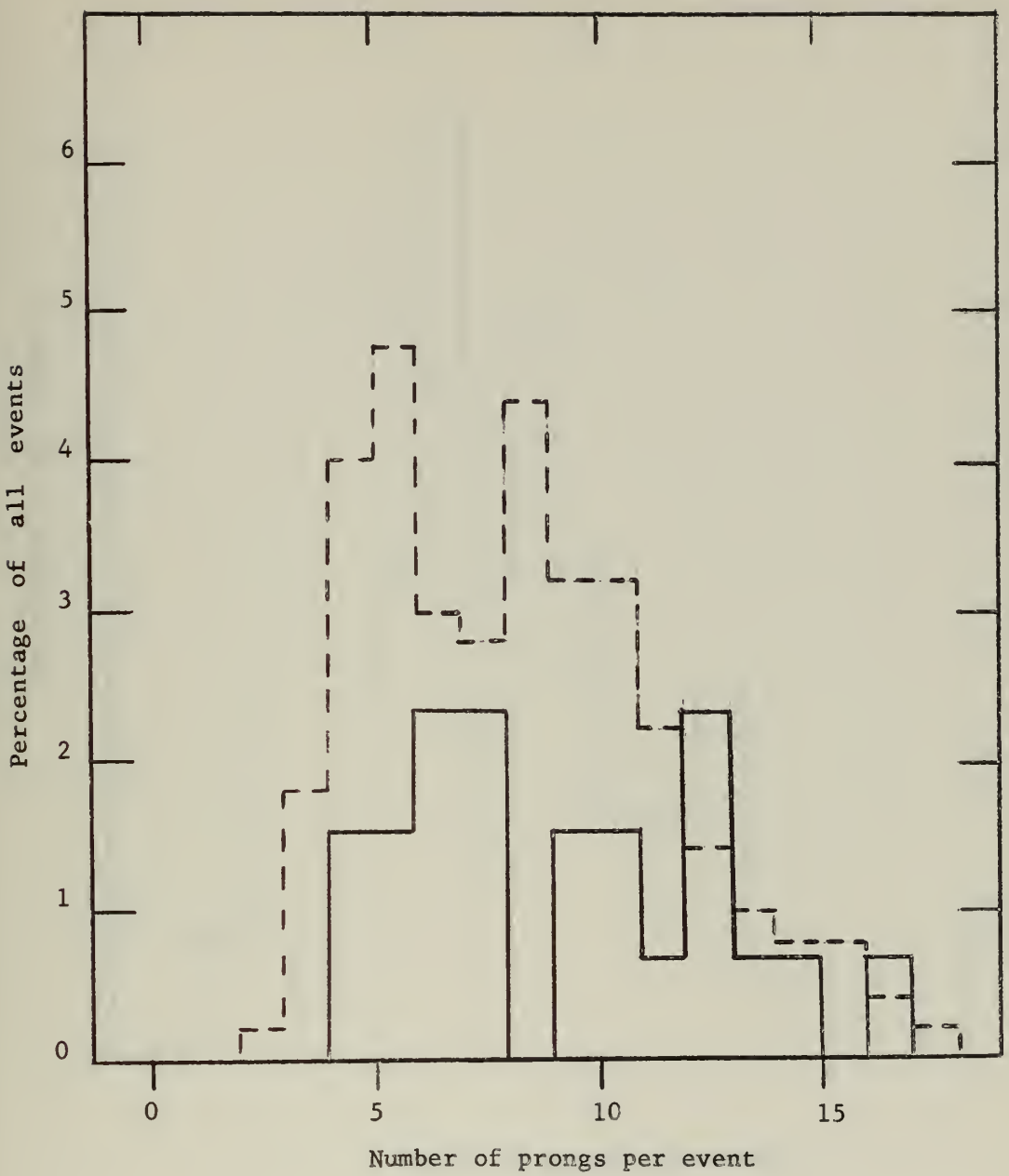

Fig. 11 Short prong distribution of hyperon parent stars, 123 events. Dashed outline indicates the distribution of short prongs for the entire sample.

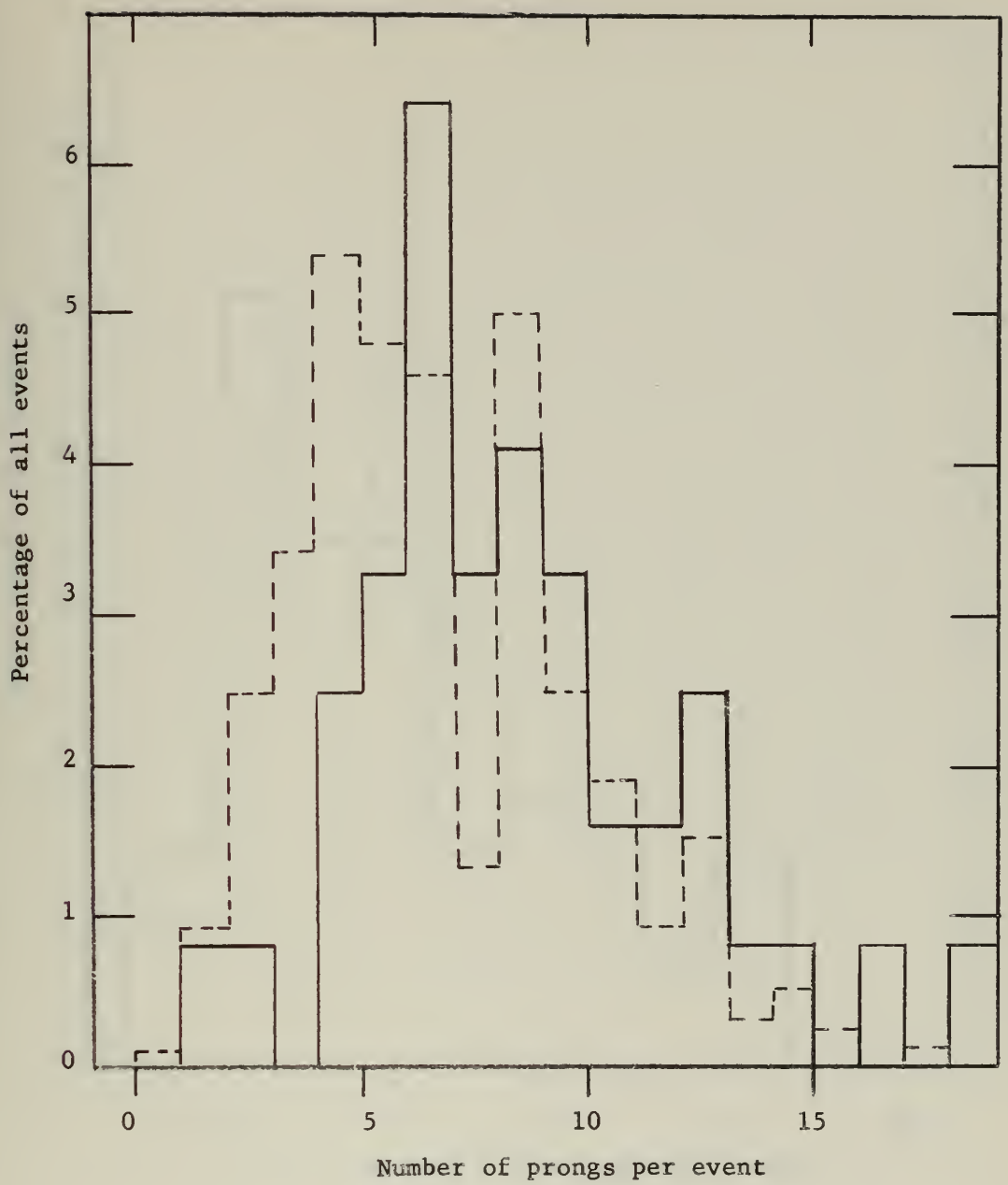

Fig. 12 Recoil prong distribution of hyperon parent stars, 123 events. Dashed outline indicates the distribution of recoil prongs for the entire sample.

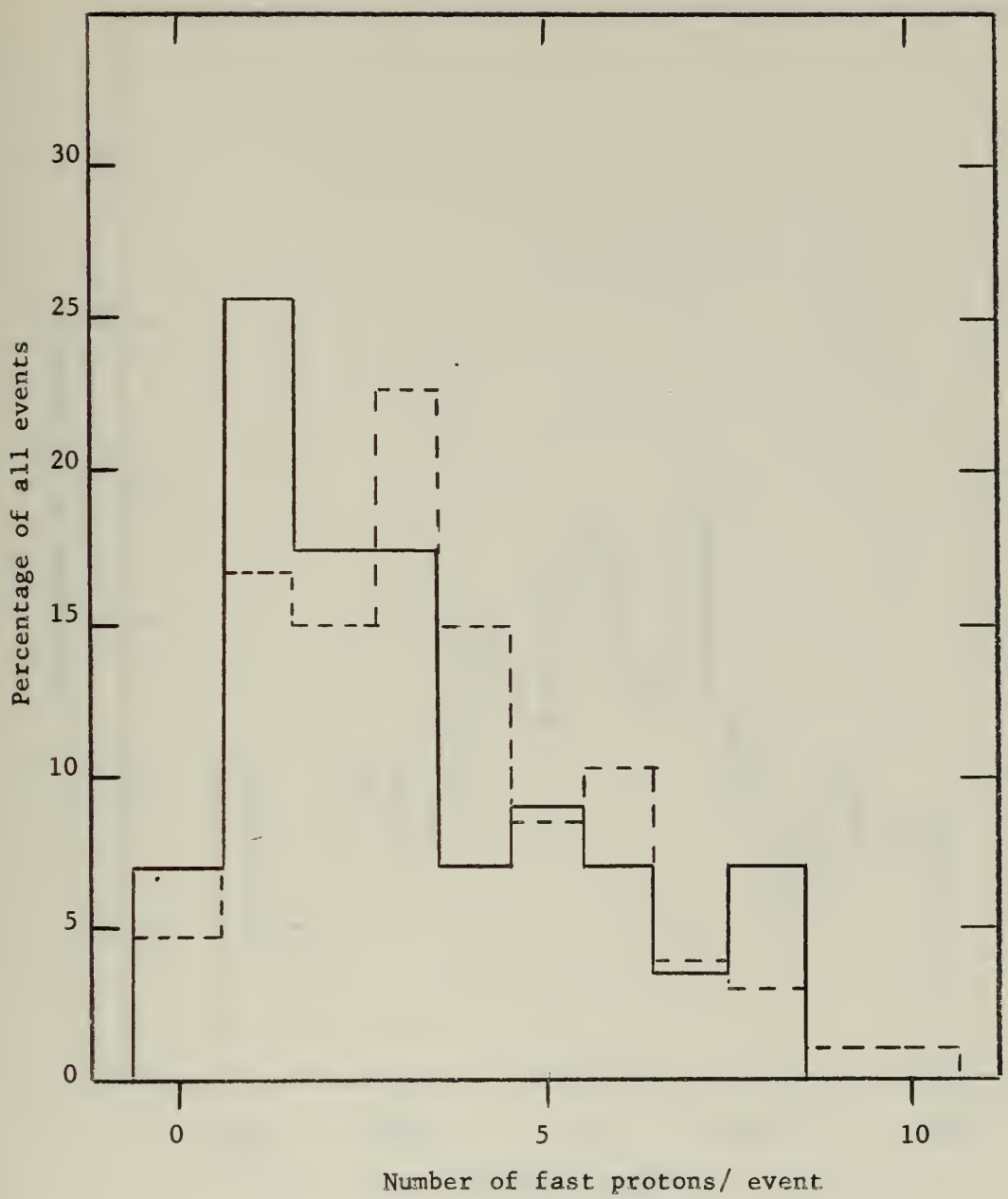

Fig. 13 Number distribution of fast protons from hyperon parent stars, 123 events. Dashed outline indicates the distribution for the entire sample.

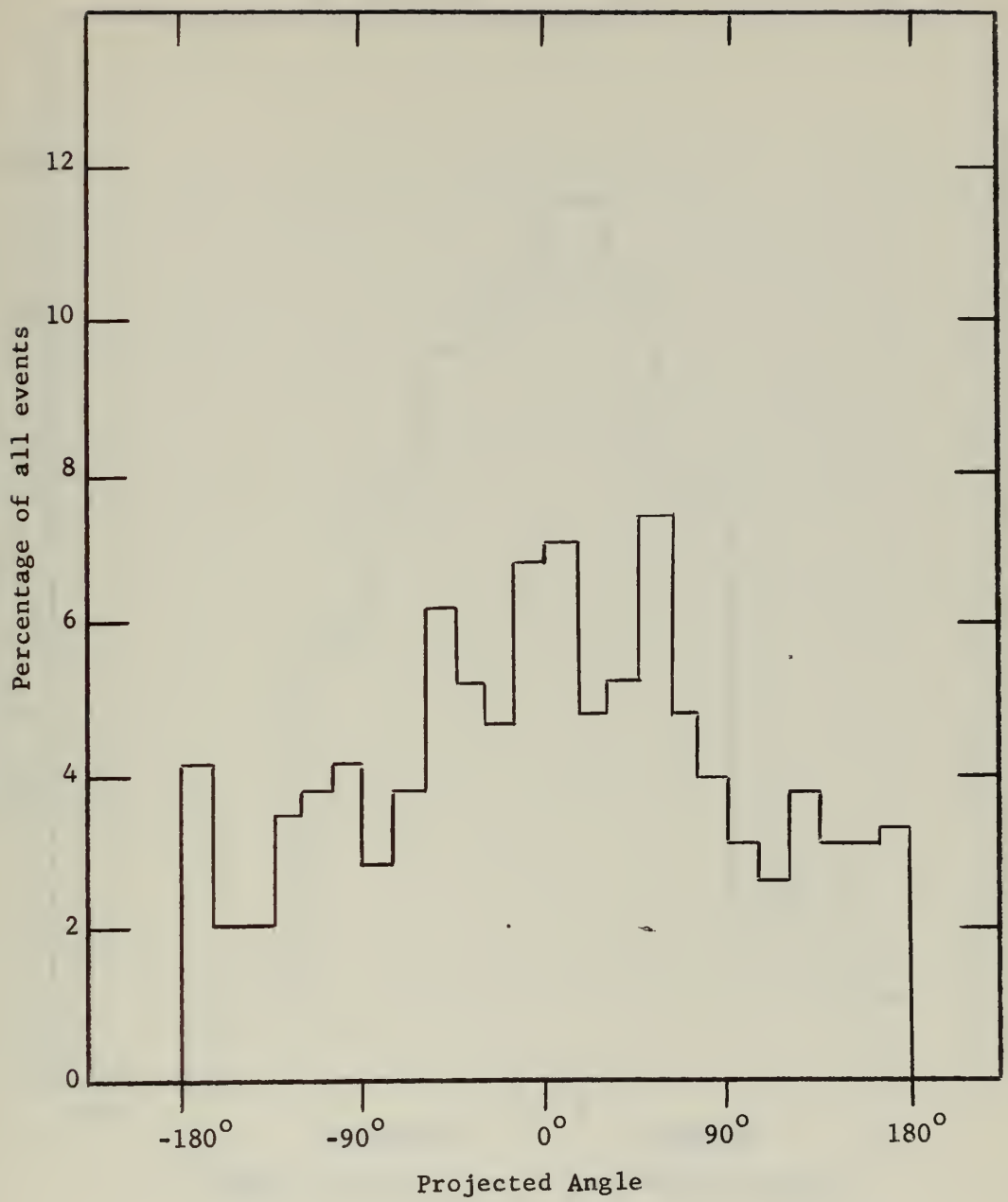

Fig. 14 Projected angular distribution in the laboratory system of all fast protons from hyperon parent stars.

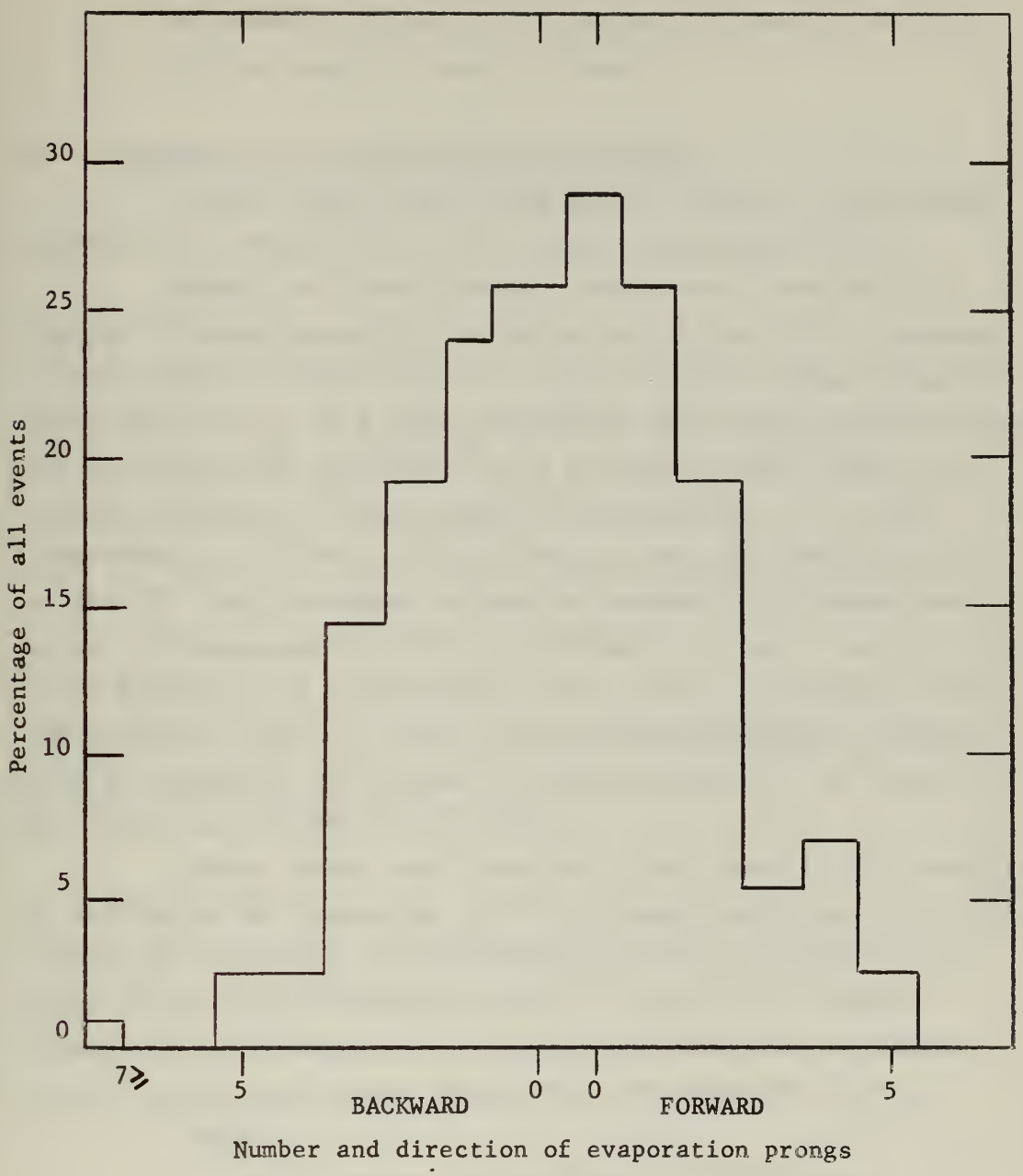

Fig. 15 Distribution of evaporation prongs with direction of emission for hyperon parent stars , 123 events.

of prongs for all events of the sample is the same as that for the hyperon events within statistical limits. The number distribution of evaporation prongs from the hyperon events is shown in Figure 15 .

E. Production of 2 or more Strange Particles

In 817 interactions there were no definite events which exhibited the production of two or more strange particles.

During the investigation 9 events were found which by virtue of kinematic analysis satisfied all criteria for a Cascade hyperon decay in flight into a π^- . This was done using ionization measurements only. In 6 cases the momenta and space angle were such as not to satisfy the conditions for a Σ^- hyperon decay within one standard deviation. In all cases the pion emitted in the decay interacted or left the stack and hence no definite identification of the Ξ^- could be made. The rate of possible Ξ^- production is not in disagreement with that reported by M. Baldo Ceolin et al /37/. However it is significant to note that in all cases in which the pion was brought to rest in the emulsion and definite identification possible, the kinematic identification of a Σ^- via the pion mode was verified to be correct.

Three events were found which could possibly be identified as indicating the production of three strange particles. In all the events the uncertainty of identification arising because of the decay of one of the hyperons by the $\Sigma^+ \longrightarrow P + \pi^o$ mode in flight in such a manner as to also fit the kinematics of proton scatter within statistics. These events are described below.

EVENT 1.

A K^- interaction yielding 5 visible prongs:

3 stable prongs with ranges 32.5, 40.1, and 97.0 millimeters.

1 $\Sigma^{\pm}$ hyperon which formed a star in flight after 7.12 millimeters.

1 Σ^+ hyperon which decayed by the proton mode after 58.0 millimeters. This could also be a proton scatter .

EVENT 2.

A K^- interaction yielding 4 prongs :

2 stable prongs with ranges 35, 500 microns

1 Σ^- hyperon which forms a two prong capture star at rest after 2.06 millimeters

1 Σ^+ hyperon which decays in flight via the proton mode after 2.1 millimeters. This also fits the kinematics of a proton scatter.

EVENT 3.

A K^- interaction yielding 7 visible prongs:

5 stable prongs with ranges 150, 180, and 780 microns and 6.6 , and 1.4 millimeters.

1 Σ^+ hyperon which decays at rest via the pion mode after 3.7 millimeters.

1 Σ^+ hyperon which decays in flight by the proton mode after 17.6 millimeters. This also could be a proton scatter.

One event was found in which a $\Sigma^{\pm}$ hyperon was produced by a re-emitted K^- particle which formed a star in flight after 141.5 millimeters. The hyperon decayed via the pion mode after 9.13 millimeters.

F. Conclusions

879 events have been completely analyzed; correcting for 7 % contamination the number of K^- interactions was calculated to be 817. It was found :

Percentage of charged hyperons emitted..... 21%

Percentage of Σ^+ hyperons emitted..... 8%

Percentage of Σ^- hyperons emitted..... 13%

The energy distribution of the charged hyperons in the laboratoy system is peaked toward low energies and is probably due to backward emission of hyperons in the center of mass system.

Charged pion production in hyperon parent stars is found in 34% of the interactions and double pion production is noticed in 12% of the hyperon producing events.

No definite Ξ^- particles noted, but 9 possible cases were found.

No definite examples of double hyperon production were found but 3 possible cases were noticed.

IV

INTERACTIONS IN FLIGHT

At the present time, no published work has been devoted completely to the study and analysis of stars in flight and disappearances in flight. In only a few isolated cases in the literature have they been mentioned, and then only by a reference to the fact that they were observed during the analyses of other interactions.

A star in flight occurs when a particle emitted from a K^--star, created by the beam, undergoes an interaction with an emulsion nucleus. This interaction occurs before the particle decays or comes to rest. The star in flight is characterized by visible prongs of varying energy.

A disappearance in flight is an interaction in flight suffered by a particle emitted from a K^--star, in which there are no visible prongs.

In this discussion, stars in flight and disappearances in flight will be dealt with utilizing the results of the analysis of all these interactions recorded from the 1240 K^--stars in the B-stack.

A. The Role Of Stars In Flight And Disappearances In Flight

The K^--meson is known to have strangeness -1. In the K^--interactions studied in this emulsion stack, due to conservation of strangeness in the strong interactions, strangeness -1 must be accounted for coming out of the interactions.

As part of our larger program to determine how often charged strange particles are emitted from 1.15 Bev/c K^--meson interactions, we have tried to identify the particles which form stars in flight (SIF) or disappearances in flight (DIF).

We assume that all DIFs are negative particle interactions. This assumption is supported by the observed fact that π^+-mesons and protons rarely, if ever, are responsible for such events, while π^--mesons and K^--mesons frequently are.

Hence, we assume that DIFs are K^-, π^-, Σ^-, or Ξ^- interactions. Each event has been inspected carefully to eliminate the possibility that it is a decay with a minimum secondary.

Considering the stars in flight, these can be caused by K^--mesons, protons, $\Sigma^{\pm}$ hyperons, Ξ^- hyperons, or π^+ and π^- mesons. Therefore, the careful analysis of SIF events separates π, K, and Baryonic mass particles. The separation of protons from hyperons is difficult and can be done with certainty in a few cases. The sections following describe the techniques and methods used to accomplish the objectives outlined above, together with the results of the work and conclusions that were drawn.

B. Measurement Techniques

1. Reticle Calibration

The personal calibration of the reticle to be used in high magnification grain counting was accomplished using standard calibration techniques. The reticle length was determined to be 112.81 $\pm$ .04 microns.

2. Variation of B with Pellicle

The variation of blob-density, blobs per 100 microns, between plates in the emulsion stack and also from top to bottom in a single pellicle was of prime importance, because of the necessity of accurate grain counting for determination of particle velocities. Plates 84 through 92 (those plates in which are located the 1240 stars under study) were searched and flat tracks (zero dip angle) of incoming beam particles were blob counted. This determined the standard minimum tracks for each plate. In each plate, tracks in the upper, middle, and lower third were selected. It was found that the blob density from top to bottom in each plate was, within statistical limits, constant. However, there is a definite blob density change from plate to plate, up to as much as 1.5 blobs/100 microns ($\pm$5.7 %), and so each plate was calibrated against a standard, plate B-89.

3. The B vs. β Curve

It was necessary to construct several empirical curves, the first of which was blob density (B) vs. β (v/c). Accordingly, a number of flat π tracks, flat fast proton tracks, and flat K^- tracks emerging from beam K^--stars were followed and their ranges

measured to within ± 2%. At several points along the track blob counts were made of 400 blobs (5 %) statistics. This gave a point on the B vs.β curve, independent of the particle involved. These data are shown in Fig. 16.

4. Dip Angle

The dip angles of all tracks forming SIF or DIF events were measured. The technique used was as described in ref. /38/, pages 89-90.

5. Dip Angle Correction

Since very few of the tracks of interest that were to be blob counted were flat, it was necessary to next make the calculations and curves needed to convert the blob density of a dipping track, B_δ , to its equivalent flat track blob density, B, in order to use the B vs. β curve.

From the theory presented in ref./39/, and from techniques in ref./40/, the curves were developed and procedures used for determining B from B_δ , as follows.

If "a" is the mean distance between centers of just resolvable grains, it is known that $B=ge^{-ga}$ where g is grain density /38/. By taking $\frac{\partial B}{\partial g} = 0$, B has a maximum value Bm at g=1/a . Thus "a" can be found for any observer and optical system by knowing the value of Bm. From Fig. 16, Bm was determined to be .599 blobs/100 microns.

So, $.599=1/ae^{-1} = 1/ea$. Therefore, a= .614 microns for the author.

From ref./39/ and /40/ :

I). $B=ge^{-ga}$, and

II). $B_\delta = g a \sec\delta\, e^{-ag\sec\delta}$

From ref./24/, Fig. 19, a universal plot was made of equation (II) above. Converting this to the specific case a=0.614, Fig. 17 was determined, plotting B_δ vs. g sec δ . The dip angle δ is that angle in the unprocessed emulsion, and B_δ is the blob density, at the angle δ, in processed emulsion.

From equations (I) and (II) above,

$$\frac{B}{B_\delta} = \frac{ge^{-ga}}{g\sec\delta\, e^{-ag\sec\delta}}$$

III). $$\frac{B}{B_\delta} = \frac{1}{\sec\delta}\, e^{+ag(\sec\delta - 1)}$$

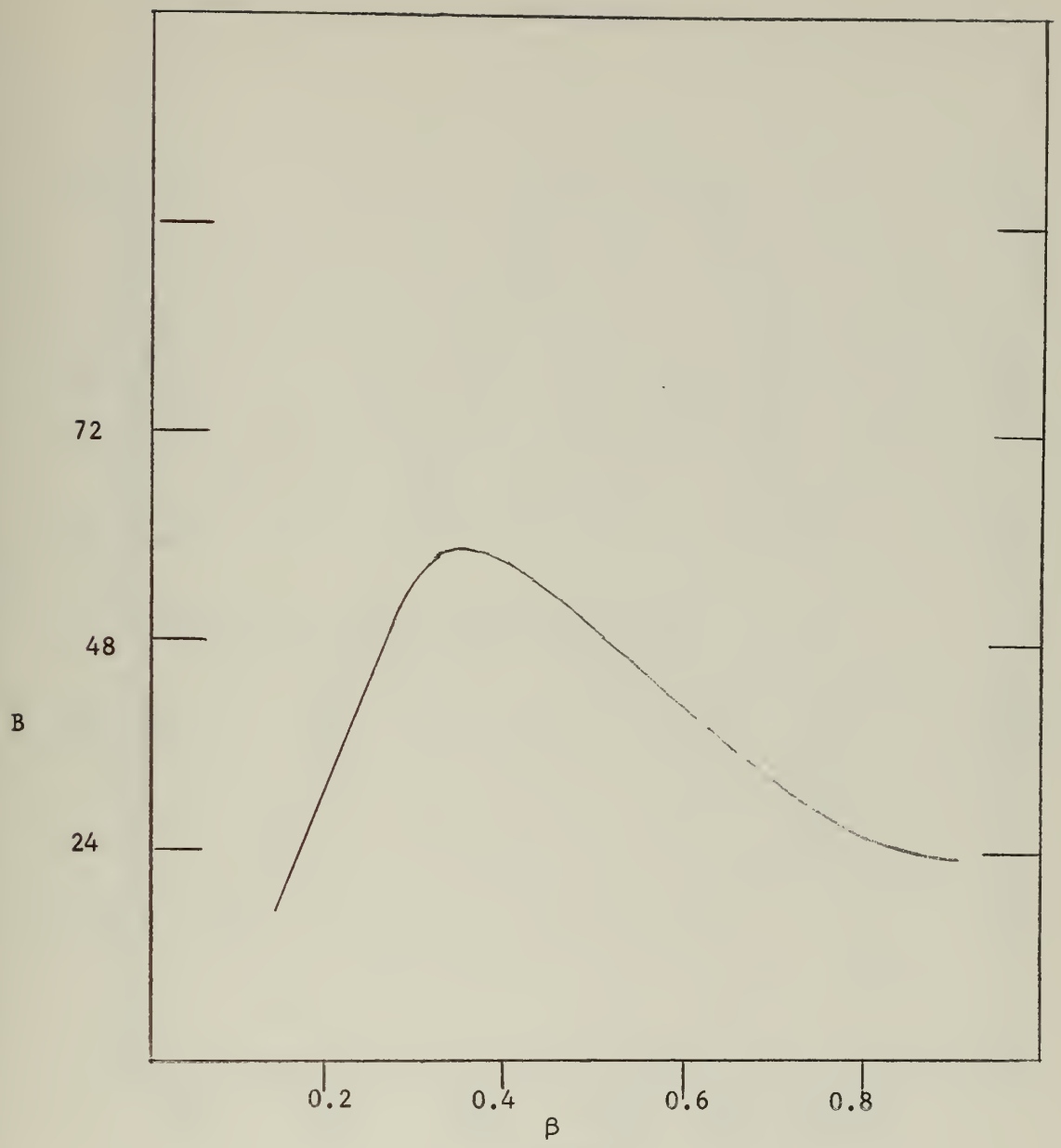

Fig. 16
Blob density (B) in blobs/100 microns vs. β (v/c)

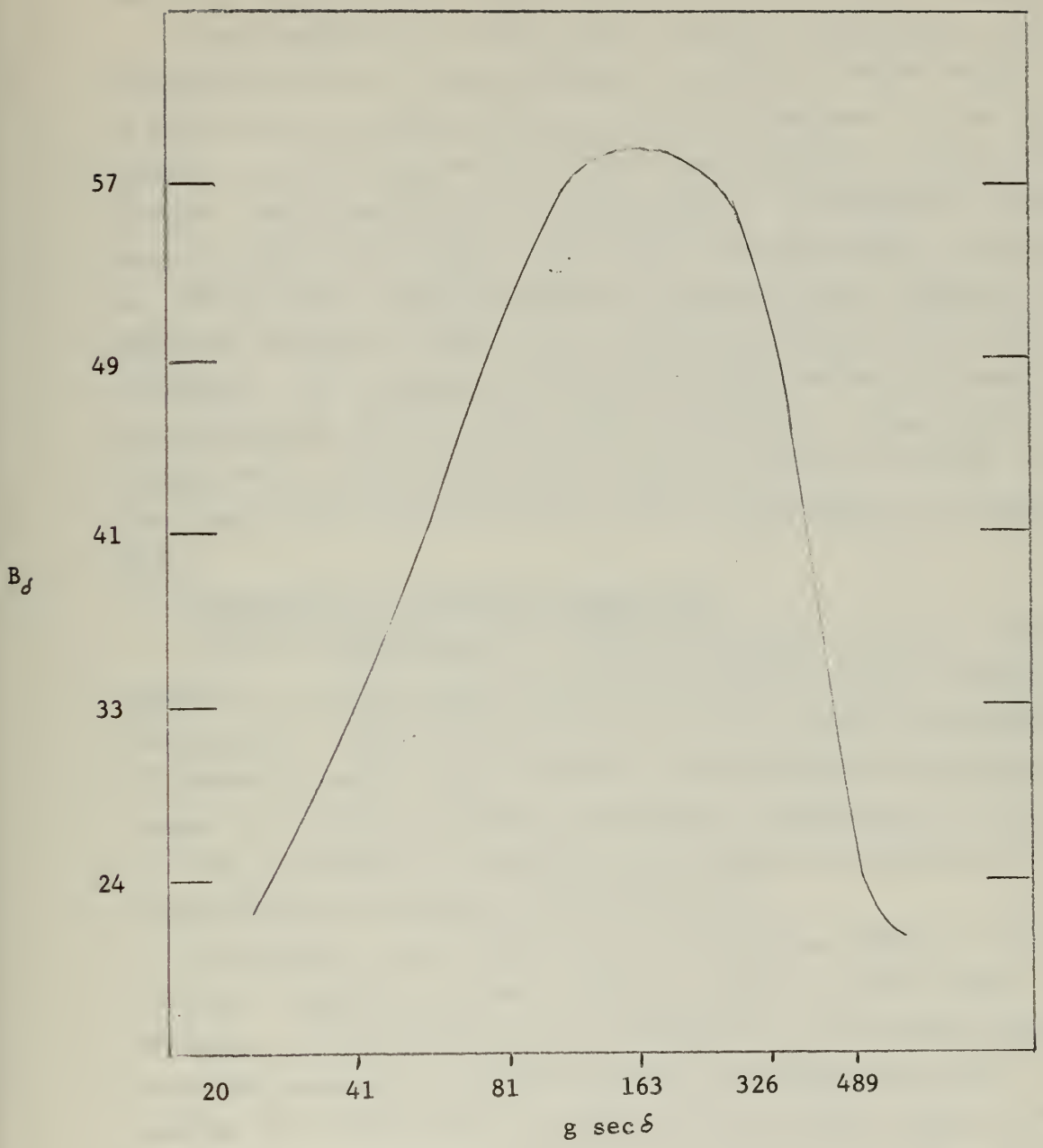

Fig. 17 B_δ in blobs/100 microns vs. g sec δ

From equation (III) a family of curves was plotted in Fig.18, plotting B/B_δ vs ag for values of δ of 0°, 10°, 20°, 30°, and 40°.

The procedure is to enter Fig.17 with B_δ, which gives g secδ. Although the curve is double-valued, the choice of which value of g secδ to use was usually obvious from the appearance of the track. Values of g secδ greater than about 150 correspond to nearly saturated tracks. Having measured δ, g is determined. Then Fig.18 is entered with 0.614g and the proper value of δ. This yields B/B_δ, and finally B. The procedure described above was used each time a dipping track was blob counted, in order to get the equivalent flat track blob density B. The curves were checked with known values of B and B_δ, and yielded the proper values within statistics. It was found that black tracks of dip angle greater than 10° could not be used, but that near minimum tracks could be used at dip angles up to about 40°.

6. Blob Density vs. Residual Range Curve

For the identification of unknown particles a curve of blob density vs. residual range was constructed for π-mesons, K-mesons, and Baryons. From the B vs. β curve, βs were found corresponding to certain B values, then converted to the energies and residual ranges for π-mesons, K-mesons, and Baryons (see Figs.19 and 20).

The procedure for identification of unknown particles was established and followed as described below.

Two points on the unknown track are selected which are sufficiently separated to give a definite change in grain count, if possible. The blob density was determined to ± 5% at each point and the range measured to ± 2% between the two points. From the blob density vs. residual range curve(Fig.19)the residual range at the two points was estimated from the blob density for the three different possible particle masses. Then the actual range between the points was compared with the difference of the two residual ranges for the three possibilities.

The principal use of this procedure was to identify the particles causing SIF and DIF events, and to determine their energy.

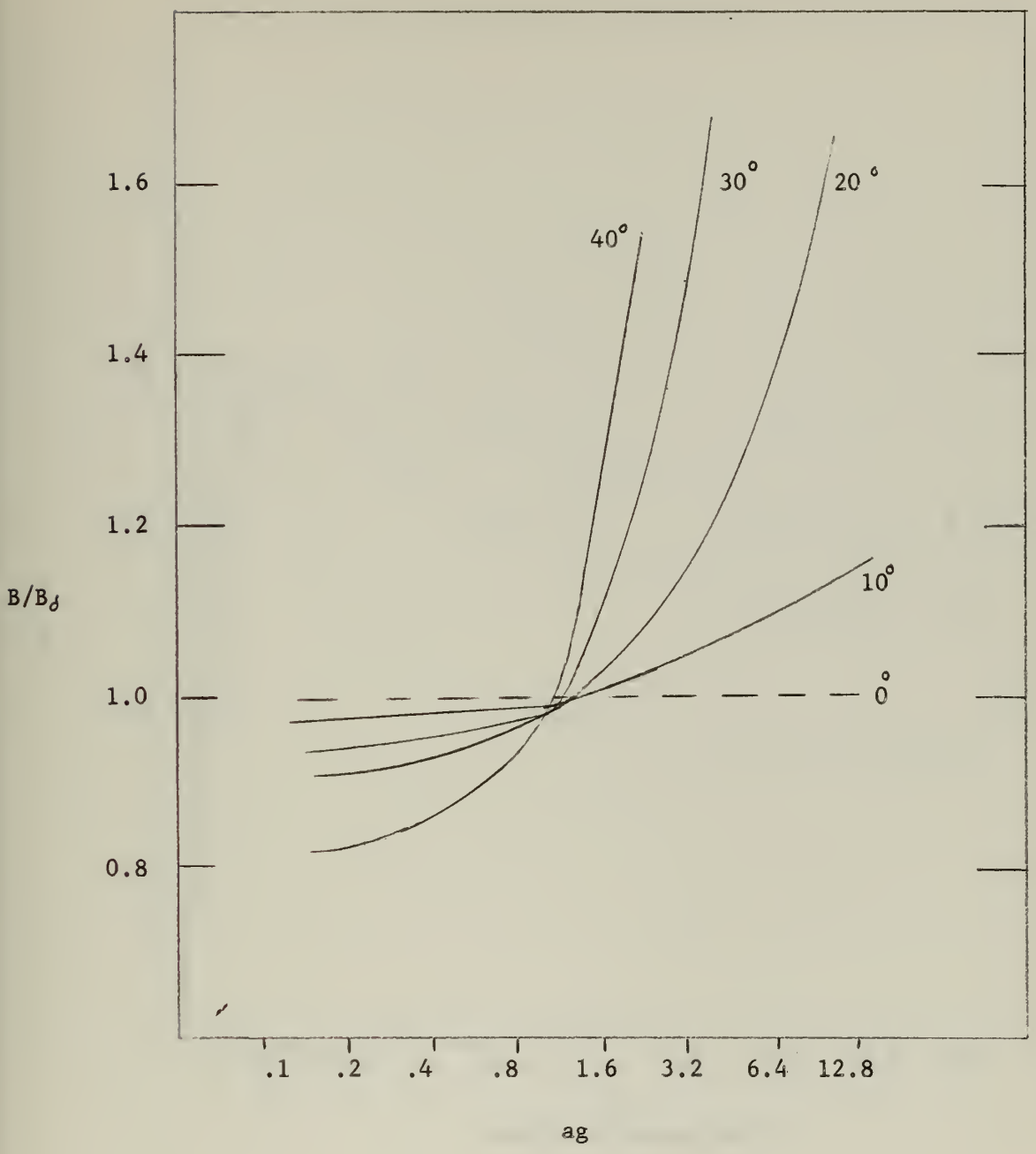

Fig. 18

A family of curves showing B/B_δ vs. ag for 5 values of the dip angle δ.

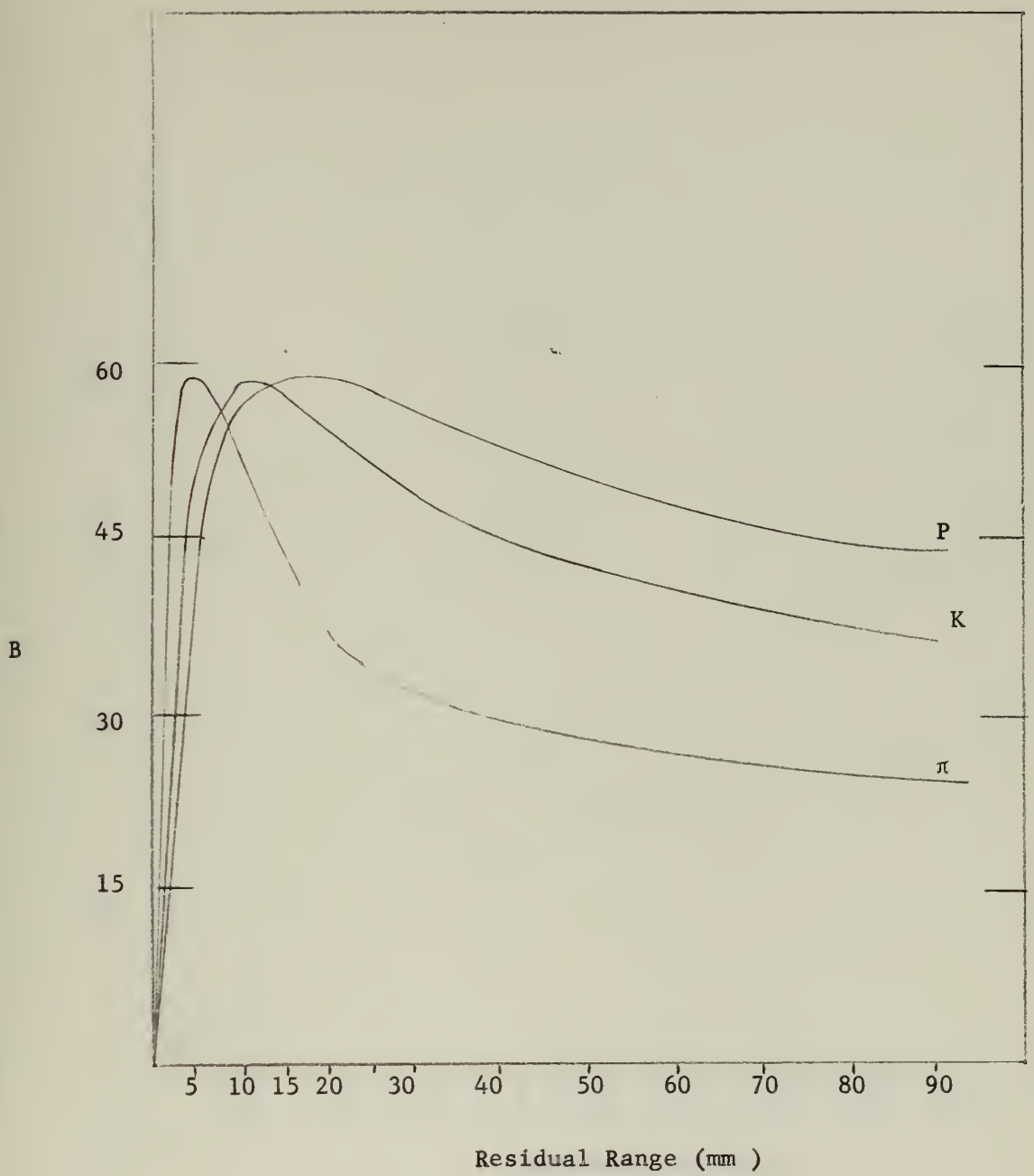

Fig. 19

Blob density in blobs/100 microns vs. residual range in mm .
Shown for π, K, and Proton.

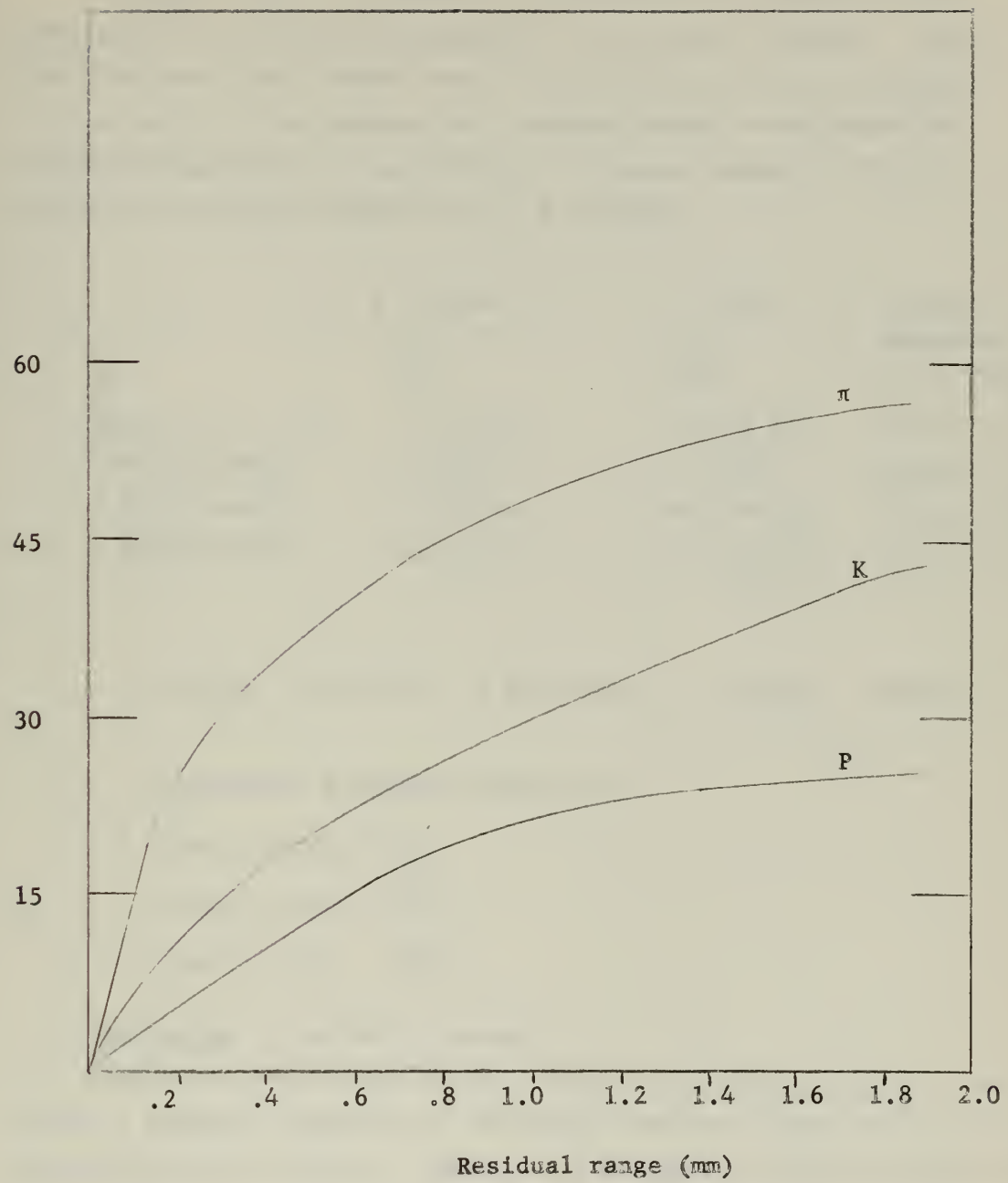

Fig. 20

Blob density vs. Residual range, expanded for the range 0-2 mm. Shown for π, K, and Proton

7. Sample Event

A sample event is included to illustrate the identification procedure and the typical magnitude of the errors involved. Since the blob count had a known error of ± 5% this error was projected to the curve of blob density vs. residual range to determine the residual range error at each point. The event number is B87-21, which was ultimately identified as a K^--meson.

	At K-Star	At SIF	Method
δ	16^o	14^o	Measured
B_δ	46.7	56.3	Blob count
$B \pm \Delta B$	47.1 ± 2.3	57.2 ± 2.9	Figs. 16,17,18
R R(π)±ΔR R(π)	$9.0^{+1.0}_{-1.5}$	$4.0^{+1.7}_{-0.5}$	Figs. 19, 20
R R(K)±ΔR R(K)	34.0 ± 4.0	$14.0^{+4.0}_{-1.0}$	Figs. 19,20
R R(B)±ΔR R(B)	64.0 ± 8.0	$25.0^{+6.0}_{-9.0}$	Figs. 19,20

Actual R R(SIF) - R R(K-star) = 20.7 mm measured

Estimated R R(SIF)-R R(K-star)

For π = $5.0 \pm ^{2.0}_{1.6}$

For K = $20.0 \pm ^{5.0}_{4.1}$

For B = $39.0 \pm ^{10.0}_{12.0}$

Conclusion: A definite K-meson.

This event was identified as a definite K^--meson, since it was within 1 standard deviation of the actual measured range for a K, but inconsistent with either a π-meson or a Baryon. In the few cases that were outside of one standard deviation, a probability of 1/3, 1/2, or 2/3 was assigned depending upon the observed variation between the two particles involved. Probabilities assigned in this event were: π=0; K=1; B=0.

C. SIF and DIF Sample Size

The original number of stars investigated was 1240, out of which the total number of SIF events was found to be 106. The total number of DIF events was found to be 19. Of these only those with dip angle less than or equal to 30° were selected for analysis. Theoretically, in an isotropic spherical distribution, one half the surface of a sphere will be contained between $\pm 30^{\circ}$ from the horizontal. This would predict, if the distribution of tracks which end in SIF events is isotropic, that 53 events would have dip angles less than or equal to $\pm 30^{\circ}$. The final number of events used, which fit the dip angle criteria, was 55.

D. Analysis of SIF Events

Each star in flight was analyzed in detail in order to learn as much about its characteristics as possible in the search for a correlation between stars in flight and the problem of the conservation of strangeness in the original beam K^- interactions. The details of each SIF and DIF are included in Table IV.

1. Range Measurement

A range measurement from the beam K^--stars to each SIF was made, accurate to an estimated $\pm$ 2 %.

2. Blob Count

Blob counts at the K-star and at the SIF of 400 blobs gave the blob density to ± 5 % accuracy.

3. SIF Prong Analysis

The number of prongs of each SIF was recorded. Each prong was followed to its end-point, and the total energy visible at each SIF was determined. Protons and π-mesons released at the SIF were followed and from visual identification of the particle, the energy was determined using the range energy curves.

4. Correlation With Other Data

In the stars in flight and disappearances in flight analyzed, there was no case of an SIF or DIF occurring from the same parent K^--star which had an associated crypto-fragment, hyper-fragment, free Λ°, or $\Sigma^{\pm}$.

TABLE IV

BARYONS

T at K star	T at SIF	Vis.T Rel(SIF)	Vis. T + Bind. Energy	No. Prongs	Range K to SIF	T vis. T in	Event No.	ID
117	21	27		1	29.3	1.3	86-31	B-scatter
68	10	8		1	27.1	0.8	87-57	B-scatter
82	63	73		2	25.6	1.1	88-78	B-scatter
104	79	60		1	20.5	0.75	88-107	B-scatter
46	11	10		1	4.95	0.9	86-15	B-scatter
145	122	53	93	5	16.8	0.75	85-25	B
132	99	66	84	4	69.3	0.85	85-35	B
120	66	19	35	2	45.0	0.55	85-54	B
40	40	9	17	1	0.0745	0.42	87-15	B
58	48	8	24	2	3.6	0.5	87-30	B(1/2K)
186	156	75	91	2	45.9	0.6	87-32	B
175	137	46	86	5	78.2	0.63	87-190	B
156	118	70	78	1	27.6	0.66	89-41	B
80	49	8	16	1	17.7	0.4	89-178	B
172	66	20	36	2	19.1	0.51	89-196	B
68	56	7	15	1	12.5	0.26	90-27	B
39	23	14	22	1	3.4	0.95	91-21	B
61	39	12	20	1	10.9	0.51	92-37	B(1/2 K)
66	39	21	29	1	8.1	0.74	92-49	B
122	94	86	102	2	74.4	1.08	84-3	B
68	53	10	18	1	9 .65	0.33	86-89	B
34	32	25	31	2	2.15	0.97	86-90	B
98	69	45	61	2	34.6	0.88	86-100	B
240	111	119	132	5	141.5	1.2	86-17	B(1/3 K)
30	15	85	93	1	2.3	6.6	85-58	B
64	7	7	23	2	13.1	3.3	89-177	α
68	55	118	126	1	7.05	2.3	90-157	B

$\bar{K}$-MESONS

58	48	8	24	2	3.6	0.5	87-30	K(1/2 B)
60	50	26	50	4	7.45	1.0	87-71	K
39	8	193	209	2	16.2	26.1	87-98	K(1/2 π)
80	48	18	32	3	20.7	0.67	87-21	K
74	58	32	58	3	14.6	1.0	88-10	K
56	7	8	14	1	14.65	2.0	88-84	K
63	20	97	120	3	11.1	6.0	88-59	K
140	135	42	50	1	22.7	0.37	89-61	K
28	11	1	1	1	3.5	0.1	89-133	K
23	22	15	33	2	0.3	1.5	90-155	K(1/3 B)
61	39	12	20	1	10.9	0.51	92-37	K(1/2 B)
115	10	134	174	5	99.1	17.4	86-91	K

TABLE IV (cont.)

π-MESONS

91	57	135	167	4	53.6	2.9	86-75	π
48	43	148	188	5	7.3	4.3	87-11	π
15	9	41	57	2	4.0	6.5	87-26	π
90	69	64	104	5	31.0	1.5	87-84	π
24	13	17	25	1	11.7	1.9	87-89	π
10	8	202	218	2	11.55	27.3	87-103	π
39	8	193	209	2	16.2	26.2	87-98	π(1/2 K)
31	21	21	37	2	3.9	1.75	87-107	π(1/3 K)
25	16	15	31	2	4.1	1.93	87-231	π
21	6	1	9	1	3.7	1.5	88-101	π
35	21	127	151	3	6.55	7.25	89-198	π
14	10	10	18	1	1.0	1.8	90-13	π
48	43	20	44	3	9.85	1.02	89-29	π
43	30	96	120	3	5.5	4.0	91-1	π
17	5	18	42	3	7.4	8.4	91-8	π
33	2	62	110	6	26.7	55.0	91-171	π
38	1	36	60	3	39.2	60.0	92-55	π

DIF Events

T at K star	T at DIF	Range K to DIF	Event No.	ID
BARYONS				
95	12	21.7	86-51	B(1/3 K)
31	18	1.0	88-102	B(1/3 K)
66	5	18.6	89-123	B
186	173	58.8	91-31	B
122	52	41.7	91-35	B
12	8	3.0	88-81	B
π^--MESONS				
55	50	7.1	87-69	π
35	3	25.6	87-150	π
17	11	4.8	88-49	π

The ranges listed in Table IV are given in millimeters. The energies are given in Mev to the nearest integer value, and no error values are listed.

Histograms have been prepared to display the data from Table IV, and are shown in Figs. 21 through 26.

5. Identification of SIFs

The total sample of stars under investigation is 1240. The beam contamination is known to be 7%, so that the sample of K^- beam interactions is 1154. From this sample, a total of 817 K^--stars had all prongs followed. There were 105 stars in flight, of which 54 were below 30° in dip angle and were completely analyzed. One event, number B87-22, was considered to be indeterminate. This was a near minimum particle which changed only slightly in blob density from the K^--star to the SIF. It was on the nearly flat portion of the residual range curve, and the errors in range from the 5% error in blob count became indeterminate. It was therefore not entered in the final statistics.

From the 54 event sample, the following are the most probable identifications on the basis of blob count:

π-mesons	16/54
K^--mesons	11/54
Baryons	27/54

The final percentages of K^--mesons, π-mesons, and Baryons in the 54 event sample are as follows:

π-mesons	30 %
K^--mesons	20 %
Baryons	50 %

The frequency of SIF production must now be determined. An unbiased sample of 206 beam stars was selected from which all prongs were followed. A total of 30 stars in flight were observed for a "production frequency for SIF" of 14.6 %. This should then hold for the entire sample of 1154 beam K^--stars, so that the estimated total number of stars in flight will be 168. Of these 168 stars in flight, 20% or 34 total, will be K^--mesons. Hence, from 1154 K^--stars we expect that there are 38 K^--mesons(3.3%) re-emitted which make interactions in flight (SIF or DIF).

E. Analysis of the DIFs

We estimate that 5 of the 9 analyzed DIFs are of baryonic mass, and therefore most probably Σ^- hyperons; that 3 are π^--mesons, and that 1 is a K^--meson. Hence we assume that 5/9 of all DIFs

in the stack are Σ^- hyperons, 1/9 are K^--mesons, and 3/9 are π^--mesons. The total number of DIFs in the 1240 stars is estimated as follows:

In a sample of 644 stars from which all prongs were followed there were 16 DIFs. The "production frequency for DIF" is therefore 16/644, 2.5%. From the total sample of 1240 stars, we therefore expect 31 DIFs. Of these, 17 should be Σ^- hyperons, 4 should be K^--mesons, and 10 should be π^--mesons. Hence, the strangeness of the K^--mesons appears in the reaction products as a Σ^- which disappears in 1.4% of all cases, and as a re-emitted K^--meson which disappears in 0.3% of all cases. We do not attempt to correct for the beam contamination of π^--mesons.

F. Conclusions

1. Re-emission of K^--mesons

From the sample of 817 beam K^--stars with all prongs followed, 11 K^--stars at rest were observed, which indicates 14 K^- stars at rest in the 1154 beam K^--stars.

a. The known number of K^--mesons that DIF or SIF is 38, or 3.3% of the total.

b. The K^--stars at rest give 1.2% of the total.

c. Thus, in 4.5% of the K^- interactions, the incident particle is re-emitted and goes on to interact in flight or come to rest in the emulsion. The energy spectrum of these re-emitted K^--mesons is shown in Fig. 21.

To determine the total number of K^--mesons re-emitted, we must estimate the number which are re-emitted and escape the emulsion stack without interaction. We have not blob counted or scattered those tracks which leave the emulsion, so we are forced to estimate this number indirectly. We can do this very roughly by assuming that the mean free path for K^--mesons is about 25 cm. With this free path, 1/3 of the K^--mesons will interact in 10 cm. of path. Since 10 cm. is about the average distance to the limits of the stack, we estimate that we have detected as interactions roughly 1/3 of the re-emitted K^--mesons. Thus we estimate that K^--meson re-emission occurs in 13.5% of all reactions. This is in agreement with the results of Chiesa, Quasiatti et al /29/ who have estimated 10 to 20 percent K^- re-emission.

2. The Interactions of Baryons-Possible Strangeness

We find 2 cases of definitely exothermic baryon interactions in flight. These two particles are both singly charged and are therefore not α particles.

Since they are both exothermic by about 50-60 Mev , one explanation is to assume that they are $\Sigma^{\pm}$ hyperons. We can justify this assumption by stating that we expected to find a small number of $\Sigma^{\pm}$ stars in flight among the baryons, and that if found, they could be exothermic.

No definite means was devised by which we could separate the protons from the $\Sigma^{\pm}$-hyperons among the stars in flight. Blob counting was not accurate enough, and multiple scattering would not have aided measurably. With this in mind, we can only say that we estimate the lower limit on $\Sigma^{\pm}$ hyperons which form stars in flight at 2/54, or 3.7%. We are not able to estimate the upper limit on Σ stars in flight from the data available.

We have previously determined, from the "production frequency for SIF", that we estimate 168 total stars in flight. The lower limit estimate for the 168 SIF's will be 168 x 2/54, or 6 in the 1154 star sample.

Thus we estimate that as a lower limit, in 6/1154 (0.52%) of all cases, the strangeness of the incoming K^-- meson re-appears in the reaction products as a $\Sigma^{\pm}$ hyperon which forms a star in flight.

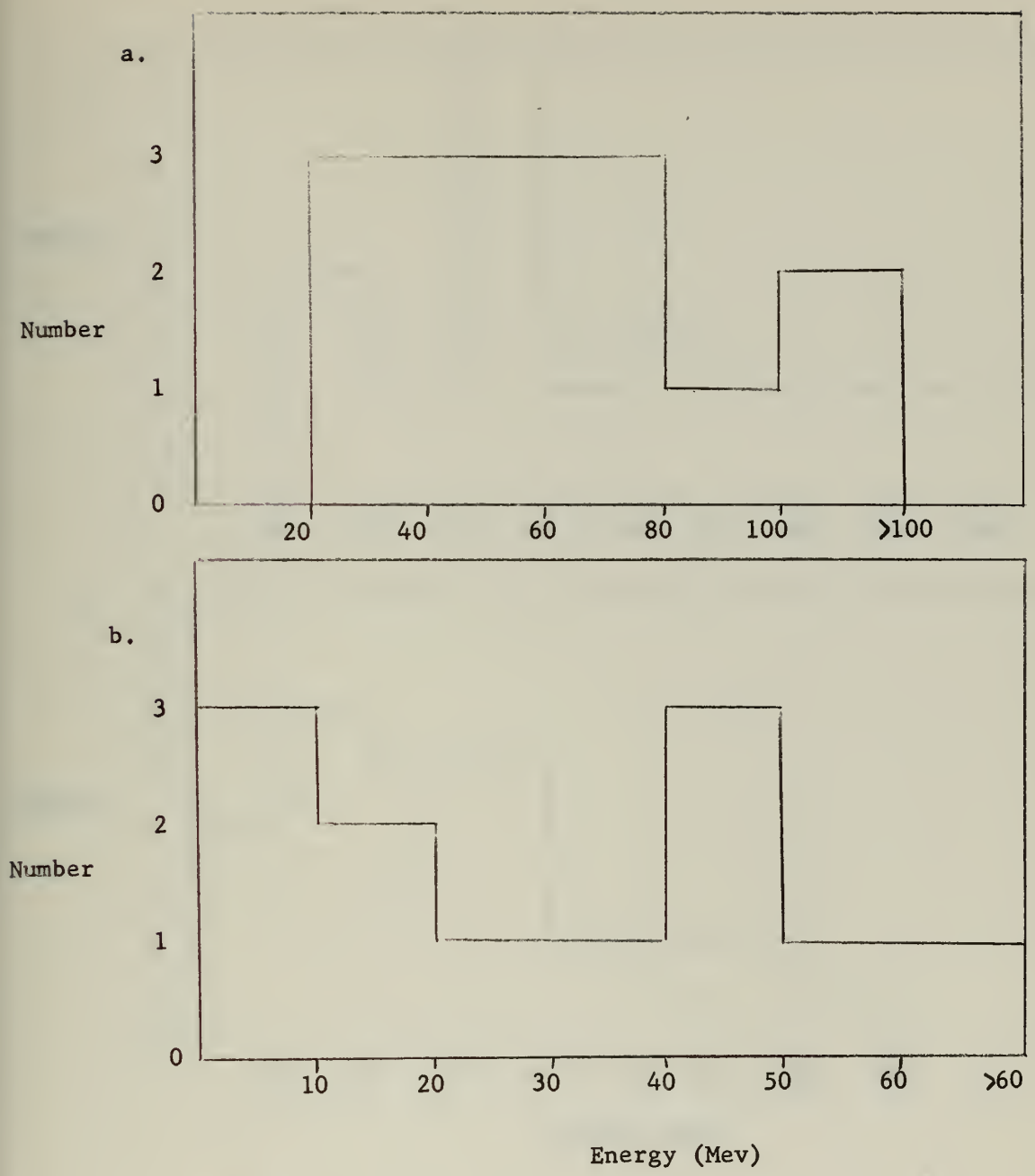

Fig. 21

Energy histogram for K^--mesons

a. At K-star

b. At SIF

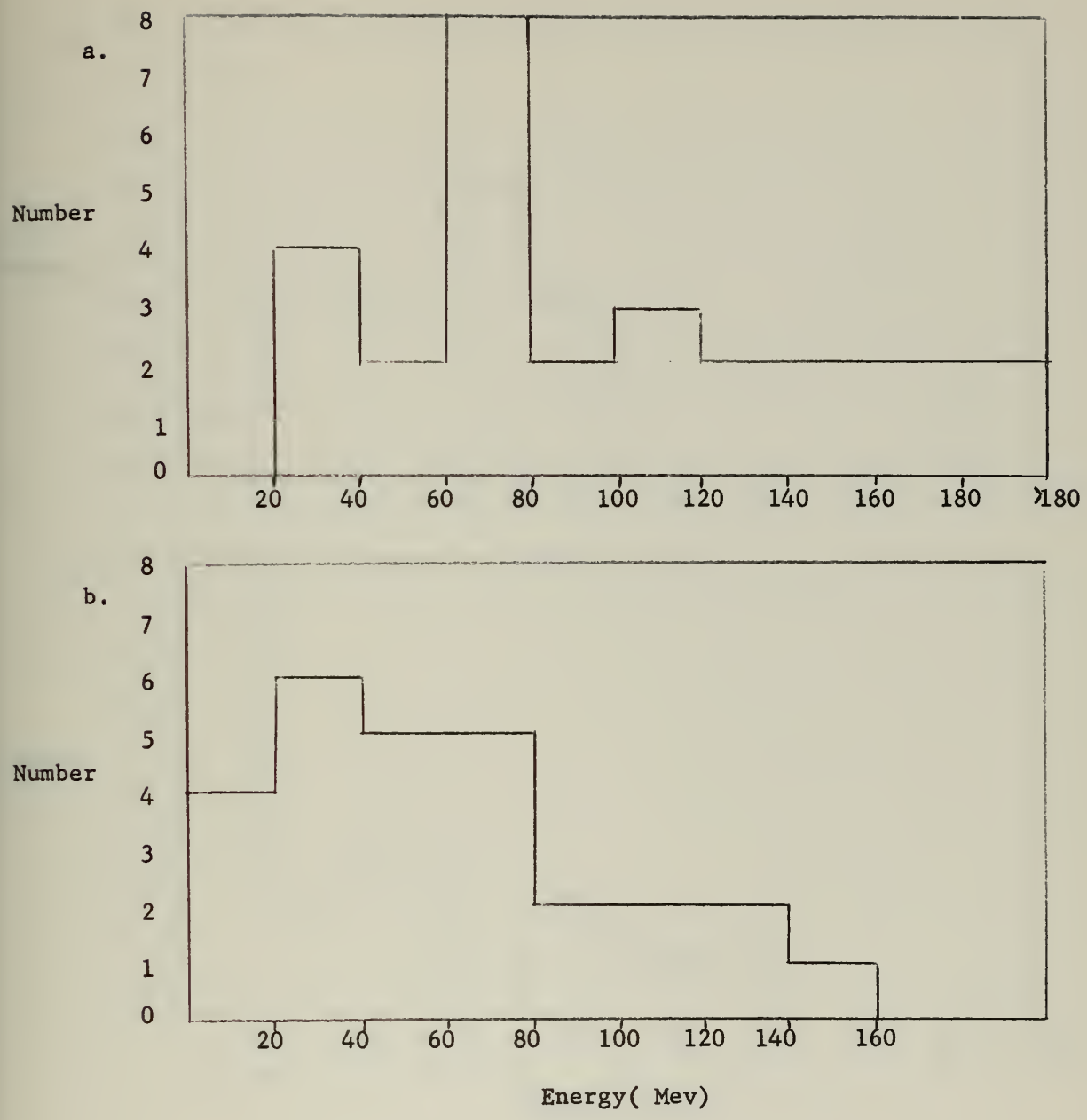

Fig. 22

Baryon Energy histogram
a. At K-star
b. At SIF

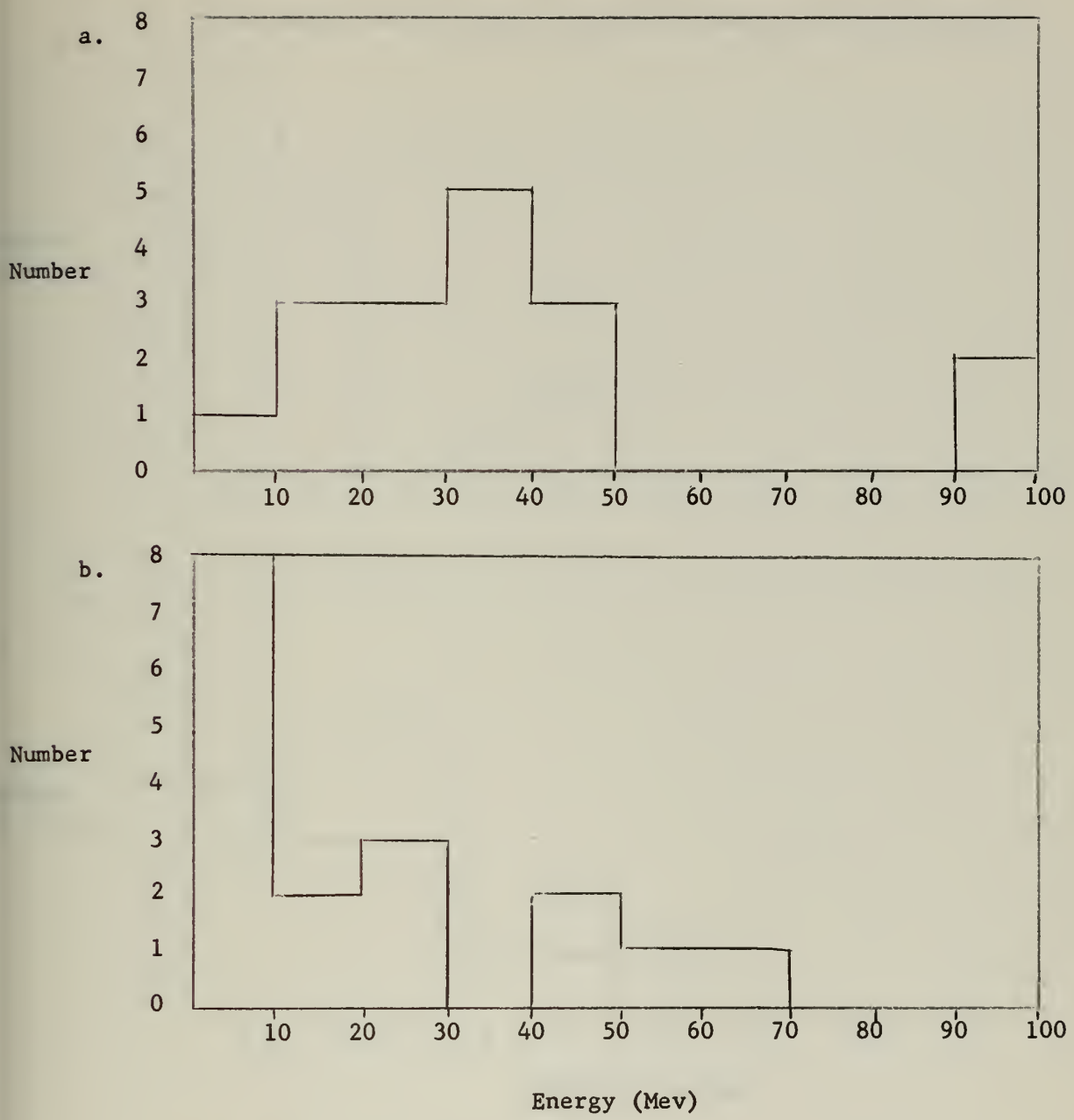

Fig. 23

π-meson energy histogram
a. At K star
b. At SIF

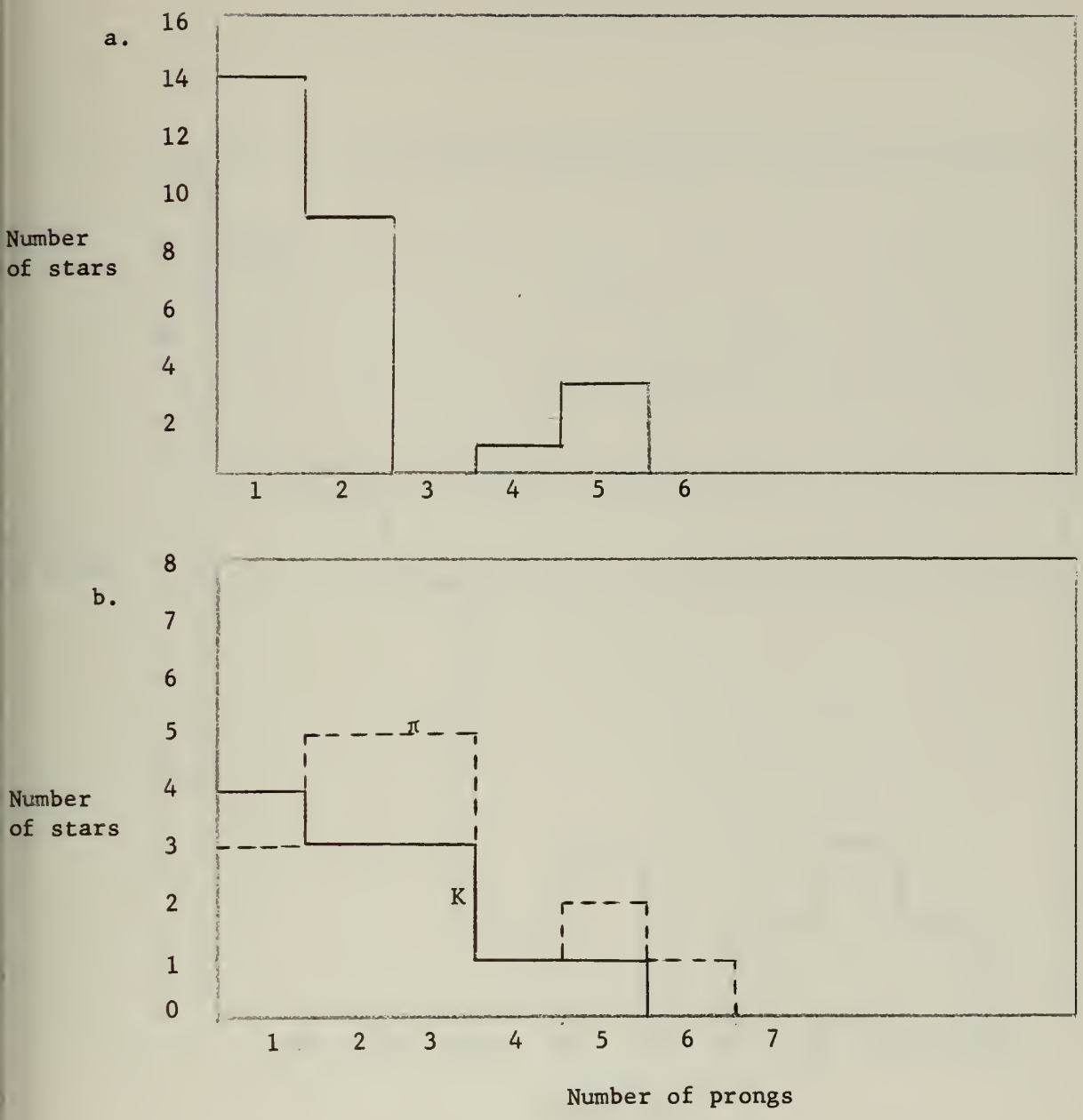

Fig. 24

Prong distribution at SIF
a. Baryons
b. K-mesons; π-mesons shown in dashed outline

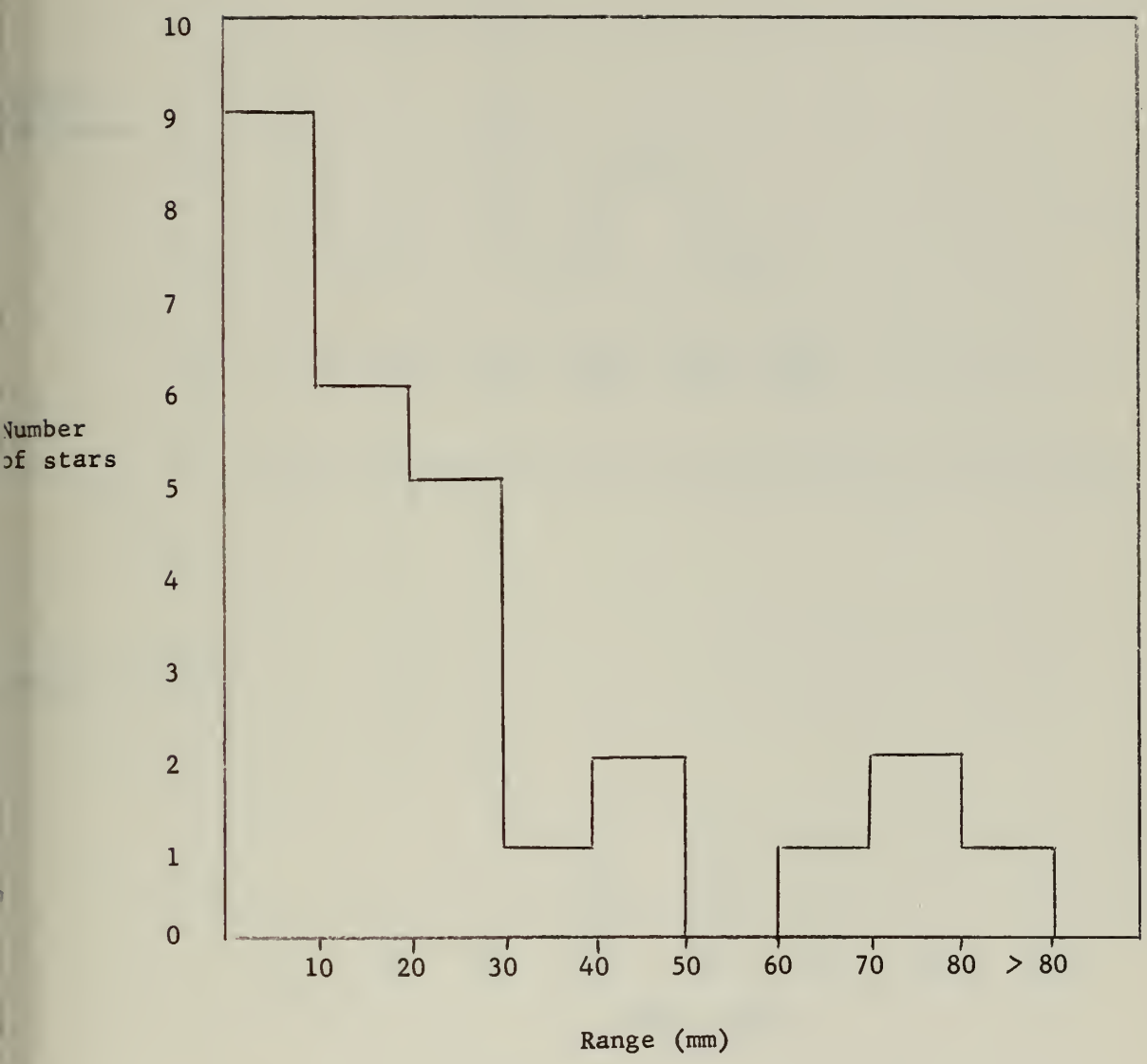

Fig. 25
Baryon K-star to SIF range histogram

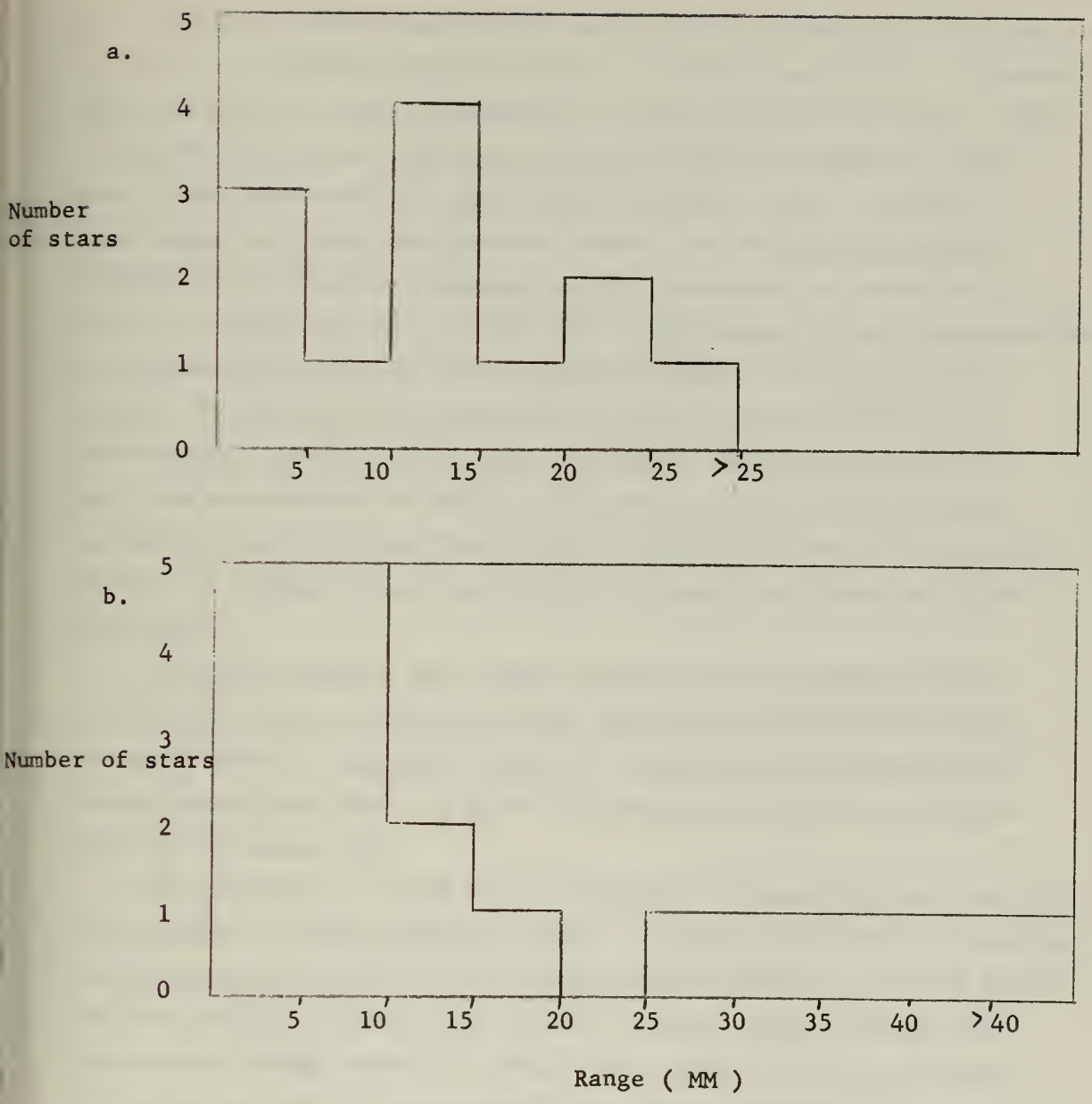

Fig. 26

Range histogram, K-star to SIF
a. K-mesons
b. π-mesons

V

LAMBDA HYPERON PRODUCTION

The first hyperfragment (HF) was observed by Danysz and Pniewski in 1955 in a nuclear emulsion exposed to cosmic rays /11/. Following their discovery, others proceeded to observe and analyze HFs. Hyperfragments were found only occasionally in stars produced by cosmic rays (less than 0.06% yielded a hyperfragment) /41/. With the development of large accelerators capable of producing beams of K^- mesons, the production frequency of HFs increased to approximately 5% /42/. Early analyses of HFs were concentrated on the interpretation of the decay modes with little attention given to the production modes. The work also concentrated on the light HF ($Z \leq 5$), for two reasons. First, these modes frequently decayed mesonically and thus were easier to analyze since few neutral particles were produced. Second, since the primary interactions were K^- absorbtion stars, not enough energy was present to enable the heavy HF to be detected.

Recently, efforts were begun to add to the knowledge of HF by studying their production modes. With the availability of high energy K^- beams, information has been compiled on the previously undetectable heavy HFs. A plausible model for heavy HF production has been proposed /12/.

Our purpose is to add to the knowledge of heavy HFs particularly with regard to their production mode. We hope to use this information in extending our study to the cryptofragments (CFs). For this paper CFs are defined as stars that produce a bound lambda hyperon (Λ°) whose decay prongs cannot be completely separated from the prongs of the parent star. Observable CF are double centered with a short separation between parent star and Λ° decay, i.e. a few microns. Non-detectable CF appear to be single centered. From the characteristics of the observed CF we made a estimate of the total CF production frequency. The probability that the incoming K^- strangeness is conserved by the production of a bound Λ° (either in a HF or CF) was then estimated.

Often the Λ° particle is produced in the primary interaction

but is not bound. It leaves the star as a free Λ° which is not readily detectable. (Since any Σ° that is produced decays electromagnetically into $\Lambda^\circ + \gamma$, this particle will be detected as a Λ°. Thus Σ° production is included in our count of the free Λ°s.) To complete the study on lambda hyperon particles we made a search for free Λ°s. Others have estimated the free lambda hyperon production frequency /43/, but their estimates have varied widely and their studies were accomplished using less energetic beams. We found a small number of free Λ°s and from their characteristics and location, estimated their production frequency.

By combining both the free Λ° and bound Λ° production probabilities, we estimated how often the strangeness could be accounted for by a lambda hyperon.

A. Hyperfragments

The characteristics of the light HF are well known /42,44-47/, i.e. their binding energies, ranges, decay modes, and frequency of production. The purpose of this section is to examine the production modes of the heavy HF and to justify or repute the model proposed by Jones et al /12/. They have stated that heavy HF and CF are produced in the following way. The incident K^- meson interacts with one or two nucleons in a heavy nucleus (silver or bromine) to produce a Λ° along with one or two very energetic particles. The energetic particles may or may not leave the nucleus with this energy since they may suffer inelastic scattering within the nucleus. Regardless, the Λ° does not leave but remains trapped and transfers its momentum to the nucleus. Before the nucleus has moved a measurable distance, it loses some of its energy by the release of a number of evaporation prongs. It then travels a few microns in the emulsion. After it has stopped, the Λ° decays producing a typical double centered star.

1. Observed Production Frequency

This sample of stars consists of 1240 events which were produced by a 1.15 Bev/c K^- beam. Previous analysis /15/ has shown that 7% of the interactions are due to π^- contamination. Thus we have about 1154 K^- interactions. Forty-nine HFs were observed for a production rate of $4.2\% \pm 0.6\%$. Because double

centered stars from which the origin of one or more prongs is in doubt were classified as a CF, the HF production rate appears low. Inclusion of the 16 observed CFs yields a total production rate for double centered stars of 5.6% $\pm$ 0.7%. This agrees with the value of 5.3% $\pm$ 0.3% reported by Jones et al /12/. Ten of the HFs decayed mesonically for a production rate of 0.9%. (This rate is not affected by the CF classification since no mesonic CFs were observed, and compares favorable with previous data /44,47,48/.)

2. Range of Hyperfragments

All observable double centered stars where the origin of all prongs could be positively determined are classified as HFs. The HFs are divided into heavy and light according to their range. If they travelled 6 microns or less they were placed in the heavy HF category. This cutoff value is slightly larger than the range of a mass 40 nucleus with a momentum of 1.0 Bev/c /49/. If the heavy HFs are indeed the remnants of the heavy emulsion elements they should be stopped in this distance. Straggling will result because their mass and the portion of the incoming momentum they absorb will vary. The range distribution for the HFs is shown in Figure 31. A sharp peaking in the number of HFs is observed at low ranges thereby indicating a large fraction of the HFs are heavy, or else they are of momentum much less than 1.0 Bev/c. Above 6 microns the number of HFs appears to be fairly well distributed. However a large number have ranges between 200 and 600 microns and 2.5 and 7 millimeters. These irregularities are believed due to the small sample size and are not significant. Of the 49 HFs analyzed, 29 are classified as heavy and 20 as light hyperfragments. All of the mesonic decays are in the light HF group. The lack of mesonic decays in HFs with range less than 6 microns, strengthens the arguement that they are indeed heavy.

3. Identification as Hyperfragments

Conceivably the "things" called heavy HF are not. They might be decays of highly excited nuclei. No positive determination can be made since the connecting track is too short. If they are not HF, one would expect to observe some other evidence of strange

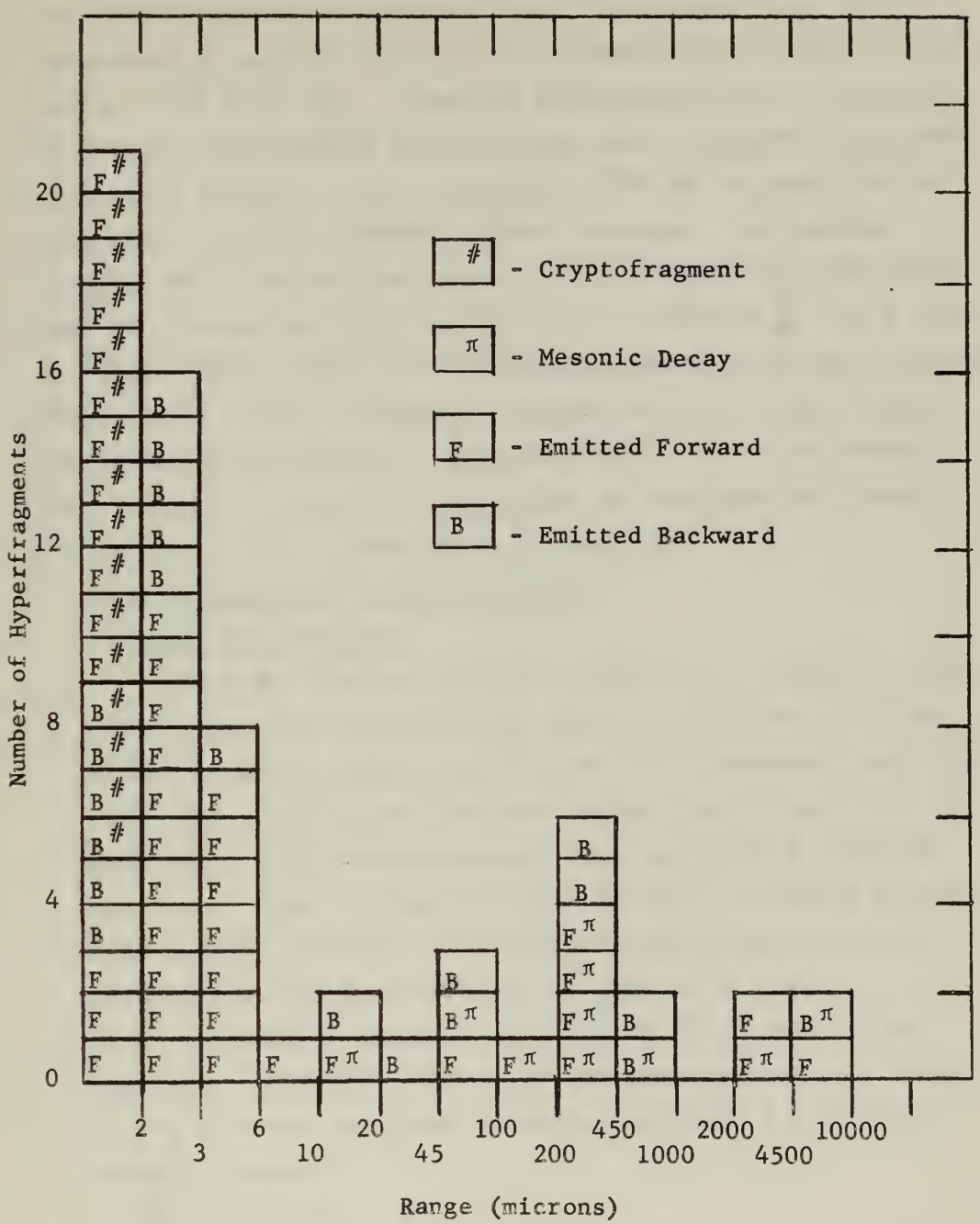

Figure 31 - Range distribution of hyperfragments from the interactions of 1.15 Bev/c K^- mesons. (CF data also included.)

particle production either as K, Σ , or light HF emission with the same frequency as observed for all the stars (i.e. 20% as determined in earlier sections or approximately 6 events in our sample of 29 heavy HF). Complete examination of all the heavy HF parent stars yielded only one star that displayed strangeness in another particle. The existence of the HF is justified in this star under the "unusual events" section. The absence of strange particles can also imply that the "HFs" are some other type of strange particle interaction. Low energy Σ^- or K^- stars in flight (SIF) might be interpreted as heavy HF if the connecting track is very short. However as shown earlier in this paper, the energy distribution of these SIF falls off at low energy. Thus in lieu of contrary information, we conclude that these events are correctly identified as heavy HF.

4. Hyperfragment Decay Characteristics

a. Prong Distribution

Heavy HFs display a greater charge, i.e. they emit more visible particles during decay than the light HFs. Figure 32 shows the prong number distribution for HF decays. Only three light HFs emitted more than two charged particles (three in each case). The maximum number of prongs from a heavy HF was five. Thus, during the decay of the Λ° in these fragments only a small portion of the nucleons were ejected if one assumes that the heavy HFs are of mass 40 or greater. In 9 of the heavy HF decays a short prong $\leq$ 2.5 microns was observed. This was taken to be the recoiling of the remnants of the HF decay and hence probably contained a fairly substantial charge.

b. Mesonic Decays

Of the 49 HFs observed, ten decayed mesonically for a non-mesonic to mesonic decay ratio of 3.9 ± 1.4. This value compares favorably to the ratios observed with slow incoming particles /50/ but is considerably less than that observed with a beam of comparable energy. However by including the 16 CF decays, we calculate a non-mesonic to mesonic ratio of 5.6 ± 1.9, which is still substantially lower than the figure

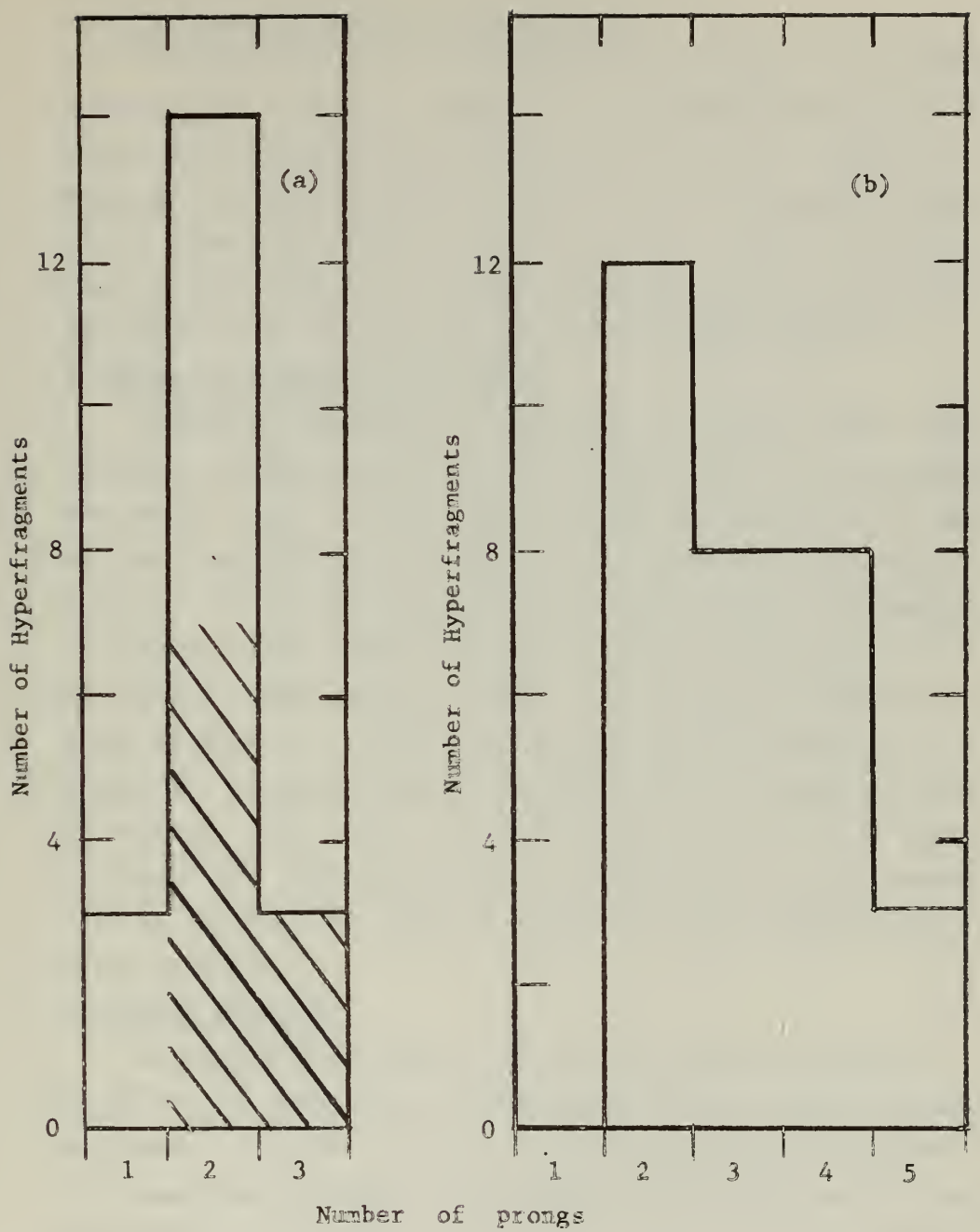

Figure 32 - Prong distribution of HF decays for (a) light HF and (b) heavy HF. Hatching indicates mesonic HF decay.

of 11.5 $\pm$ 0.6 reported by Jones et al /12/.

c. Hyperfragment Angular Distribution

For each HF the projected angle with respect to the incoming particle was measured. Light HFs are emitted isotropically since their forward/backward ratio is 1.2 $\pm$ 0.5. However heavy HF and CF production is peaked in the forward direction with a forward/backward ratio of 2.8 $\pm$ 0.9. This indicates that the heavy HFs are emitted during the primary interaction and absorb some of the momentum of the incoming particle.

d. Range of Prongs from HF Decay

During the HF decay, a relatively low energy event, the classical coulomb barrier for the nucleus should not be greatly disturbed. Hence a proton would require an energy of 3.3 Mev and an alpha particle 6.5 Mev /47/ to escape from a bromine nucleus. If they escaped with this minimum amount of energy, the proton would travel 75 microns and the alpha particle 30 microns before coming to rest. If the heavy HFs are as heavy as silver or bromine, no prongs except recoils (i.e. prongs $\leq$ 5 microns) should be observed with a range less than 30 microns. The short prong distribution for all HF is shown in Figure 33. Whereas short prong production is quite common (30% of the time) in light HF decay, it is not observed in heavy HF decay.

e. Energy Released

To estimate the upper limit for the binding energy of the Λ° in the heavy HFs, an examination of the energy released was made. The range of all HF prongs was measured and from the Range-Energy curves, the corresponding energy was determined. All prongs are assumed to be protons. To the value obtained for the visible energy, eight Mev is added to compensate for the approximate binding energy of each particle. Figure 34 shows the number of HFs versus the visible energy released. The maximum value of 133 Mev gives an upper limit for the binding energy of the Λ° of 51 Mev. ($B.E._{\Lambda^\circ} = M_{\Lambda^\circ} - M_n + B.E._n - Q$) Previous work by other groups has reduced this upper limit to 25 Mev /13/.

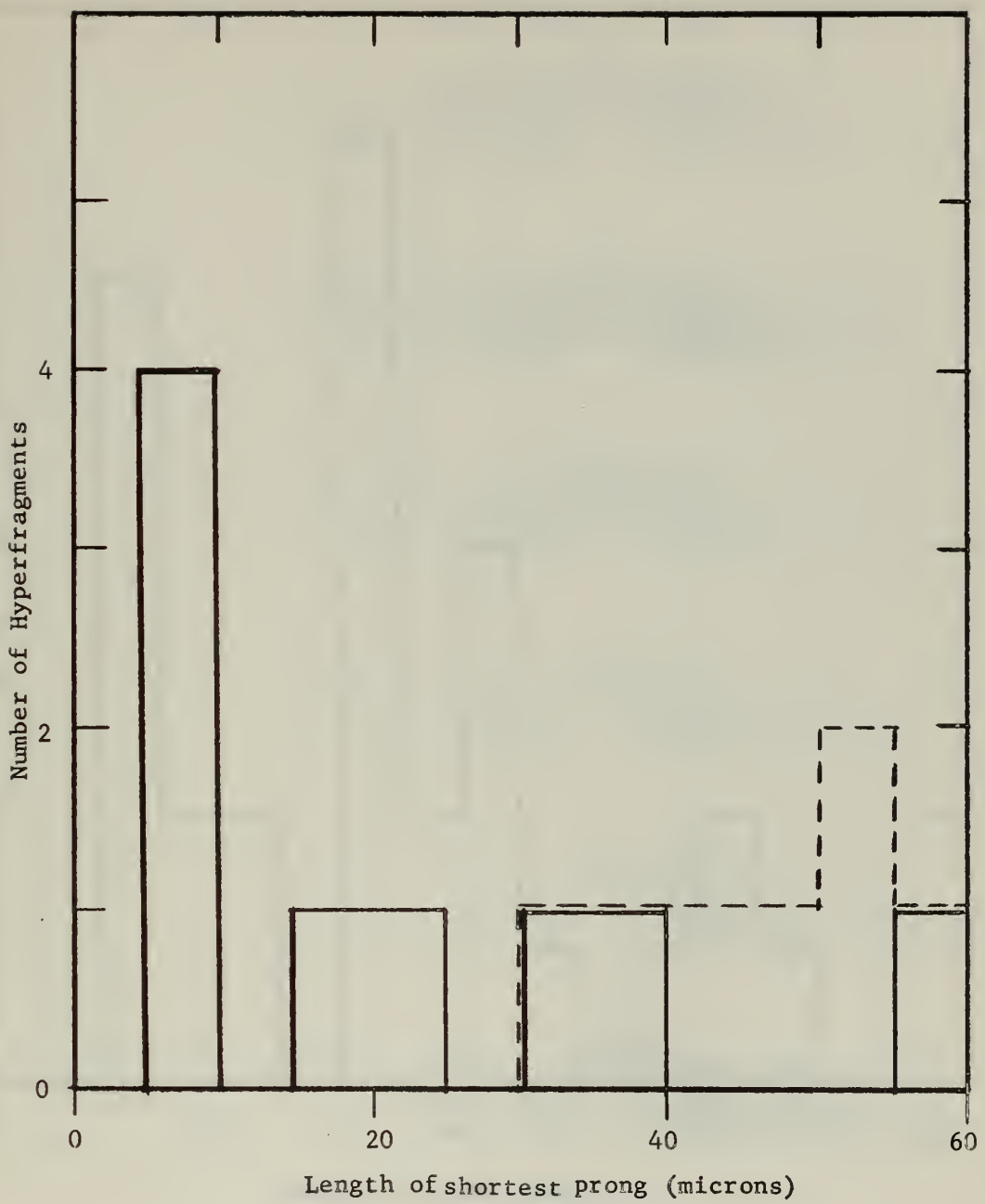

Figure 33 - Short prong distribution of HF decays. Solid outline indicates light HF decays. Broken outline indicates heavy HF decays.

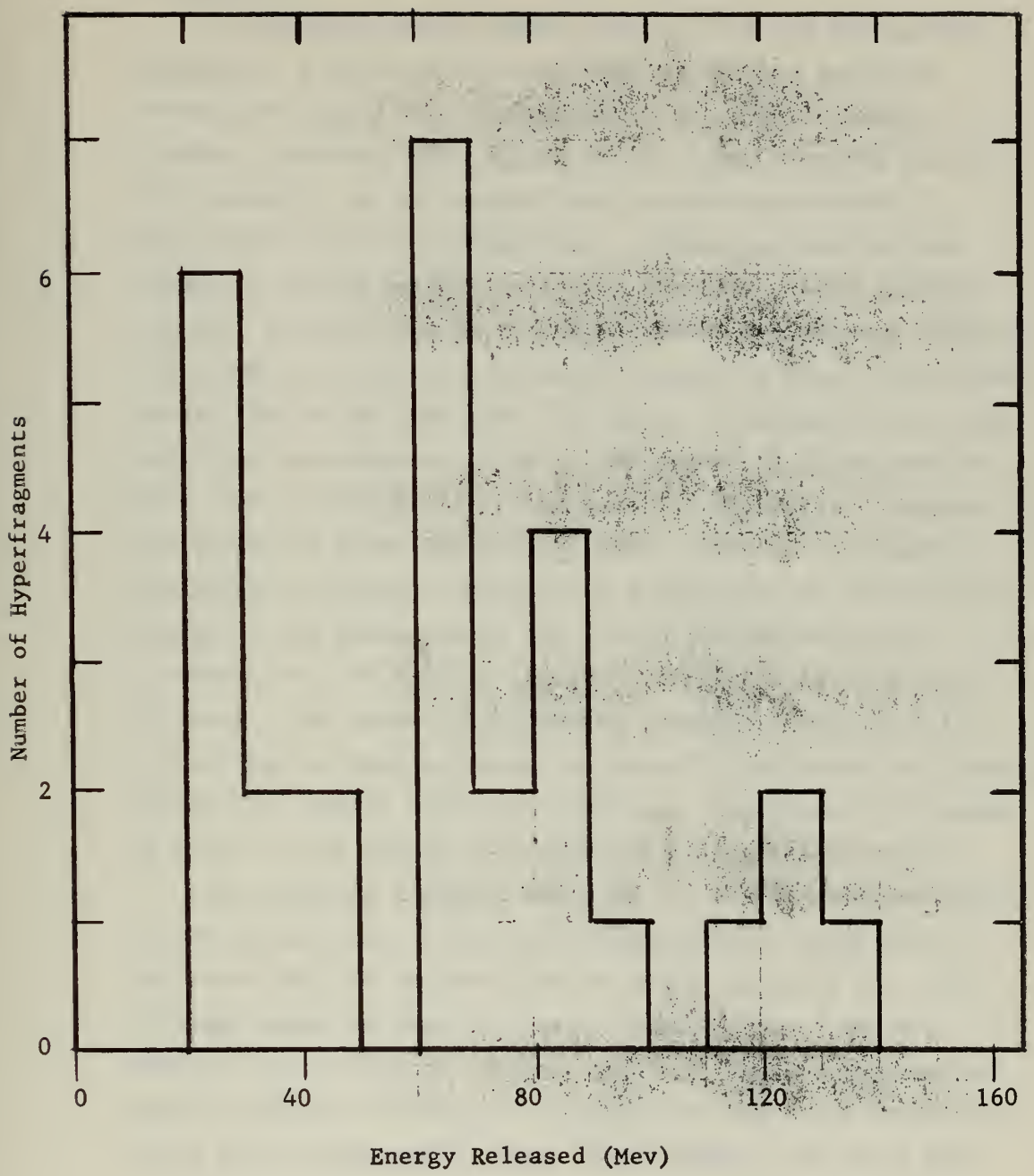

Figure 34 - Visible energy distribution for heavy HF decays.

5. Parent Star Characteristics

a. Identity

To identify the HF parent star, all of its prongs were examined. A determination was made of whether heavy HF production occurs more frequently in the light elements (carbon, nitrogen, and oxygen) or the heavy elements (silver and bromine). To accomplish this the minimum charge of each parent star was determined. A count was made of the number of prongs emitted both from the star itself and from the HF. All pion tracks and the track of the HF were excluded. Conceivably, if the star produced a negative pion, the minimum charge can be one less than the number of prongs if all other particles are protons. However the number of alphas emitted more than compensates for this possible reduction of charge /12/. Our criterion gives the desired lower limit of the charge of the parent nucleus. Figure 35 is a histogram of the minimum charge of the parent stars for both light and heavy HF. For a comparison, the minimum charge distribution for all stars is shown. The latter distribution compares favorable with a distribution obtained when one scans by following the incoming tracks /51/ rather than area scanning. Therefore this sample of stars is not biased toward the more spectacular events.

One observes a strong shift in the average minimum charge of the parent star. From the distribution at least 83% of the heavy HFs are emitted from the heavy elements (i.e. the minimum charge is nine or more). Thus the heavy HFs are heavier than the light elements and conceivably approach the mass of silver or bromine. Light HFs are produced from stars which also display more charge than average. At least 50% of the light HFs are produced in the heavy elements. As a comparison only 26% of our sample of all stars are definitely an interaction in the heavy elements.

b. Short Prong Distribution

According to the classical coulomb barrier discussed in an earlier section, prongs less than 30 microns but greater than 5 microns should not be observed from interactions in

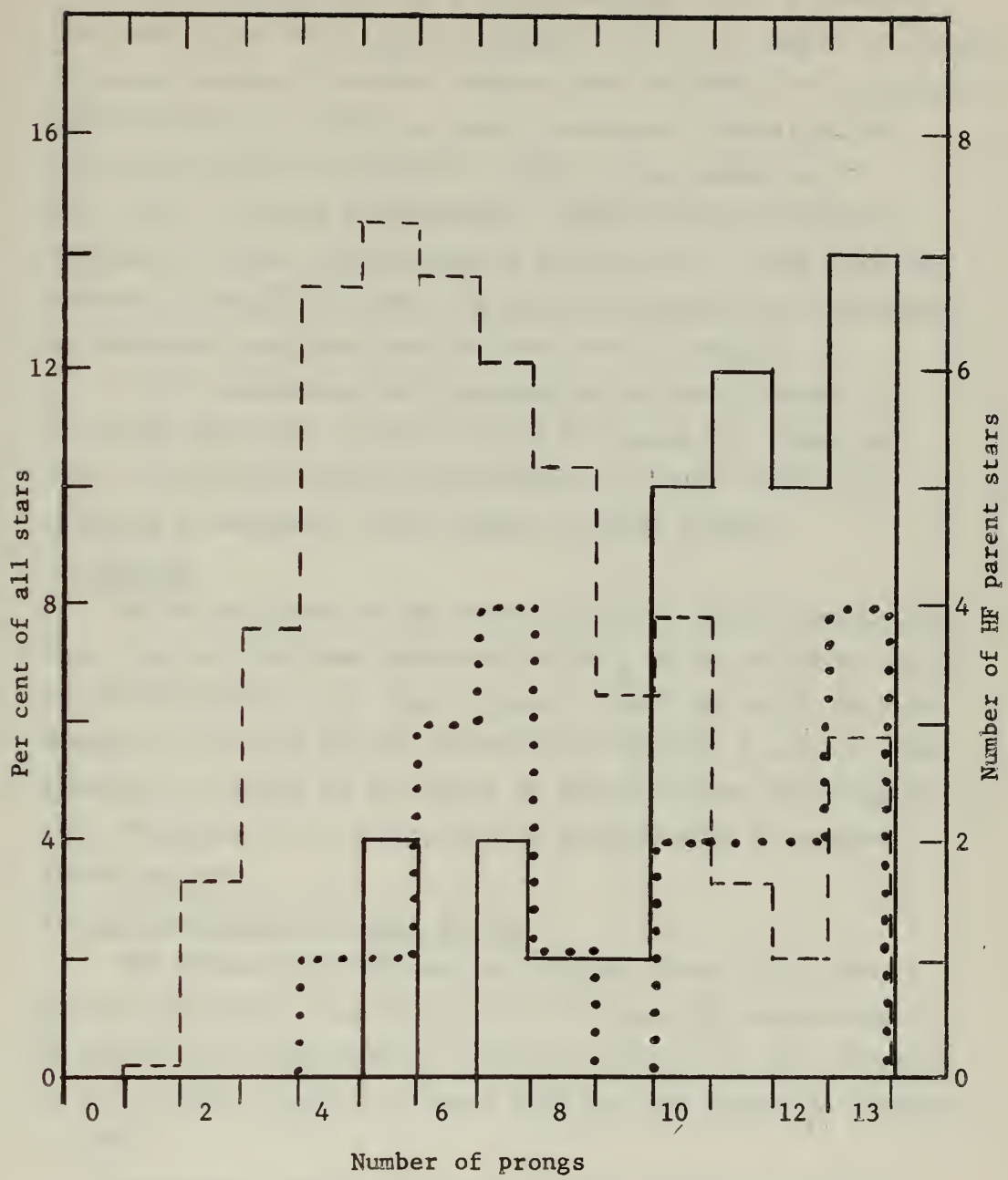

Figure 35 - Prong distribution of HF parent stars. Solid outline indicates heavy HF. Dotted line indicates light HF. (Prong distribution of all stars is indicated by dashed outline.)

the heavy elements. This is often one of the tests to determine whether the parent star is a light nucleus /47/. A check of the short prong distribution (Figure 36) in our sample of stars produced negative results. Rather than following the classical coulomb barrier, stars that were previously identified as heavy nuclei had a frequency of short prong emission of 25% $\pm$ 4%. This was significantly higher than the overall average for short prong emission of 16% $\pm$ 2 %. Thus when the nucleus is highly excited, the effective radius of the nucleus is increased and hence the coulomb barrier reduced.

For a comparison the distribution of short prongs in the heavy HF stars is also plotted in Figure 36. Comparing this to the short prong distribution for heavy stars, one observes a decrease in the number of short prongs.

c. Recoils

In the analysis of the parent stars, a recoil (prong less than five microns) was observed in 55% $\pm$ 9% of the heavy stars. In the 29 parent stars that produce a heavy HF, only one has a recoil. None of the CF parent stars display a recoil. The absence of recoils in the heavy HF and CF parent stars indicates that the HF or CF is the recoiling nucleus with a captured lambda hyperon.

d. Associated Pion or Fast Proton

The production frequency of minimum tracks, both fast protons and pions, was observed in the heavy HF parent stars. No significant difference is noted in this group when compared to the complete sample of stars (59% for the former as compared to 53%).

The kinetic energy of pions emitted from the HF parent stars was determined and the results are plotted in Figure 37. A bias against very energetic pions was introduced since steep minimum tracks were not followed. Of the 48 parent stars, one emitted two charged pions, 16 emitted one charged pion and 31 produced no charged pion.

6. Unusual Events

A number of events were observed that can not be fully

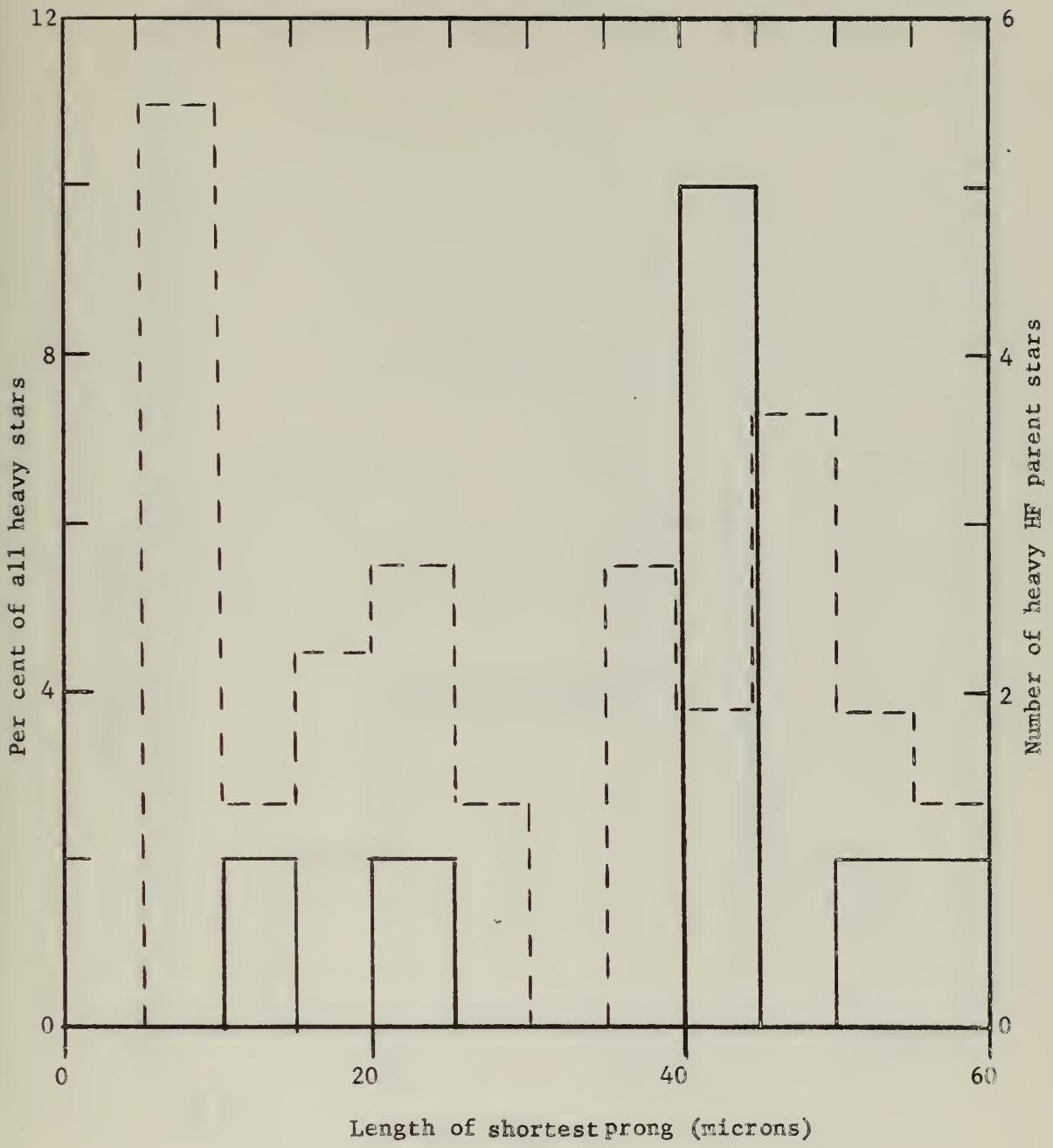

Figure 36 - Short Prong distribution of interactions in heavy nuclei. Solid outline indicates heavy nuclei stars that produce a HF. Dashed outline indicates all heavy nuclei stars.

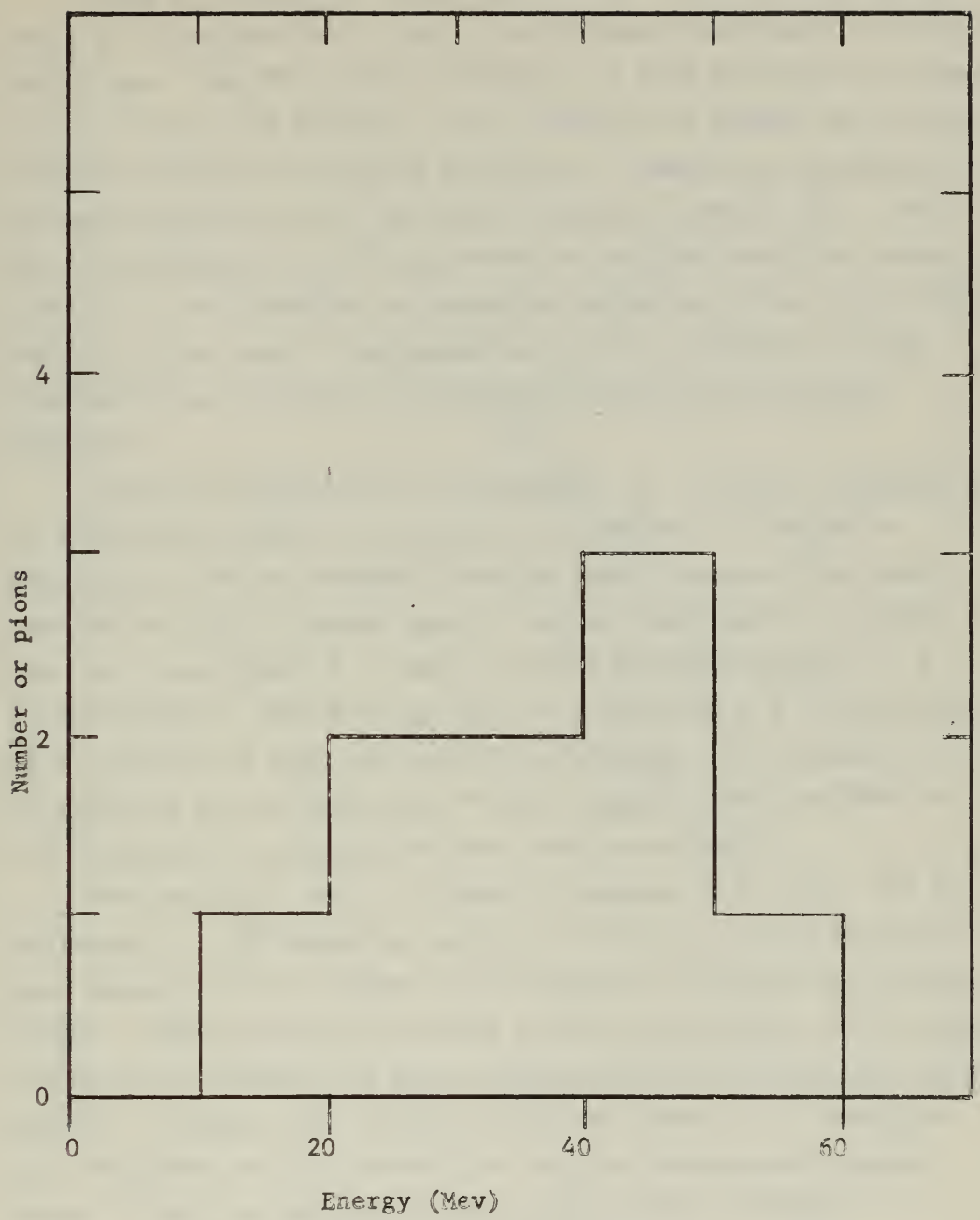

Figure 37 - Kinetic energy distribution of pions emitted from interactions that produce a HF or a CF.

justified yet are included in the data as HF.

Prong A in Figure 38 is an apparent HF. The track is definitely of a particle with charge two or more since there are many delta rays. The HF travels a distance of 5.89 mm before apparently coming to rest and decaying into a particle of charge one or two plus most likely two neutral particles. However the appearance of two electrons at the "HF decay" is most uncommon /38/. Thus the event might also be interpreted as an alpha particle scatter since it is not possible to establish definitely that the incident particle is at rest. The appearance of the electrons is then reasonable but one would also expect a recoiling scattering particle.

Prong B in Figure 39 is an apparent HF. Prong C disappears in flight (DIF) after 6.12 mm and is a baryon. It might be considered a proton forming a neutral star, however, the cross section for this is quite small. Another explanation is that the "HF" is actually a K^- meson and the apparent "decay" is a K^- interaction. The DIF can then be considered a Σ^- interacting with a proton to form two neutral particles. The presence of an electron at the "decay star" also suggests that the "HF" is a K^- emitted from the parent star with low velocity.

Both prongs D and E in Figure 40 appear to be HFs. One is definitely a ${}_{\Lambda}H^4$ decaying into a π^- and an α. The other event also appears to be colinear and consists of a recoil and a short prong. However since the recoil is only two microns, the colinearity could not be checked and hence neutral particles could have been emitted. Because the incoming track was steep, it is possible that the "HF" was not actually at rest at the apparent decay point. Thus the event might be a proton star in flight.

Prong F in Figure 41 is a HF and prongs G and H are from a CF decay. The minimum prong was multiple scattered at both ends and grain counted and the particle was found to be a K meson. If the K was positively charged, the following interactions most likely took place:

$$K^- + p \longrightarrow \overline{\overline{=}}^- + K^+$$

$$\overline{\overline{=}}^- + p \longrightarrow \Lambda^\circ + \Lambda^\circ$$

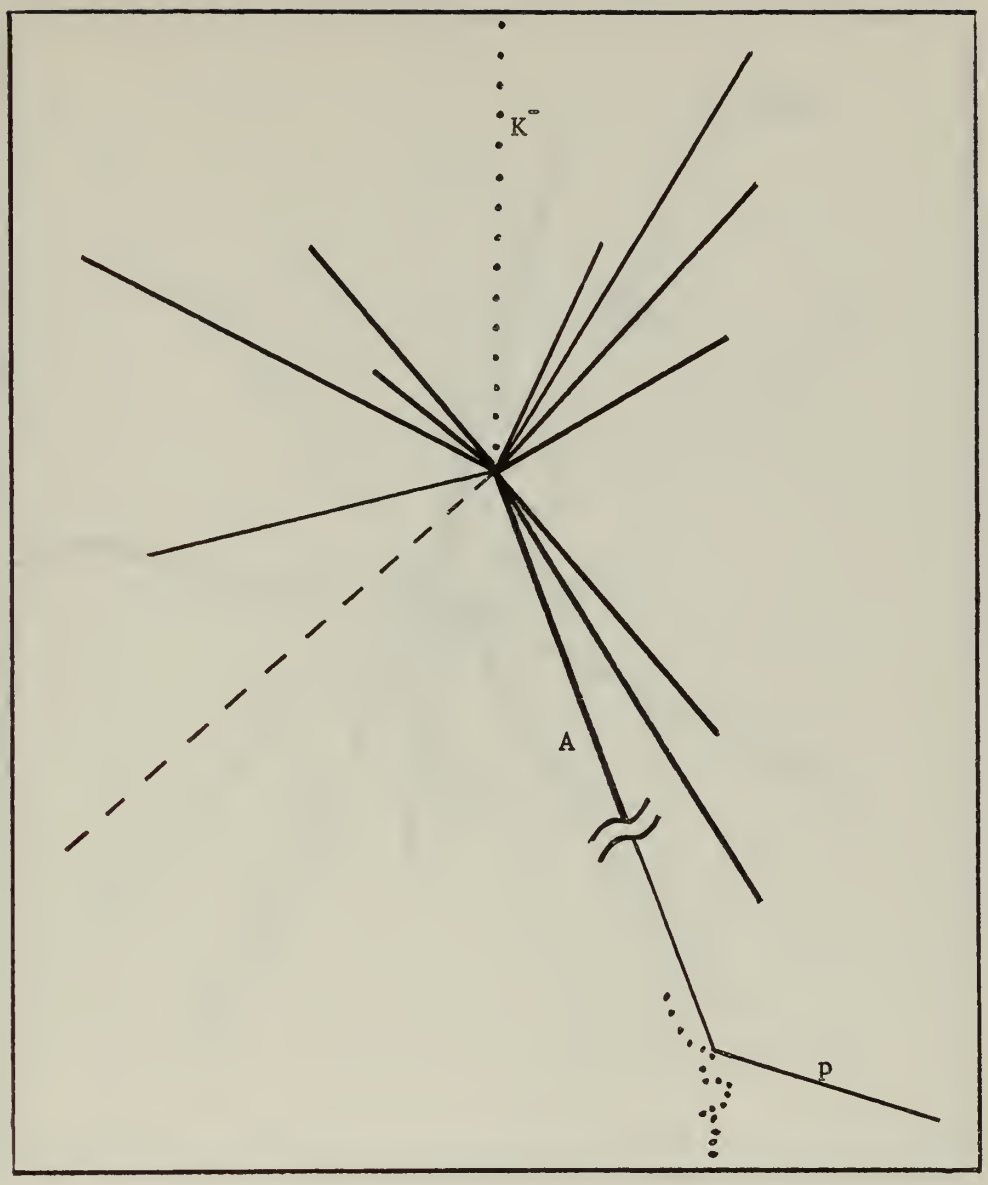

Figure 38 - Interaction of a 1.15 Bev/c K^- meson with the emission of a possible HF.

Track	A	p
Range	5.89 mm	599 um

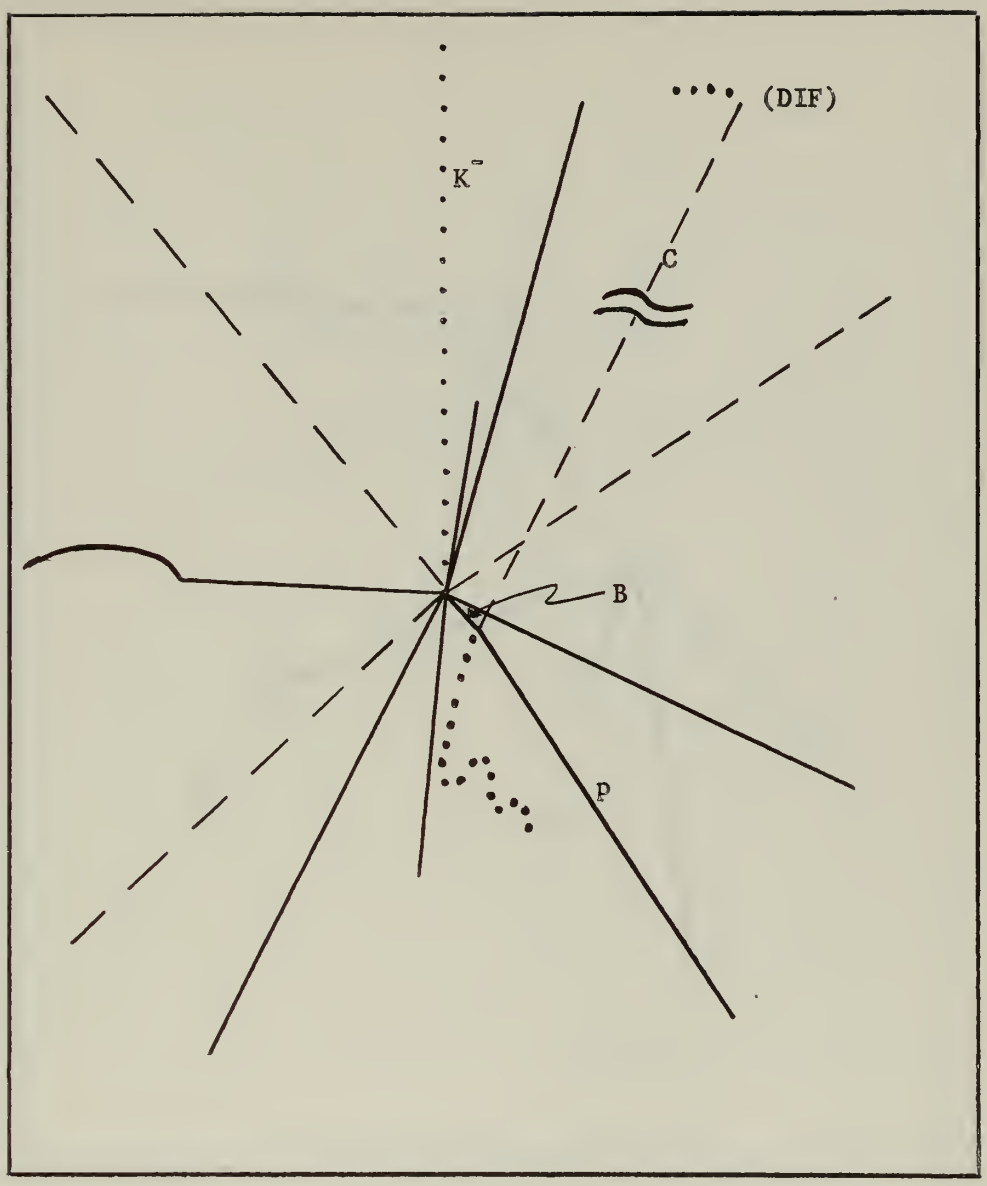

Figure 39 - Interaction of a 1.15 Bev/c K^- meson with the emission of a possible HF.

Track	B	C	p
Range	1.9 um	6.12 mm	591 um

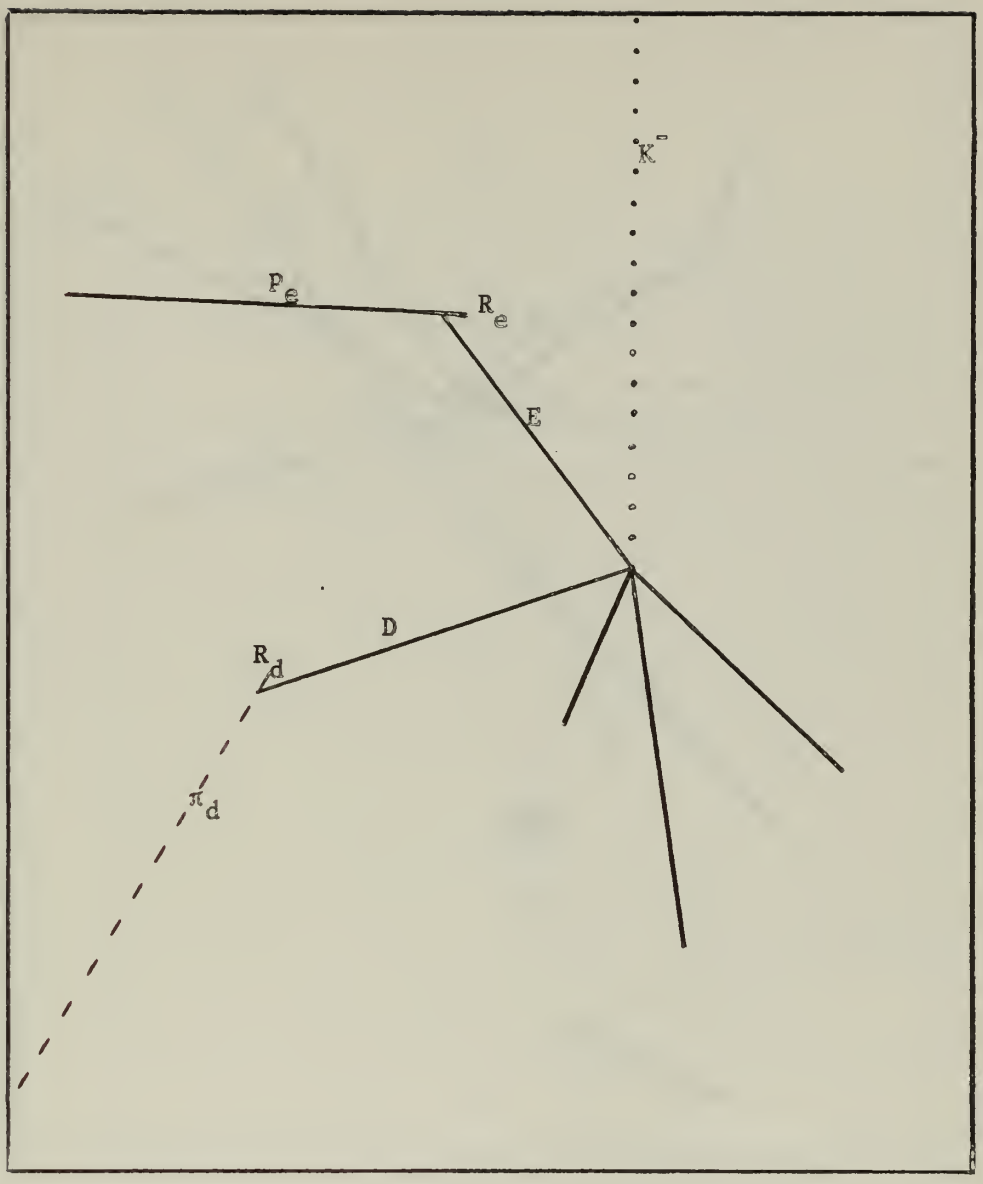

Figure 40 - Interaction of a 1.15 Bev/c K^- meson with the emission of one definite HF and one possible HF.

Track	D	R_d	π_d	E	R_e	p_e
Range	234 um	3.9 um	40.7 mm	455 um	2.4 um	1.77 mm

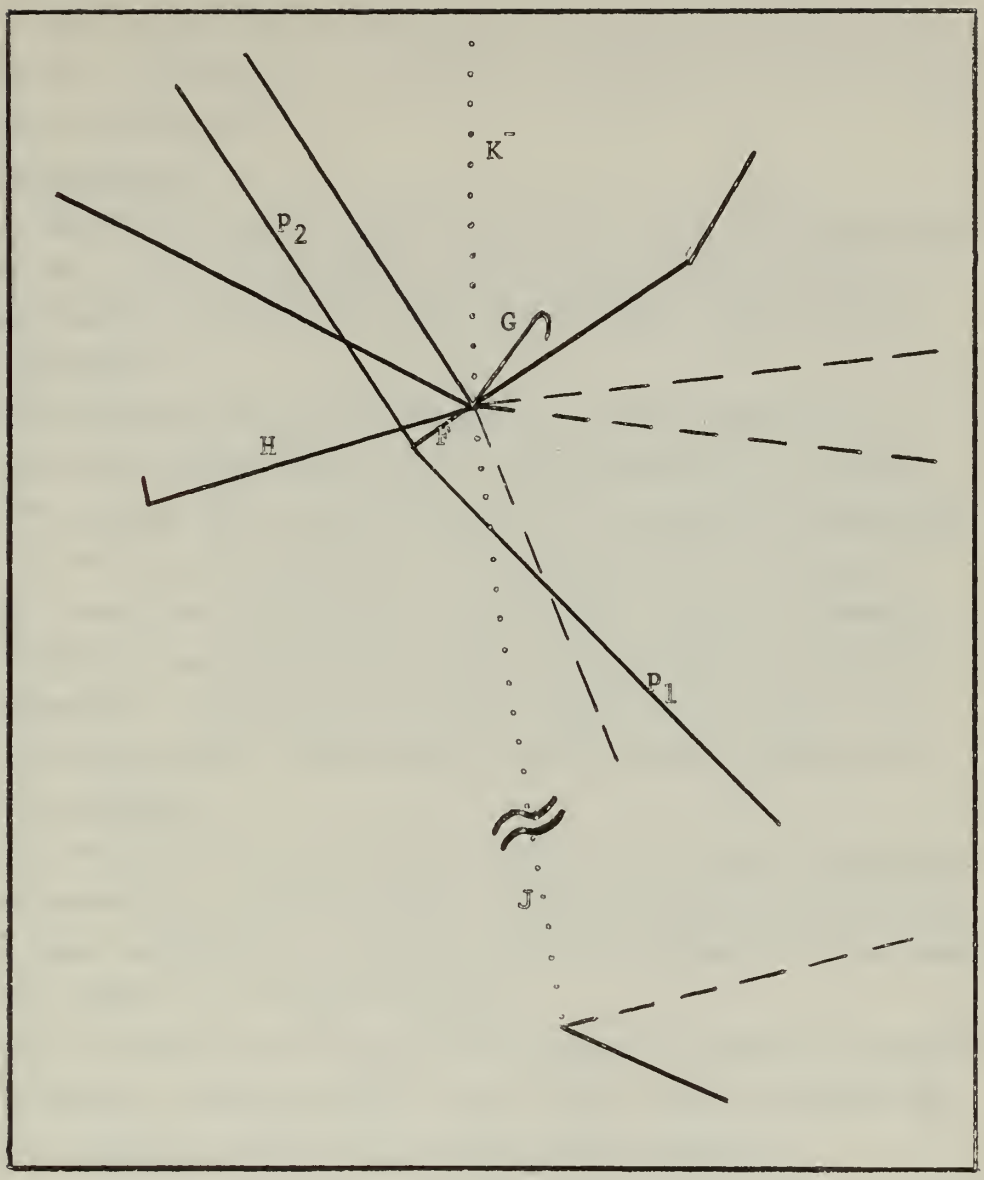

Figure 41 - Interaction of a 1.15 Bev/c K^- meson with the emission of a CF, HF and K meson.

Track	F	P_1	P_2	J
Range	4.1 um	264 um	187 um	72 mm

One of the lambda hyperons was trapped in the parent nucleus and resulted in the CF decay while the other Λ° formed a HF.

Even though some of the above events are not definite HF, they were included in the data since contamination due to other events is rare /12/.

7. Conclusions

The observations listed above lead to the conclusion that heavy HF are the combination of the recoiling nucleus with a bound lambda hyperon. The following evidence supports this the strongest:

(a) The fact that the heavy HFs are peaked forward means that they absorb some of the incoming momentum. They are not "boiled off" but are emitted in the primary interaction.

(b) The fact that nearly all (at least 83%) of the heavy HFs come from interactions in the heavy emulsion elements, indicates that they have a charge greater than the light elements. If the heavy HF had a charge of 8 or less, one would anticipate their production in all the elements of the emulsion.

(c) The fact that the heavy HF decays are without any prong of range less than 30 microns indicates that these HFs have a mass comparable to the heavy emulsion elements if one considers the effect of a coulomb barrier.

(d) The fact that the parent stars show an absence of recoils (normally a fairly common event) implies that the heavy HFs are recoiling nuclei with a bound lambda hyperon.

In estimating the mass of these heavy HFs we note that the average number of prongs emitted by the parent star is 11. Considering that some of these are multicharged, and assuming that the HF maintains the rest of the parent star charge, we estimate that the heavy HF are of charge 15 less that the parent star or approximately of charge 20 to 32. Stable nuclei of this charge have mass values between 40 and 75. The absence of short prongs from the HF decay strengthens the argument for a mass of at least 40.

B. Cryptofragments

As previously stated, a cryptofragment is defined to be a double-centered K^- star with interconnecting track between centers and having one or more prongs whose origin cannot be definitely placed with one center or the other.

An initial sample of possible cryptofragments (henceforth, cryptofragment is abbreviated to CF) was gathered from a sample of 1240 stars by examination of each star under 2500X magnification to determine if one or more prongs appeared not to emanate from a common center.

This initial sample of possible CF was subjected to the scrutiny of two scanners, operating independently, to further refine and reduce the sample. As a final check, the refined sample of possible CF was further reduced using a R-4 Koristka microscope under 3200X magnification.

The final sample contained 16 CF. This sample is assumed to be all of hypernuclei decays in that there is no evidence of any contamination at short range (see section V-A-3 of this paper).

The ranges of the hypernuclei examined were all less than 1 micron with one exception whose range was 1.8 microns. The CF data is added to the HF data to produce the number-range relationship of Fig. 31.

The forward to backward ratio (henceforth, abbreviated to FBR) for the emission of CF is 3.0 ± 1.7. If all CF and heavy HF (heavy HF are defined to be those with range less than 6 microns and are henceforth abbreviated to HHF) are considered, the FBR becomes 2.8 ± 0.9.

1. General Characteristics

A study of the characteristics of the parent stars of CF was made to determine if any of these characteristics differed from the overall 1240 K^- star sample characteristics. Details of the 16 CF stars are given in Table 5.

a. Prong Distribution

The prong-number distribution of the CF stars is compared to the prong-number distribution of a random sample of 541 stars in Fig. 42. From an examination of this, we see that 12 of 16 of the CF stars have 9 or more prongs. The prong number used is all the prongs from the parent star plus all the prongs from the hypernuclei decay. The interconnecting track is not counted. These data agree well with the HHF data (83% of HHF stars had 9

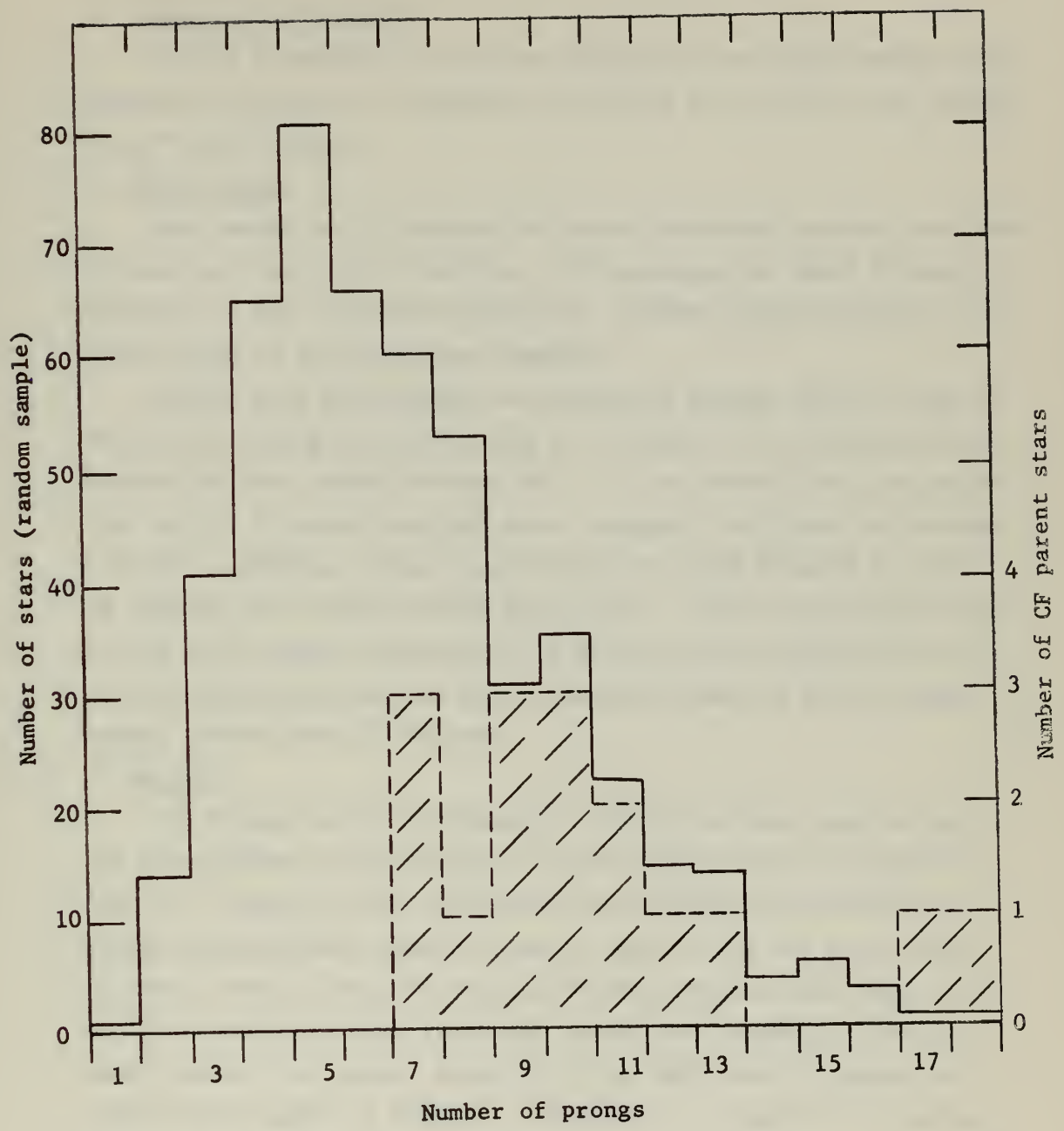

Figure 42 - Number-prong distribution of CF parent stars. Solid line indicates distribution of a random sample of 541 stars. Dashed line indicates CF parent stars.

or more total prongs) and implies that at least 75% of all CF come from the heavy nuclei (Ag or Br) of the emulsion.

b. Electrons and Blobs

Within statistical error, no difference was found between the relative occurrence of electrons and blobs on the 1240 star sample and CF parent stars.

c. Short Prongs

Our sample of CF hypernuclei decays displayed prongs less than 30 microns long 25% of the time. The presence of short prongs is contrary to the evidence obtained in the HHF study where only one short prong in 29 decays was observed.

Nuclei with Z=50 should not evaporate prongs shorter than 30 microns (assuming that the prong is the path of an alpha particle) because of the coulomb barrier /47/. If we assume that the parent star of the CF which displays short prongs is Br, then the average Z of the remaining nucleus containing the bound Λ^{o} would be about 18 (taking into account alpha particles). Since the average range of the short prongs observed is 22 microns, it is plausible that the coulomb barrier of the CF is reduced enough to allow prongs of length shorter than 30 microns.

d. Recoils

The prong-number distribution of stars without recoils and the prong-number distribution of stars with recoils is shown in Fig. 43. From this the conclusion can be drawn that the heavy nuclei (prong number greater than or equal to 9) are more likely to have a recoil than the stars with prong number less than 9. It could be inferred that, since HHF and CF are primarily from the heavy nuclei, the parent stars of CF and HHF should display an appreciable number of recoils. However, in a sample of 46 parent stars of CF and HHF, only one recoil is observed.

The FBR of recoils from known heavy nucleus stars is $1.39 \pm .22$, while the FBR of the recoils from stars with less than 9 prongs is $1.93 \pm .21$. The possible significance of this discrepancy will be discussed in the conclusion section.

The recoils from the HHF and CF hypernuclei decays are isotropically distributed within statistical error. The FBR of emmission is 1.1 ± 0.5.

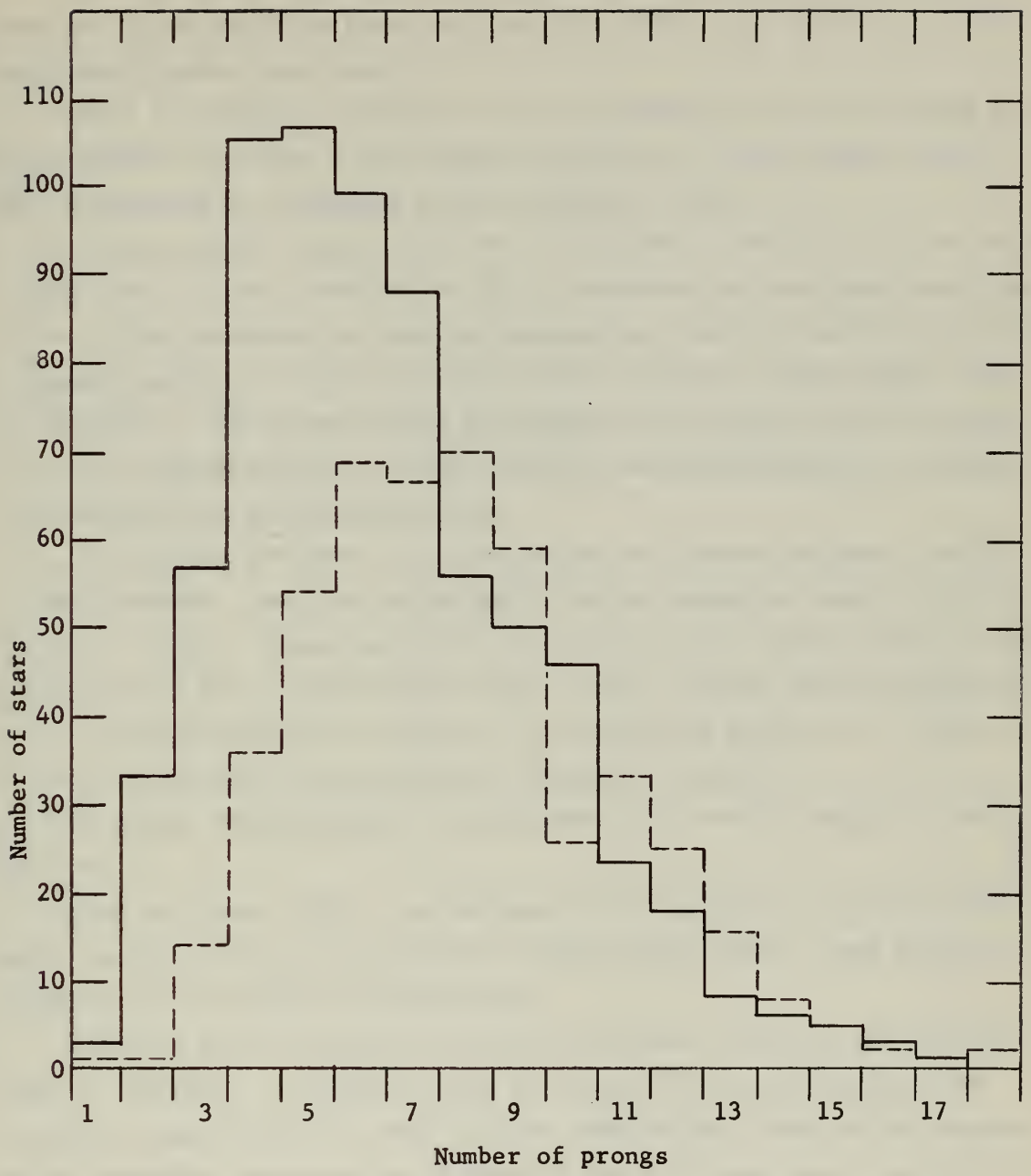

Figure 43 - Number-prong distribution of stars with and without recoils. Dashed line indicates distribution with recoils. Solid line indicates distribution without recoils.

2. Conclusions

A difference is observed in the experimental FBR of the recoils from the known heavy nucleus stars and the FBR of the recoils of stars with prong number less than 9.

There is evidence to believe that practically all of the stars with prong number less than 9 that have a recoil are in fact heavy nuclei. This assumption is supported by the following facts:

a. If all nuclei with recoils are considered to be Ag or Br, we estimate from our data that 70% of the K^- interactions are with heavy nuclei. This estimate is made by considering that the known heavy nucleus stars display a recoil more often than stars with prong number less than nine. The above stated percentage is the same as that arrived at by using geometrical cross-sections and calculating the expected percentage of such interactions;

b. If recoils are used as an indication of a heavy nucleus, then we would expect a smaller percentage of short prongs on stars that display a recoil. Experimentally, 43% of all stars display short prongs, while only 16% of stars that have a recoil display short prongs; and

c. If the interaction is with C, N, or O, then by Fig. 43, there is very little left of the original nucleus to recoil.

We assume hereafter that the presence of a recoil implies a heavy nucleus.

From our data, 80% of the HHF and CF are produced from the known heavy stars, 33% of the hypernuclei decays have recoils, and these recoils have an isotropic distribution.

Assuming that only heavy nucleus stars show recoils, the discrepancy in the FBRs' of recoils might be explained by superimposing an isotropic distribution of recoils from undetectable hypernuclei decays on the expected distribution of recoils for the known heavy nuclei. In the following, we will assume that the FBR of recoils from K^- stars is peaked forward, but that our observed ratio is modified by the presence of undetected CF which display isotropic recoils among the K^- stars. We further assume that the different ratios observed can be attributed to different fractions of unobserved cryptofragments in the samples with greater than or equal to 9 and less than 9 prongs. It is reasonable that the presence of a CF is correlated with the existence of stars with greater than or equal to 9 prongs, both from the observed

fact that 80% of all observed HHF and CF come from such stars, and from the assumed fact that the trapped Λ^o causes greater excitation which leads to a larger number of evaporation prongs.

Utilizing the above assumptions and data, a calculation has been carried out in Appendix C to determine the number of undetectable CF. We estimate that a Λ^o is trapped in the nucleus to produce an unobservable CF (no double center) in 29±22% of the K^- interactions.

TABLE V

Cryptofragment Data

Event No.	No. of prongs from parent star + CF	Probable No. of prongs from CF decay	Presence of: Recoil	Blob	Minimum	Electron	θ	$\bar{R}$ (u)
85-9	10	3-4	Y(CF)	N	1	N	+58°	0.6
85-53	9	1	N	N	N	1	-70°	0.5
86-47	11	2	N	N	N	N	+42°	1.8
87-16	9	2	N	N	1	N	-52°	0.3
87-77	10	1(15u,CF)	N	N	N	N	~10°	0.8
87~90	11	2(24u,CF)	Y(CF)	N	1	1	+85°	0.2
88-118	13	2	N	N	1	N	+50°	0.8
89-32	10	2~3	N	N	N	N	+20°	0.3
89-43	17	3(29u,CF)	N	N	1	N	-30°	0.4
89-120	7	2	N	N	1	1	+120°	0.7
89-191	18	2(25u,CF) (26u,CF)	N	N	N	N	+110°	0.8
90-134	7	3	Y(CF)	N	N	1	+110°	0.5
91-146	12	4	Y(CF)	N	N	N	-105°	0.9
91-191	7	2	Y(CF)	N	1	1	-85°	0.5
91-249	8	2	Y(CF)	1	1	N	+25°	0.6
91-257	9	2	N	N	N	N	-45°	0.6

(CF) indicates from hypernuclei decay.

N indicates not present.

θ is the horizontal angle between the projected K^- track and the interconnecting track between double centers. $\bar{R}$ is the length of this track.

C. Free Lambda Production

Preliminary calculations were made to determine the feasibility of conducting a search for the free Λ^0 decay downstream from the parent star. These calculations and the assumptions utilized in the calculations are shown in Appendix B.

The decision to search the area as shown in Fig. 44 was arrived at by considering; (1) the diminishing probability of finding a free Λ^0 further downstream if one confines the search to one plate because, if we consider a cone with opening angle of 60°, the relative volume of the cone that lies within the plate becomes increasingly smaller as we go downstream (see calculations in Appendix B), and (2) the difficulty of correlating the free Λ^0 with a parent star if it should be found outside the plate from the parent star.

From the results of calculations, it was estimated that a maximum of 20 free Λ^0 decays could be found in scanning the specified area around each star in the 1240 star sample. This figure of 20 free Λ^0 decays assumes that Λ^0's are produced in 75% of the stars and are produced backwards in the center-of-mass coordinate system.

1. Results and Conclusions

A total of six free Λ^0 decays were found, of which five could be correlated with a parent star.

Identification with the parent star was accomplished by following the π^- and proton tracks from the point of decay of the free Λ^0, determining momentum from the range-momentum curves by Barkas, and extrapolating the vector sum of the momenta back to the parent star.

Table VI is a summation of some of the characteristics of the free Λ^0's found in the search.

In the initial calculations, it was assumed that the free Λ^0 came off backwards in the center-of-mass system when considering the reactions:

$$K^- + P \rightarrow \Lambda^0 + \pi^0$$
$$K^- + P \rightarrow \Lambda^0 + \pi^-.$$

An upper limit for the momentum of the free Λ^0 in the above mentioned case is 778 Mev/c. Our results show no Λ^0 with momentum greater than 411 Mev/c. Therefore, our original assumption that the Λ^0 comes off backward in the center-of-mass system appears to be valid.

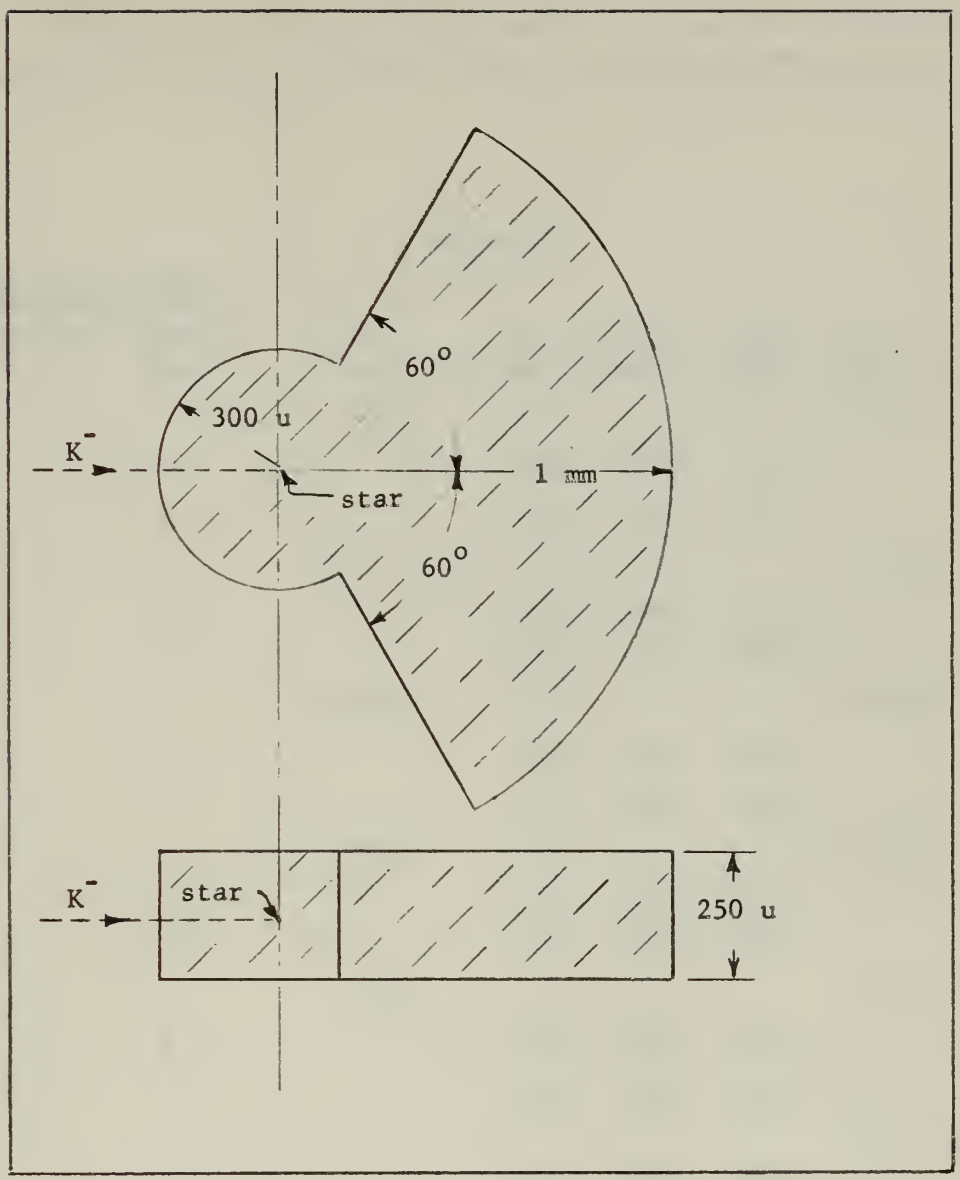

Figure 44 - Search area about the parent star for free Λ°'s.

The momentum spectrum achieved with our limited sample is also compatible with multi-pion production modes /53/.

Utilizing our original calculations and our data inserted where possible, we arrive at a rough figure of 20% free Λ^{o} production.

TABLE VI

Free Lambda Data

Event No.	Particle Type	θ (o)	R (mm)	K (Mev/c)	T (Mev)	T (Mev)	K (Mev/c)
1		252				38.1	33.4
	P		.18	85.8	3.9		
	π^-		19.1	102	34.2		
2		007				70.9	274.5
	P		6.8	286	41.9		
	π^-		14.6	94.5	29.0		
3		-017				95.4	358.0
	P		4.1	247	31.6		
	π^-		53.1	148	63.8		
4		-042				57.6	212.2
	P		2.9	122	26.1		
	π^-		16.7	98.6	31.6		
5		141				44.1	120.6
	P		0.5	131	9.1		
	π^-		19.9	104	35.0		
6*		---				111.0	411.5
	P		23.5	408	85.0		
	π^-		12.2	89.2	26		

* Unable to correlate with a parent star.

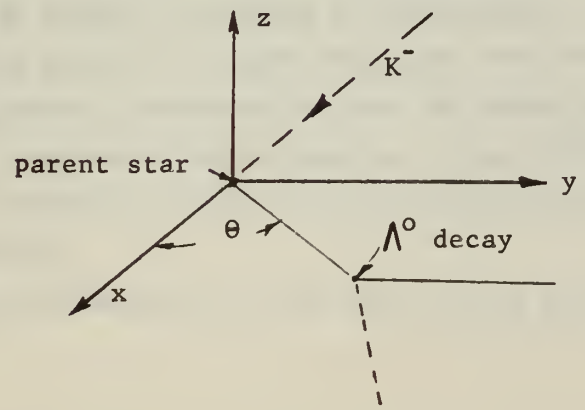

VI

CONCLUSIONS

The strangeness of the incoming 1.15 Bev/c K^- meson was conserved by the emission of the following particles, with production frequencies as indicated.

Particle	K^-	Σ^{+}_{-} & Ξ^-	Free Λ°	HF	CF	Total
Prod. Rate	14%	24%	20%	4.2%	29%	91%

According to our estimates for each mode of strange particle production, strangeness can be accounted for 91% of the time. Strangeness could also have been conserved by the emission of a $\overline{K}^o$, however no attempt was made to determine its frequency of production. Our unique method of examining the recoil direction to determine the CF production rate was subject to large error primarily because of our small sample size. We believe that this method could be used more successfully with a larger sample of interactions to obtain very accurate results.

Free lambda hyperon production is also subject to large error since we found only five Λ° decays. Extension of this investigation to a larger sample is not recommended since such a study would be very time consuming.

The characteristics of the short range HFs are similar to those observed by Jones et al /12/. Specifically, the HFs were produced predominantly forward, they generally were emitted from an interaction in a heavy emulsion element, few of their decay particles were short range, and the parent star was without a recoil. We thus concur with Jones et al in their interpretation of this data and their proposal of a model for heavy HF production.

Eleven possible cascade particles were observed. Two of the cascade hyperons interacted within the parent nucleus to produce in each case two bound lambda hyperons. The other nine possible cascade hyperons decayed in flight and had characteristics similar to a sigma hyperon decay.

In the examination of the short prong distribution from parent

stars, short prongs were observed more often from interactions in heavy emulsion elements than from interactions in light elements. Thus the emission of a short range prong is not an effective test to determine which interactions are in the light elements when the incoming particle is fairly energetic.

APPENDIX A

TRACK IONIZATION MEASUREMENTS

It has been previously shown that the range of the particle through the emulsion may be measured, and with a knowledge of the identity of the particle, determinations of the energy, momentum, velocity and the like can be made by using published tables and graphs. For the particles on which range measurements cannot be made, measurement of the track ionization can often be utilized to acquire the same information. Since the rate of energy loss is velocity-dependent, it is possible to find velocity as a function of any parameter equivalent to the rate of energy loss. For the purposes of this paper, the parameter chosen was blob density (the number of blobs per 100 microns). This parameter is plotted as a function of velocity β in the region of $\beta = 0.11$ to $\beta = 0.92$.

A statistical treatment of the geometry of the emulsion media and the theory of track structure by Barkas /39 / develops the relationships between some observable track parameters. Barkas has shown that the gap length distribution is exactly exponential , a fact determined empirically and reported by O'Caellaigh in 1954 . /55 / Barkas also has demonstrated that the gap length coefficient and the true grain density are the same quantity. A brief review of the treatment follows.

A charged particle traversing the emulsion causes ionizations which leave a series of developable grains along the particle trajectory. These ionizations are revealed by the formation of " grains" in the developed track. The number of grains per unit length is a function of particle velocity; however, grain density is not an observable track parameter since many grains coalesce into " blobs". A track to the observer is actually a series of blobs separated by gaps of varying length and not the series of grains mentioned above. It is these observable features which must be related to the particle velocity.

The density of gaps exceeding some length (L) is exponential of the form:

$$H(L) = B\, e^{-gL} \qquad (A\text{-}1)$$

where H (L) is the density of gaps of length exceeding length L .
B is the blob density, or the density of gaps of length exceeding zero.
g is the true grain density.

The relationship between blob density and grain density is also exponential and of the form :

$$B = ge^{-g\alpha} \qquad (A-2)$$

where α is the mean distance between " just resolvable " grains, and which becomes the mean grain diameter in the limit of perfect resolution. The value of α is calculated using the maximum value of the experimental blob density curve.

$$\alpha = \frac{1}{e\, B_{max}} \qquad (A-3)$$

Using the equations above , the relationship between blob density and grain density can be obtained for various parameters. An experimental curve of blob density as a function of velocity (β) was plotted in Figure A-1 .

Since most tracks in the emulsion are inclined to the surface of the emulsion, these relationships must be extended to include measurements on these " dipping " tracks. Defining the dip angle (δ) as the inclination of the track to the surface of the emulsion as measured in the unprocessed emulsion , equations A-1 and A-2 become :

$$H_\delta (L) = B_\delta e^{-gL \sec\delta} \qquad (A-4)$$

$$B_\delta = g \sec\delta\, e^{-\alpha g \sec\delta} \qquad (A-5)$$

where the subscripts δ indicate measurements per unit projected length for a track with dip angle δ . A plot of αB_δ as a function of $ag \sec\delta$ using equation A-5 above is shown in Figure A-2 .

Using equations A-2 and A-5 , the relation between blob density (B) and the observed blob density (B_δ) is calculated to be:

$$\frac{B}{B_\delta} = \frac{1}{\sec\delta}\, e^{\alpha g\,(\sec\delta - 1)} \qquad (A-6)$$

and a plot of B/B_δ as a function of αg for various values of δ is shown in Figure A-3 .

In using ionization measurements for the determination of the particle velocity the following standardized procedure was used.

The observed blob density was corrected to true grain density using Figure A-2 and the computed value of α of 0.61 microns. Grain density and observed dip angle were used in Figure A-3 to find the correction factor for dip. The observed blob density corrected for dip was then used to determine velocity using Figure A-1, the calibration curve of velocity as a function of blob density.

Experimental verifications of the results of these calculations were performed on tracks of various particles, velocities, and dip angles . The corrections for inclined tracks were found to be valid up to dip angles of 40° for tracks of minimum ionization.

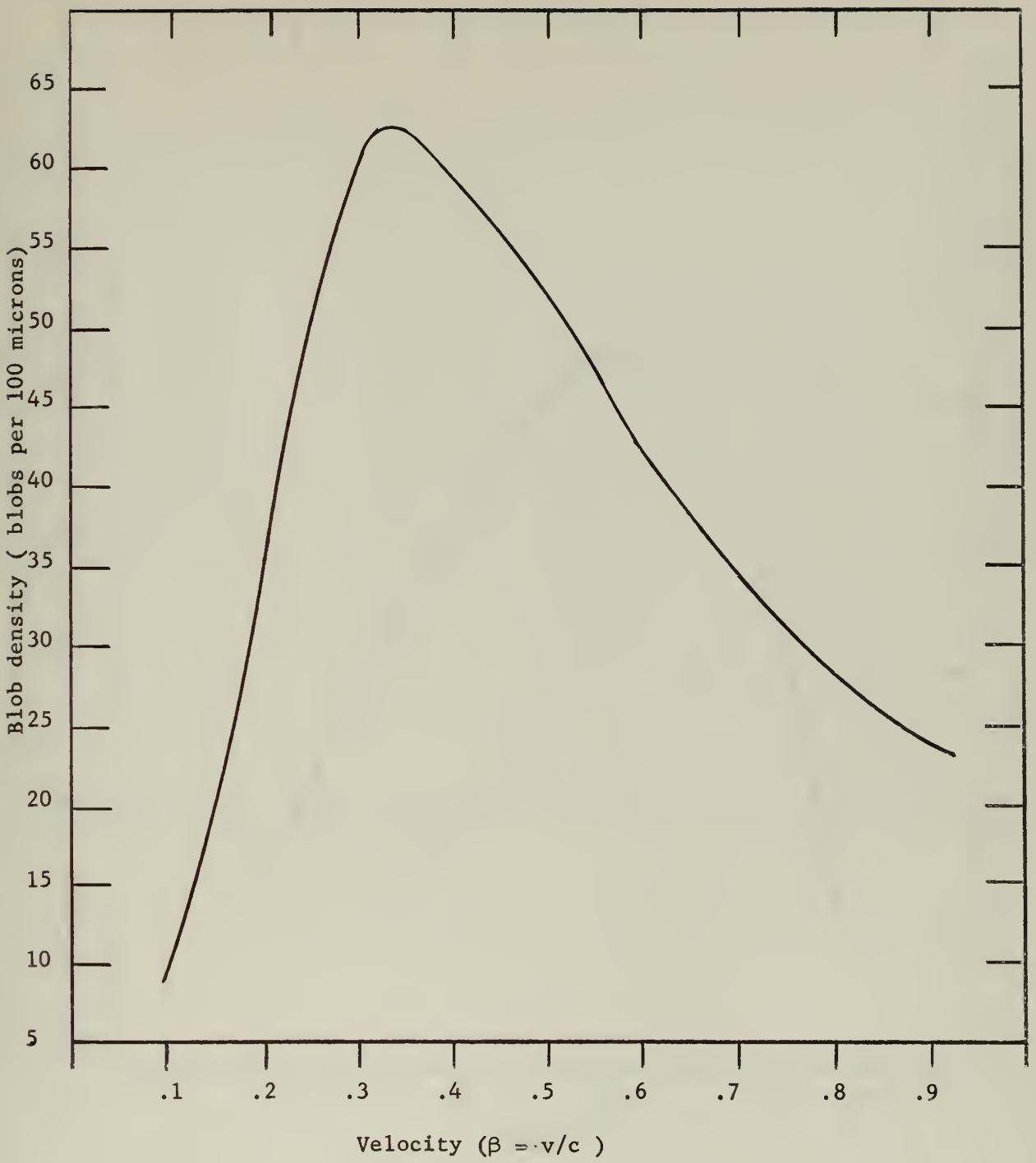

Figure A-1 Experimental curve of blob density as a function of normalized velocity , β.

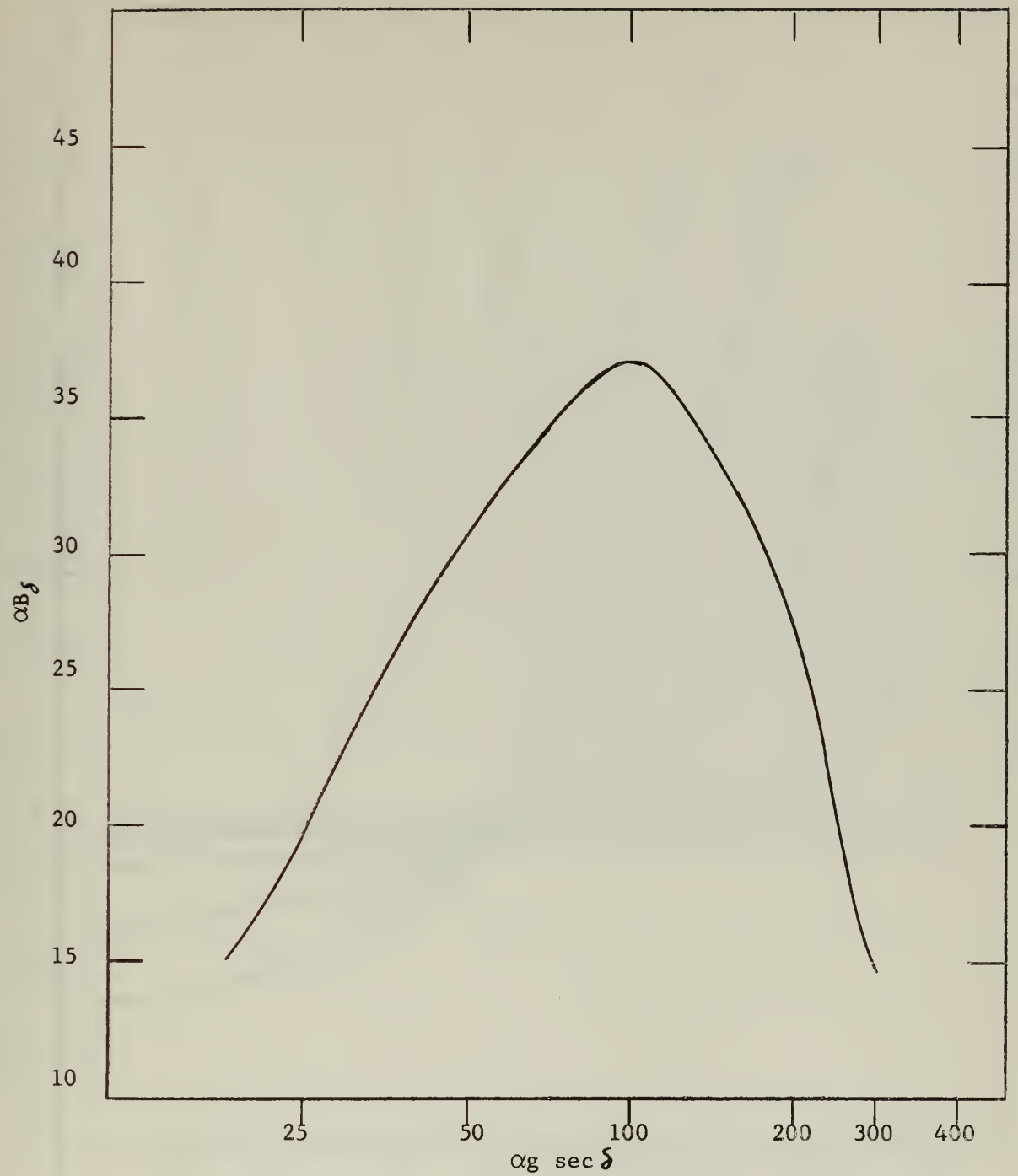

Figure A-2 The relation $\alpha B_\delta = \alpha g \sec \delta (\exp. -\alpha g \sec \delta)$ with αB_δ plotted against $\alpha g \sec \delta$.

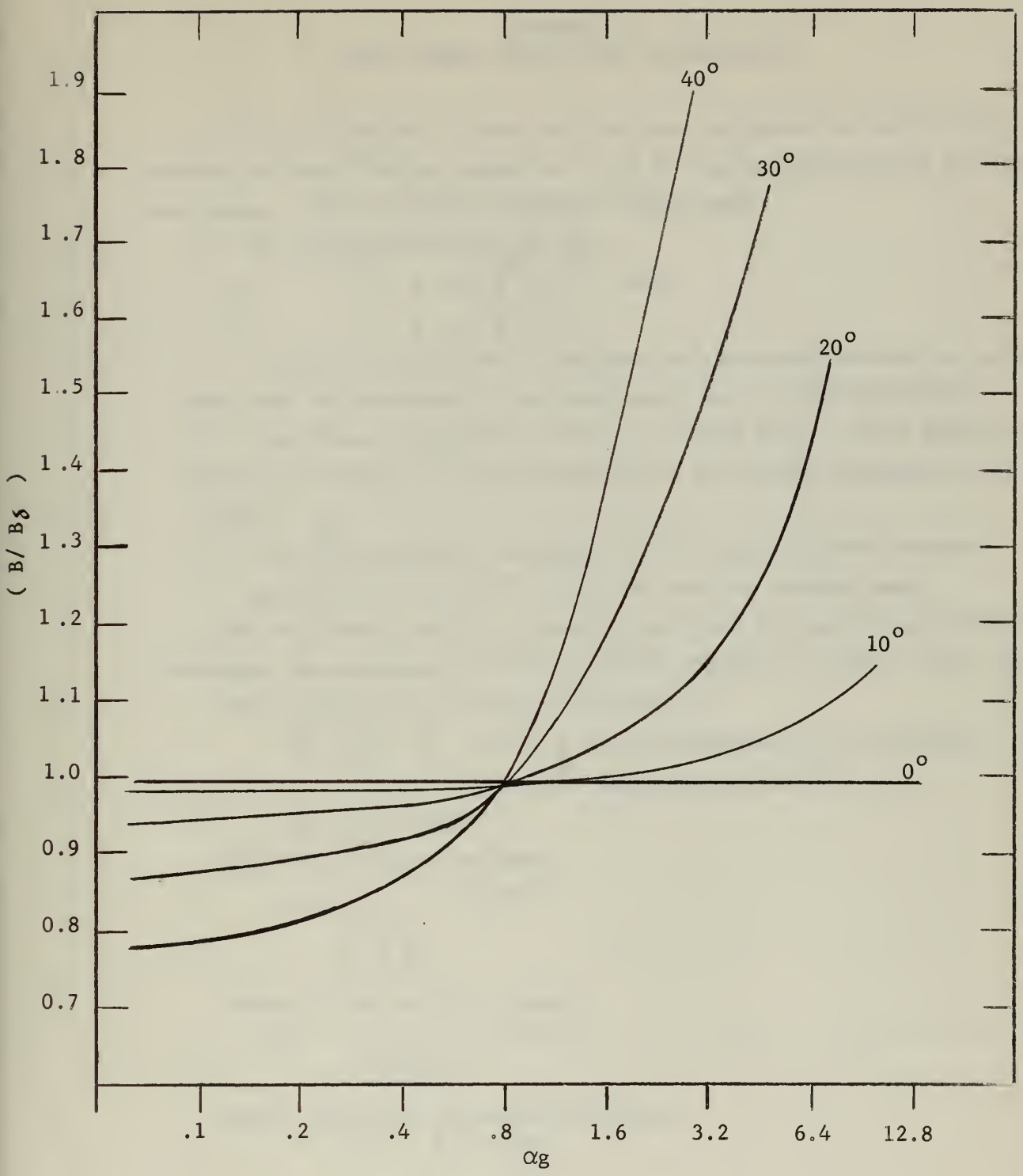

Figure A-3 The relation $B/B_\delta = 1/\sec\delta\ (\exp.\ \alpha g\ (\sec\delta - 1))$ with B/B_δ plotted against αg for various values of δ.

APPENDIX B
FREE LAMBDA PRODUCTION CALCULATIONS

The calculations in this section were performed to predict the number of free Λ^o's that might be found in a given area around the parent stars. The following assumptions were made.

1. The production reactions are:
   a. $K^- + P \longrightarrow \Lambda^o + \pi^o$ and
   b. $K^- + n \longrightarrow \Lambda^o + \pi^-$.

   Production reaction a. was used for calculations and no attempt was made to calculate b. as there would not be much difference.
2. Free Λ^os are produced in 75% of all beam stars. This rough figure was arrived at in considering lack of visible strangeness in K^- stars.
3. Free Λ^os are emitted backward in the center-of-mass system.
4. Two-thirds of the Λ^o decays are via the charged mode.

The following series of calculations /54/ are performed below to determine the parameters of the momentum ellipse as shown in Fig. B1.

The incoming total energy available is:

$$E_k^2 = M_k^2 + K_k^2$$ where $\frac{K}{c}$ is the momentum of the incoming K^- and M is the rest mass of the K^-.

$$E_k = 1251.6 \text{ Mev}$$

Beta of the center-of-mass:

$$\beta = \frac{K_k}{E_k + M_p} = 0.525$$

Gamma of the center-of-mass:

$$\gamma = \frac{1}{(1 - \beta^2)^{1/2}} = 1.175$$

Total energy in the center-of-mass:

$$N^2 = M_k^2 + M_p^2 + 2E_k M_p$$

$$N = 1863.5 \text{ Mev}$$

Momentum of the Λ^o in the center-of-mass:

$$K'^2 = \frac{1}{4N^2}\left(\left(N^2 - (M + M_\pi)^2\right)\left(\left(N^2 - (M - M_\pi)^2\right)\right)\right.$$

$$K' = 587.6 \text{ Mev/c}$$

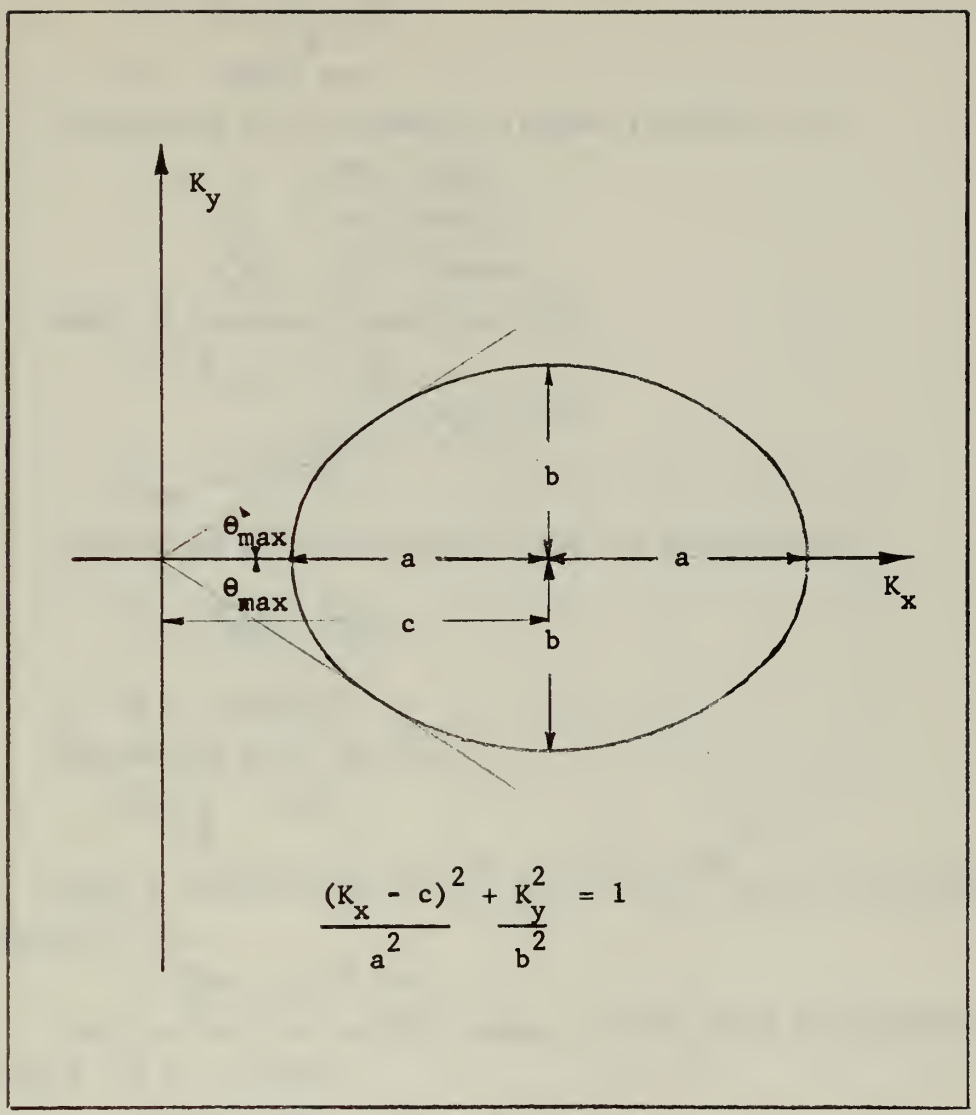

Figure B1 - Momentum ellipse in the lab system for the emission of the Λ°.

Energy of the Λ^o in the center-of-mass:

$$E' = \frac{N^2 + M^2 - M_\pi^2}{2N}$$

$$E' = 1260.1 \text{ Mev}$$

Coordinates of the momentum ellipse (see Fig. B1):

$$a = K' = 690.4 \text{ Mev/c}$$

$$b = K' = 587.6 \text{ Mev/c}$$

$$c = \beta\gamma E' = 777.7 \text{ Mev/c}$$

Angle of maximum θ (see Fig. B1):

$$\tan \theta_{max} = \frac{b}{c(1 - a^2/c^2)^{1/2}}$$

$$\theta_{max} = 58^o\ 40'$$

The average Λ^o momentum that might be expected is:

$$\bar{K} = \frac{K_{max} + K_{min}}{2}$$

$$\bar{K} = 200 \text{ Mev/c}$$

The average β of the Λ^o is:

$$\gamma\bar{\beta} = \frac{\bar{K}}{M} = 0.18$$

Using a lifetime for the Λ^o of 2.5×10^{-10} sec = α, the average range will be:

$$\bar{R} = \gamma\beta\alpha c = 13.7 \text{ mm.}$$

Starting with an initial sample of 1240 stars and applying assumptions 2 and 4, we have

$$1240 \times 0.75 \times 2/3 = 620 = N_o$$

where N_o is the number of free Λ^o we would expect to find if we searched a cone (with opening angle of $58^o\ 40'$) "downstream" from the star. See Fig. B2.

Assuming an exponential decay law:

$$N = N_o(1 - e^{-\frac{r}{13.7}}).$$

For r=0.351 mm

$$N = 16 \text{ decays}$$

For r=1 mm

$$N = 44 \text{ decays}$$

From Fig. B2, we see that for r=0.351 mm, the volume in question lies entirely within one plate while for r=1 mm, a considerable por-

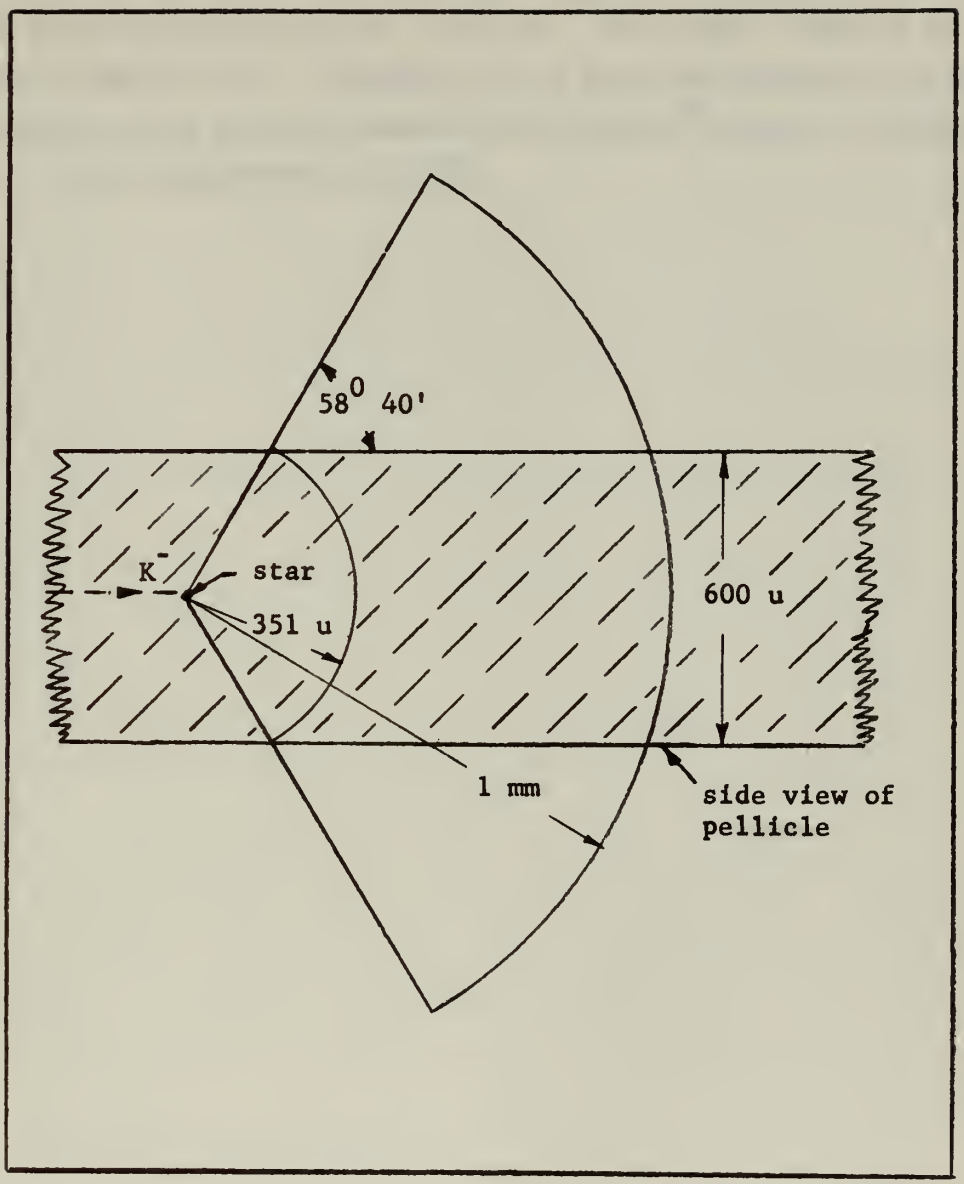

Figure B2 - Geometry of the emission cone for the Λ^0 in the lab system.

tion lies outside of one plate. To find the number of Λ^0s in the second volume we take a ratio of the area inside the plate to that outside and multiply this by 44 - 16 = 28. The number expected in the second volume is 3.9. Therefore, if an area downstream of the star as shown in Fig. B2 were scanned for visible Λ^0 decays, we would expect to find approximately 20 Λ^0's.

APPENDIX C

CALCULATION OF THE NUMBER OF UNDETECTABLE BOUND LAMBDA IN CF FORM

We estimate here the percentage of K^- stars that have a bound Λ° in undetectable CF form. Although the difference in the FBRs' used is barely significant, we consider the calculations instructive as it leads to an estimate of Λ° trapping independent of any search for free Λ° decays or production of any other strange particles.

The following data are utilized in the calculations:

a. the experimental FBR of the recoils from the decay of hypernuclei is isotropic;

b. the experimental FBR of the recoils from known heavy nucleus stars is 1.39 ± 0.22;

c. the experimental FBR of the recoils from stars with less than nine prongs is 1.93 ± 0.21;

d. the experimentally determined percentage of CF and HHF decays that display a recoil is 33.3;

e. the experimentally determined percentage of CF and HHF that occur in known heavy nuclei is 80; and

f. the number of recoils observed from the known heavy stars is 177.

We assume that the sample of stars with prong number less than 9 contains no CF's. The recoils from stars with prong number less than 9 have a FBR of 1.93, while the stars with prong number greater than or equal to 9 have a FBR of 1.39 for recoils. We assume that the more isotropic distribution in the latter sample is due to recoils from decays of unobservable cryptofragments.

Let X = the fraction of recoils from stars with prong number greater or equal to 9 which are from undetectable CF's. Let f_c = the fraction of CF (undetectable) recoils which go forward, f_n = the fraction of non-CF recoils which go forward, and f_o = the observed fraction of recoils which go forward.

Then

$$f_o = Xf_c + (1 - X)f_n .$$

To solve for X, we assume that f_c is 0.5, which means an isotropic distribution of recoils from CF decays. $f_o = \frac{1.38}{1.38+1}$ is direct experimental data. We take $f_n = \frac{1.99}{1+1.99}$, which involves the following

assumptions:

a. the sample of stars with prong number less than 9 contains no CF's; and

b. the non-CF stars from the total sample of stars with prong number greater than or equal to 9 are assumed to have the same angular distribution of recoils as the stars with prong number less than 9.

Solving for X:

$X = 0.48$

By f:

$0.48 \times 177 = 85$ recoils from undetectable hypernuclei decays in the known heavy stars.

By d and e:

$\frac{85}{.333 \times .80} = 319$ undetectable hypernuclei decays from all stars.

The percentage of the sample that contains bound lambda in undetectable CF form is 29 ± 22.

ACKNOWLEDGMENTS

We are grateful to Dr. John N. Dyer for suggesting and guiding this research, and to Dr. Fred R. Buskirk and Dr. Harry E. Handler for their interest and encouragement.

Our sincerest thanks go to the scanners, Mrs. Gail Henderson and Mrs. Sue Bearry.

We are also indebted to our wives, without whose assistance it would have been difficult to have completed this work.

This research was done under the auspices of the Office of Naval Research and the United States Atomic Energy Commission.

BIBLIOGRAPHY

1. L. Leprince-Rinquet and M. Lheritier, Comptes rendus 219, 618 (1944).
2. W. Fowler, R. Shutt, A. Thorndike, W. Whittemore, Phys. Rev. 91, 1287 (1953) & 93, 861 (1954).
3. R. Hill, E. Salant, M. Widgoff, L. Osborne, A. Persner, D. Riston, J. Crussard, W. Walker, Phys. Rev. 94, 797 (1954).
4. R. Hill, E. Salant, M. Widgoff, Phys. Rev. 94, 1794 (1954); 95, 1699 (1954); & 99, 229 (1955).
5. J. Hornbostel and E. Salant, Phys. Rev. 93, 902 (1954); 98, 218 (1955); 98, 1202 (1955); & 99, 338 (1955).
6. W. Barkas, W. Dudziak, P. Giles, H. Heckman, F. Inman, C. Mason, N. Nickols, and F. Smith, Phys. Rev. 105, 1417 (1957).
7. L. Kerth and D. Stork, Bull. Am. Phys. Soc. 30, 41 (1955).
8. J. Murray, Coaxial Static-Electromagnetic Velocity Spectrometer for High Energy Particles, UCRL-3492, May 1957.
9. J. Dyer, Analyses of the K^- beam transmitted by the Murray Spectrometer, UCRL-8364 Suppl., Jan. 1959.
10. J. Dyer, Analysis of the Bevatron K^- beam by means of an Emulsion Stack, UCRL-8364, July 1958.
11. M. Danysz and J. Pniewski, Phil. Mag. 44, 348 (1953).
12. B. Jones et al, Phys. Rev. 127, 236 (1962).
13. D. Davis et al, Phys. Rev. ltr. 9, 464 (1962).
14. E. Fletcher et al, Phy. ltr. 3, 280 (1963).
15. W. Barkas, N. Biswas, D. DeLise, J. Dyer, H. Heckman, and F. Smith, Interactions of 1.15 Bev/c K^- Mesons in Emulsions, UCRL-8745, Apr. 1959.
16. W. Barkas and D. Young, Emulsion Tables I, Heavy Particle Functions, UCRL-2579 (Rev), Sept. 1954.
17. Private communication from Dr. J. N. Dyer, USNPGS.
18. W. Barkas, Equiptment and Methods for Automatic Track Analysis, UCRL-8482, Aug. 1958.
19. Reynolds, J. Dyer, C. Mason, N. Nichols, F. Smith, H. Heckman and W. Barkas, Keysort Card System for Emulsion-data Recording, UCRL-8307, 1958.
20. W. Barkas, The Range-Energy Relation in Emulsion, Part 2 The Theoretical Range, UCRL-3769, Apr. 1957, & Nuovo cimento 8, 201 (1958).
21. D. DeLise, Scanners Notes, Lawrence Radiation Laboratory, 1958 (Unpublished).
22. W. Barkas, The Range-Energy Relation in Emulsion, Part 1 Range Measurements, UCRL-3768, Apr. 1957, & Nuovo cimento 8, 185 (1958).
23. W. Barkas, J. Dyer, C. Mason, N. Nickols, and F. Smith, Phys. Rev. 124, 1209 (1961).

24. J. Dyer, Charged Hyperon Production and Decay: Energetics, Lifetimes, and Branching Ratios (Ph.D. Thesis), UCRL-9450, Nov. 1960.

25. Bonetti, Levi-Setti, Panetti, and Tomasini, Nuovo cimento 10, 1736 (1953).

26. C. York, R. Leighton, and E. Bjornerud, Phys. Rev. 90, 167 (1953).

27. W. Fry, J. Schneps, C. Snow, M. Swami, and D. Wold, Phys. Rev 104, 270 (1956); & 107, 257 (1957).

28. S. Freden, F. Gilbert, and R. White, High Energy K^- Meson Interactions and Decays, UCRL-5629, Aug. 1959.

29. B. Quassiate et al, Nuovo cimento 13, 1294 (1959); 16, 960 (1960); & 19, 1171 (1961).

30. W. Barkas et al, Phys. Rev. ltr. 11, 466 (1959).

31. D. Evans et al (K^- Collaboration Part III), Nuovo cimento 15, 873 (1960).

32. H. White, Identification Curves for Heavy Meson and Hyperon Decays, UCRL-3514, Sept. 1956.

33. B. Bhowmik et al (K^- Collaboration Part II), Nuovo cimento 14, 315 (1959); & B. Jones et al, Nuovo cimento 19, 1077 (1961).

34. L. Alvarez, P. Eberhard, M. Good, W. Graziano, H. Ticho, and S. Wojiciki, Phys. Rev. ltr. 2, 215 (1959).

35. D. Davis and O. Skjeggstad, EFINS 63-7 Internal Report, 1963 (Unpublished).

36. M. Garelli, B. Quassiati, and M. Vigone, Nuovo cimento 17, 786 (1960).

37. M. Baldo Ceolin et al, Nuovo cimento 17, 804 (1960).

38. C. Powell, P. Fowler and D. Perkins, The Study of Elementary Particles by the Photographic Method, (Pergamon Press, New York, 1959).

39. W. Barkas, Emulsion Track Structure, UCRL-9181, June 1960.

40. W. Barkas, Information Content of Particle-tracks, UCRL-9578, May 1961.

41. C. Castagnoli, G. Cortini, and C. Franzinetti, Nuovo cimento 2, 550 (1955).

42. W. Fry in Annual Review of Nuclear Science 8, ed. by E. Segre (Annual Reviews Inc., Palo Alto, Calif., 1958).

43. D. Davis, M. Csejthey-Barth, J. Sacton, B. Jones, B. Sanjeevaiah, and J. Zakrzewski, Nuovo cimento 22, 275 (1961).

44. P. Prakash, P. Steinberg, D. Chandler, and R. Prem, Nuovo cimento 21, 235 (1961).

45. R. Ammar, R. Levi Setti, W. Slater, S. Limentani, P. Schlein, and P. Steinberg (EFINS-NU Collaboration Part I), Nuovo cimento 15, 181 (1960).

46. R. Ammar et al (EFINS-NU Collaboration Part II), Nuovo cimento 19, 20 (1961).

47. D. Aleledo, L. Choy, R. Ammar, N. Crayton, R. Levi Setti, M. Raymund, and O. Skjeggestad (EFINS-NU Collaboration Part III), Nuovo cimento 22, 1171 (1961).

48. J. Sacton, Nuovo cimento 15, 110 (1960).

49. H. Heckman, B. Perkins, W. Simon, F. Smith, and W. Barkas, Phys. Rev. 117, 544 (1960).

50. J. Sacton, Nuovo cimento 18, 266 (1960).

51. N. Nickols, S. Curtis, and D. Prowse, Phy. ltr. 1, 327 (1962).

52. S. Wojcicki, Pion-Hyperon Resonances (Ph.D. Thesis), UCRL-9835, Aug. 1961.

53. M. Alston, L. Alvarez, P. Eberhard, M. Good, W. Graziano, H. Ticho, and S. Wojcicki in Proceedings of the 1960 Annual International Conference on High-Energy Physics at Rochester (Interscience Publishers, Inc., New York, 1960).

54. Private communication from Dr. F. R. Buskirk, USNPGS.

55. C. O'Ceallaigh , CERN Report B.S. 11 (1954)